# A NEW LATTICE FLUID EQUATION OF STATE FOR ASSOCIATED $CO_2$ + POLYMER AND $CO_2$ + IONIC LIQUID SYSTEMS

A Thesis
Presented to
The Academic Faculty

by

Mohammad Zahid Hossain

In Partial Fulfillment
of the Requirements for the Degree
Doctor of Philosophy in the
School of Chemical and Biomolecular Engineering

Georgia Institute of Technology
December 2014

# A NEW LATTICE FLUID EQUATION OF STATE FOR ASSOCIATED $CO_2$ + POLYMER AND $CO_2$ + IONIC LIQUID SYSTEMS

Approved by:


Dr. Amyn S. Teja, Advisor
School of Chemical and Biomolecular Engineering
*Georgia Institute of Technology*

Dr. William J. Koros
School of Chemical and Biomolecular Engineering
*Georgia Institute of Technology*

Dr. Peter J. Ludovice
School of Chemical and Biomolecular Engineering
*Georgia Institute of Technology*

Dr. David Bucknall
School of Materials Science and Engineering
*Georgia Institute of Technology*

Dr. Sheldon M. Jeter
School of George W. Woodruff School of Mechanical Engineering
*Georgia Institute of Technology*


Date Approved: 08/20/2014

I dedicate my dissertation to my family and friends. I would especially like to express my deepest gratitude to my parents Abdul Ghani and Monwara Begum for making me who I am and for their unconditional love that motivates me to set ambitious goals.

# ACKNOWLEDGEMENTS

First and foremost, I would like to thank my advisor Dr. Amyn S. Teja for his continuous help and guidance in my research. His insightful discussions on different aspects of the thermodynamics and engineering fundamentals helped me to achieve my professional goals. The enthusiasm and professionalism he has demonstrated for his research was motivational for me, even when times were difficult in my Ph.D. pursuit. It has been an honor to be his Ph.D. student. I would also like to acknowledge my committee members, Dr. Koros, Dr. Ludovice, Dr. Bucknall, and Dr. Jeter for their assistance and recommendations in different stages of my research.

I would like to express my heartiest gratitude to past and present members of the Teja research group, Yanhui Yuan, Pei Yoong, Pramod Warrier, Nelson Green, and Mohamad Kassaee for their generous help and friendship. They have added much to my personal and professional development. I am especially indebted to Mohamad Kassee, Pei Yoong, and Pramod Warrier for their willingness to provide inspiration and feedback, and Mohamad Kassaee for his help in FTIR peak analysis.

I wish to acknowledge my friends and family for their inspiration and support they have provided during my PhD work. Most importantly, I would like to thank my wife, Kamrun Nahar and my son, Naqeeb Mohammad Hossain for their love and support which was the driving force to accomplish my goals.

## TABLE OF CONTENTS

# LIST OF TABLES

# LIST OF FIGURES

# LIST OF SYMBOLS AND ABBREVIATIONS

Symbols

| | |
|---|---|
| $c$ | Velocity of light in vacuum in Equation 2.10 |
| $d_p$ | Penetration distance |
| $k$ | Force constant in Equation 2.10 |
| $m_i$ | Mass of the atom $i$ in Equation 2.11 |
| $\mu$ | Reduced mass in Equation 2.10 and 2.11 |
| $\omega$ | Interchange energy |
| $z$ | Coordination number |
| $\Gamma_{ij}(r,T)$ | Intermolecular pair-potential energy |
| $p$ | Polarizability in Equation 2.2 |
| $\mu$ | Dipole moment in Equation 2.2 |
| $Q$ | Quadrupole moment in Equation 2.2 |
| $E$ | Intermolecular attraction energy in Equation 2.3 |
| $\Delta E_V$ | Molar energy of vaporization |
| $V$ | Liquid molar volume in Equation 2.3 |
| $V_i$ | Molar volume of component $i$ |
| $x_i$ | Mole fraction of component $i$ in Equation 2.4 |
| $\phi_i$ | Volume fraction of component $i$ |
| $E_d$ | Intermolecular attraction energy for dispersion |
| $E_p$ | Intermolecular attraction energy for polar interaction |
| $E_h$ | Intermolecular attraction energy for hydrogen bonding or other interactions |

| | |
|---|---|
| $\rho_r$ | Reduced density of fluid in Equation 2.7 |
| $\rho_{r(liquid)}$ | Reduced density of liquid at its normal boiling point in Equation 2.7 |
| $P_c$ | Critical pressure |
| $T_c$ | Critical temperature |
| $V_c$ | Critical volume |
| $\chi_a$ | Association interaction constant |
| $\chi_u$ | Dispersion interaction constant |
| $K$ | Equilibrium constant for association |
| $T_0$ | Reference temperature, 298.15 K |
| $K_0$ | Equilibrium constant for association at a reference temperature $T_0$ |
| $\Delta H_{ab} / \Delta H_a$ | Enthalpy of association |
| $\alpha$ | Association ratio |
| $\nu$ | Vibration frequency |
| $\xi$ | Number of segments in a polymer molecule |
| $N$ | Total number of sites in the lattice |
| $C_i$ | Constant of component $i$ |
| $[C]$ | Concentration |
| $A$ | Absorbance |
| $\mu$ | Binding ratio in Equation B.1 |
| $\mu_i$ | Chemical potential of component $i$ |
| $\tilde{T}$ | Characteristic reduced temperature |
| $\tilde{P}$ | Characteristic reduced pressure |

| | |
|---|---|
| $\tilde{\rho}$ | Characteristic reduced density |
| $r_i$ | Number of segments in a molecule of component $i$ |
| $S_w$ | Swelling ratio |
| $T^*$ | Characteristic temperature |
| $P^*$ | Characteristic pressure |
| $\rho^*$ | Characteristic density |
| $v_i^*$ | Characteristic segment volume of component $i$ |
| $\varepsilon_i^*$ | Characteristic segment energy of component $i$ |
| $R$ | Gas constant |
| $V_{solvent}$ | Volume of the solvent in equation 2.9 |
| $M$ | Molecular weight in Equation 2.33 |
| $\delta_i$ | Solubility parameter of component $i$ |
| $G$ | Gibbs free energy |
| $A$ | Helmholtz energy |
| $k$ | Boltzmann constant |
| $\theta_c$ | Critical incidence angle of IR beam |
| $n_i$ | Refractive index of medium $i$ |
| $\lambda$ | Wavelength of IR beam in Equation 2.12 |
| $\theta$ | Incidence angle of IR beam |
| $\varepsilon$ | Molar absorptivity in Equation 2.13 |
| $L$ | Path length of IR beam |
| $I$ | Intensity of the IR radiation |

| | |
|---|---|
| $I_0$ | Intensity of the background radiation |
| $\Delta\upsilon_{OH}$ | Hydroxyl stretching frequency shift |
| $\Delta\upsilon_{CO}$ | Carbonyl stretching frequency shift |
| $m_a / n_a$ | Correlation constants of acid |
| $k_a^b$ | Correlation constant of base |
| $Z$ | Compressibility factor |
| $m_i$ | Effective segment number of component *i* in Equation 2.19 |
| $\kappa^{AB}$ | Volume of interactions between sites A and B |
| $\varepsilon^{AB} / k$ | Association energy of interaction between site A and B |
| $v^0$ | Temperature independent molar volume |
| $u^0 / k$ | Temperature independent dispersion energy of interaction |
| $\chi_{FH}$ | Flory – Huggins interaction parameter |
| $r$ | Number of segments in a polymer chain in Equation 2.22 |
| $M_i$ | Degree of polymerization for component $i$ in Equation 2.23 |
| $\Delta G_H$ | Free energy for hydrogen bonding in Equation 2.23 |
| $K_2 / K_A / K_B$ | Equilibrium constants |
| $V_i[T, P]$ | Specific volume of component $i$ at temperature T and pressure P |
| $P$ | Polymer segment |
| $S$ | Solvent molecule |
| $\rho$ | Molar density of chain molecule |
| $k_{ij} / \eta_{ij}$ | Binary interaction parameters |
| $zq$ | Number of external contacts per molecule |

| | |
|---|---|
| $\Gamma_{00}$ | Nonrandom factor between holes |
| $N_{ij,H}$ | Total number of hydrogen bonds between a donor $i$ and an acceptor $j$ |
| $\theta_i$ | Surface (contact) fractions for component $i$ in Equation 2.39 |
| $N_i$ | Number of molecules of component $i$ |
| $\sigma$ | Symmetry number |
| $\tau$ | Flexibility parameter |
| $N_0$ | Number of holes on a lattice |
| $\hat{r}\hat{N}$ | Total number of segments (polymer and solvent) on a lattice |
| $N_q z / 2$ | Total number of non-bonded pairs |
| $\Omega_R$ | Partition function of random contribution |
| $\Omega_{complex}$ | Partition function of complex contribution |
| $Q$ | Associated lattice fluid partition function |
| $E$ | Lattice energy in Equation 3.8 |
| $V$ | Lattice volume in Equation 3.9 |
| $f_0$ | Fraction of holes in the lattice |
| $V_0$ | Volume of the dry polymer in Equation 3.27 |
| $V$ | Volume of the solution in Equation 3.27 |
| $C_A / E_A$ | Empirical constants for the acidity |
| $C_B / E_B$ | Empirical constants for the basicity |
| $\nu_0$ | Carbonyl stretching peak of the solute in the gas phase |
| $\nu_s$ | Carbonyl stretching peak of the solute in the solvent |
| $C$ | Constant in equation 4.1 |

| | |
|---|---|
| $\varepsilon$ | Dielectric constant of the solvent in equation 4.1 |
| $k$ | Constant in equation 4.1 |
| $AN$ | Gutmann acceptor number of the solvent |
| $[P...CO_2]$ | Concentration of the associated complex |
| $[P]$ | Concentration of the free polymer unit |
| $[CO_2]$ | Concentration of the free $CO_2$ |
| $\varphi_i$ | Fugacity coefficient in Equation 6.1 |
| $\lambda_i$ | Thermal conductivity of the molten salt $i$ |
| $U$ | Speed of sound in the salt |
| $V$ | Molar volume of the salt in Equation A.1 |
| $N_{\mathrm{A}}$ | Avogadro's number |
| $\gamma$ | Ratio of heat capacities $\left(C_{\mathrm{p}} / C_{\mathrm{v}}\right)$ |
| $A$ | Constant in Equation A.2 |
| $B$ | Constant in Equation A.3 |
| $M_{\mathrm{w}}$ | Molecular weight in Equation A.2 |
| $T_{\mathrm{m}}$ | Melting temperature |
| $V_{\mathrm{m}}$ | Melt molar volume |
| $n$ | Number of ions in each molecule of a molten salt |
| $\hat{V}_{\mathrm{m}}$ | Specific volume of the melt |
| $\lambda_c$ | Characteristic thermal conductivity |
| $V_c$ | Characteristic volume in chapter Appendix A |
| $T_c$ | Characteristic temperature in chapter Appendix A |

| | |
|---|---|
| $C_\eta$ | Coupling constant for viscosity |
| $C_\lambda$ | Coupling constant for thermal conductivity |
| $V_0$ | Molar volume at closest packing in Equation A.8 |
| $\sigma$ | Molecular diameter in chapter Appendix A |
| $V_s$ | Solid molar volume of salt |
| $\lambda^*_{MS}$ | Reduced thermal conductivity of the molten salt |
| $\xi$ | Reduced volume in Equation A.11 |
| $m$ | Number of components in a mixture in Equation A.12 |
| $x_i$ | Mole fraction of the $t^{th}$ component |
| $\Delta U_{mix}$ | Molar internal energy change of mixing mix ΔU |
| $\Delta G_{mix}$ | Gibbs energy of mixing |
| $[C_n mim][Tf_2N]$ | 1-n-alkyl-3-methylimidazolium bis(trifluoromethylsulfonyl)imide |
| $[C_n mim][BF_4]$ | 1-n-alkyl-3-methylimidazolium tetrafluoroborate |
| $[C_n mim][PF_6]$ | 1-n-alkyl-3-methylimidazolium hexafluorophosphate |
| $[C_n mim][TFA]$ | 1- n-alkyl -3-methylimidazolium trifluoroacetate |

**Superscripts and Subscripts**

| | |
|---|---|
| *n* | 1 to 10 in chapter 5 |
| *vdW* | van der Waals (volume) |
| *MS* | Molten Salt |
| *hs* | Hard sphere |
| *chain* | Hard sphere chain |
| *disp* | Dispersion |
| *assoc* | Association |
| *c* | Critical point |

| | |
|---|---|
| *p* | Polar |
| *r* | Reduced |
| *ab* | Acid-base |
| *res* | Residual |
| *mix* | Mixture |
| * | Characteristic |
| ˆ | Average |
| *s* | Solid |
| *T* | Total |

**Abbreviations**

| | |
|---|---|
| UCST | Upper Critical Solution Temperature |
| LCST | Lower Critical Solution Temperature |
| MP2 | Second order Møller–Plesset perturbation theory |
| SCF | Self-consistent field theory in section 2.2.2 |
| ALF | Associated lattice fluid |
| MW | Molecular Weight |
| EDA | Electron donor-acceptor complexes |
| SCF | Supercritical fluid |
| NRHB | Nonrandom Hydrogen Bonding |
| SL | Sanchez Lacombe |
| SAFT | Statistical Association Fluid Theory |
| PC – SAFT | Perturbed chain – SAFT |
| CPA | Simplified cubic plus association |
| PHSC | Perturbed hard-sphere-chain |
| MIE | Methyl isopropyl ether |

| | |
|---|---|
| PEA | poly (ethylene adipate) |
| EIE | Ethyl isopropyl ether |
| IBA | Isobutyl acetate |
| MIK | Methyl isobutyl ketone |
| PEA | poly (ethyl acrylate) |
| PE | poly (ethylene) |
| PMA | poly (methyl acrylate) |
| PMMA | poly (methyl methacrylate) |
| MMA | methyl methacrylate |
| PTFPME | poly (tetrafluoroethylene –co – perfluoromethylvinyl ether) |
| PTFE | poly (tetrafluoroethylene) |
| PVDF | poly (vinylidene fluoride) |
| PC | Poly (carbonate) |
| PS | Poly (styrene) |
| LDPE | low density polyethylene |
| HDPE | high density polyethylene |
| PBS | Poly (butylene succinate) |
| PBMA | poly (butyl methacrylate) |
| PP | poly (propylene) |
| PTFE | Polytetrafluoroethylene |
| PVAc | Poly (vinyl acetate) |
| PEG | poly (ethylene glycol) |
| PDDMA | poly (dodecyl methacrylate) |
| DDMA | dodecyl methacrylate |
| DME | dimethyl ether |

| | |
|---|---|
| PVC | poly (vinyl chloride) |
| EVA | Poly (ethylene-co-vinyl acetate) |
| PVME | Poly (vinyl methyl ether) |
| PLA | Poly (lactic acid) |
| PLGA | Poly (lactide-co-glycolide) |
| PCL | Poly (ε-caprolactone) |
| PEG | Poly (ethylene glycol) |
| CFC-22 | chlorodifluoromethane |
| PPO | poly (2,6-dimethyl phenylene oxide) |
| PEO | poly (ethylene oxide) |
| PES | poly (ether sulfone) |
| PIB | poly (iso-butene) |
| L61 | (PEO)2−(PPO)31−(PEO)2 |
| L81 | (PEO)3−(PPO)42−(PEO)3 |
| L62 | (PEO)5−(PPO)34−(PEO)5 |
| 17R2 | (PEO)15−(PPO)10−(PEO)15 |
| 17R4 | (PEO)15−(PPO)26−(PEO)15 |
| 25R2 | (PEO)22−(PPO)14−(PEO)22 |
| PA-11 | nylon polyamide-11 |
| PDMS | Poly (dimethyl siloxane) |
| PEMS | Poly (ethylmethyl siloxane) |
| PHMA | poly (hexyl methacrylate) |
| POMA | poly (octyl methacrylate) |
| PDMA | poly (decyl methacrylate) |
| PFHMA | poly (1H,1H,2H,2H-tetrahydroperfluoro hexylmethacrylate) |

| | |
|---|---|
| PFOMA | poly (1H,1H,2H,2H-tetrahydroperfluoro octylmethacrylate) |
| PFDMA | poly (1H,1H,2H,2H-tetrahydroperfluoro decyl methacrylate) |
| PBA | poly (butyl acrylate) |
| PEHA | poly (ethylhexyl acrylate) |
| PODA | poly (octadecyl acrylate) |
| PIPA | Poly (isopropyl acrylate) |
| PIDA | Poly (isodecyl acrylate) |
| PDA | Poly (n-decyl acrylate) |
| IDA | isodecyl acrylate |
| PIPMA | Poly (isopropyl mehtacrylate) |
| PPA | Poly (n-propyl acrylate) |
| IPA | isopropyl acrylate |
| IPMA | isopropyl methacrylate |
| PCHA | poly (cyclohexyl acrylate) |
| PCHMA | poly (cyclohexyl methacrylate) |
| CHA | cyclohexyl acrylate |
| CHMA | cyclohexyl methacrylate |

# SUMMARY

The phase behavior of $CO_2$ + polymer systems is of interest in polymer synthesis, flue and natural gas processing, polymer foam and nanoparticle processing, and drug delivery. Theoretical and experimental evidence suggests that $CO_2$ is able to interact with electron donating functional groups in polymers to form weak Lewis acid – base or EDA (Electron Donor Acceptor) complexes. These complexes can have a significant effect on the phase behavior of associated $CO_2$ + polymer systems. In spite of this, however, the phase equilibria of only a few associated $CO_2$ + polymer systems have been measured. Some success in modeling the phase behavior of polymer solutions has been achieved by various versions of the Statistical Association Fluid Theory (SAFT), as well as by several Lattice Models. However, many of these models incorporate two to four adjustable parameters that often depend on temperature (T), pressure (P), and/or molecular weight ($M_W$). As a result, a large amount of experimental data is required to apply these models. The goal of the present work was therefore to develop a new thermodynamic model for associating systems that would include no more than two temperature-independent adjustable parameters. The new model presented in this work is based on the Guggenheim-Huggins-Miller lattice and includes complex formation in the development of the partition function.

The EOS obtained from the resulting partition function includes two mixture parameters – the enthalpy of association or complex formation $\Delta H_a$ and a reference value of the equilibrium constant for complex formation $K_0$. Most importantly, $\Delta H_a$ can be obtained from *in situ* Attenuated Total Reflection Fourier Transform Infrared (ATR – FTIR) measurements. This work therefore demonstrates the use of ATR – FTIR spectra

to obtain molecular level information regarding the interaction of $CO_2$ and electron donating functional groups in polymers. Unlike other studies, this work uses the bending vibration of $CO_2$ to estimate the enthalpies of association ($\Delta H_a$) of $CO_2$ + polymer systems. Values of $\Delta H_a$ were directly incorporated in the new model and were found to lie between -7 and -12 kJ/mol for the systems investigated in this work. They increased (i.e. became more negative) in the order: $CO_2$ + PS-co-PMMA < $CO_2$ + PMMA <$CO_2$ + PBMA < $CO_2$ + PSF < $CO_2$ + PVAc < $CO_2$ + EVA40 < $CO_2$ + PEG.

Values of the second parameter in the new EOS ($K_0$) were obtained by fitting solubility data at one temperature. Both $\Delta H_a$ and $K_0$ were found to be temperature independent. The application of the new EOS was demonstrated by calculating the solubility (sorption) of $CO_2$ in polymers, the extent of swelling of polymers due to $CO_2$, and the solubility of polymers in $CO_2$ (cloud points). Both sorption and cloud point behavior in $CO_2$ + polymer systems could be calculated using a single value of $K_0$ for each binary system.

Ionic Liquids (ILs) can also incorporate electron donating functional groups in their structure. Evidence for the interaction of such ILs with $CO_2$ can be found in the large values of the enthalpies of absorption of $CO_2$ in these ILs. The ALF EOS was therefore extended to $CO_2$ + IL systems using the enthalpy of absorption as a measure of association ($\Delta H_a$) in these systems. $K_0$ was again treated as an adjustable parameter in the calculation of the $CO_2$ solubility in ILs. A single value of $K_0$ was sufficient to predict swelling in these systems within experimental error.

Chapter 1 of this thesis discusses the importance of $CO_2$ + polymer and $CO_2$ + IL systems, and outlines the goals of this work. Chapter 2 presents a review of experimental data and models used for such systems. Chapter 3 presents the derivation of the new EOS and its application to $CO_2$ + polymer systems. Chapter 4 describes the ATR – FTIR studies and presents results for the enthalpy of association for $CO_2$ + polymer systems. Chapter 5 describes the extension of the EOS to $CO_2$ + IL systems. Finally, in Chapter 6, major conclusions of this thesis are summarized and suggestions for future work are provided.

# CHAPTER 1: INTRODUCTION

$CO_2$ has attracted significant attention over the last few decades because of the tunability of its properties. For example, properties of $CO_2$ such as the density (and hence its solvent power) can easily be varied from gas-like to liquid-like values by slight changes in pressure. This tunability makes $CO_2$ attractive as a solvent in many applications. $CO_2$ can also be used to manipulate the physical and chemical properties of polymers in process synthesis, particle formation, drug delivery, crystallization, tissue engineering, foaming, drying, extraction, impregnation, injection molding, and lithography [27-32].

Many of the applications described above depend on sorption, cloud point, and swelling behavior of $CO_2$ + polymer systems. These phenomena are governed by microscopic intermolecular interactions, such as dispersion and association [33]. Unfortunately, because of the many physical variables and the complexity of the intermolecular forces that must be considered, experimental measurements of these phenomena are not available for all $CO_2$ + polymer systems of practical interest. It is always expensive to measure experimental data for any system at all conditions of practical interest. However, it is also expensive to use inaccurate models in the simulation and design of processes [34]. Therefore, significant effort has been devoted to derive accurate thermodynamic models to calculate phase equilibria and related properties of $CO_2$ + polymer systems. Examples of such models include versions of the Statistical Association Fluid Theory (SAFT), as well as activity coefficient models based on the Flory – Huggins theory. A good model should contain a minimum number of adjustable parameters and make use of all available molecular level information. Unfortunately, available models for polymer systems generally incorporate many adjustable parameters and fail to

account for all the intermolecular forces mentioned previously. In particular, very few models account for association between a polymer and a solvent.

It is known that Lewis acids such as $CO_2$ interact with electron donating functional groups (e.g. carbonyl, C=O) in polymers to form electron donor-acceptor (EDA) complexes. Qualitative evidence for such complexes has been provided in a number of studies [35-37]. On the other hand, quantitative information related to EDA complexes in polymer systems appears to be scarce and mostly confined to carbonyl polymers interacting with $CO_2$ [1, 35, 38]. One exception appears to be the ATR – FTIR study of Yuan and Teja [38, 41] who reported quantitative values of the enthalpy of association between $CO_2$ and polymers containing other functional groups (e.g. ether or sulphonyl). Such interactions have been noted between $CO_2$ and small molecules containing ether, alcohol, or amine groups using *ab initio* calculations by Jamroz et al. [39]. Since data for $CO_2$ + polymer systems are lacking, there is a need for methods that can obtain the specific interaction from the structure of the polymer. Therefore, the ATR-FTIR study of Yuan and Teja has been extended in this work for several polymer and copolymers, including $CO_2$ + PBMA, $CO_2$ + EVA40, and $CO_2$ + PS – co – PMMA systems. In addition, an attempt has been made to develop structure-property relationships between the strength of the interactions and the structure of the polymers and their functional groups.

The main goal of the present study was to develop a new thermodynamic model for phase equilibria and volumetric properties of associating $CO_2$ + polymer systems. The new model follows previous work on the Compressible Lattice Model (CLM) for associated solutions proposed by Ozkan and Teja [40]. This model has achieved considerable success in correlating $CO_2$ + polymer phase equilibria using two parameters that are not dependent on temperature or molecular weight. In addition, one of these parameters is directly obtained from ATR – FTIR

spectra [38, 40, 41]. The CLM model was modified by Kasturirangan and Teja who were able to correlate experimental data both at high pressure (cloud point) [42] and low pressure (sorption) [11] for different $CO_2$ + biopolymer systems. The calculated cloud points and solubilities agreed well with experiments [43]. The CLM model was extended to $CO_2$ + cosolvent + polymer systems by Yuan and Teja [41, 44]. However, the CLM model is an activity coefficient model and is not directly applicable to the calculation of volumetric properties such as swelling. Yuan and Teja therefore developed an EOS model for $CO_2$ + polymer systems [41] by combining the Flory Huggins lattice fluid partition function [45] with an association contribution of Shukhadia and Variankaval [46, 47]. They successfully correlated the solubility of $CO_2$ in polymers and the extent of swelling due to $CO_2$ over a wide range of temperature and pressure. However, in the Flory Huggins formulation, freely jointed polymer segments are arranged on the lattice via a random walk and hence multiple occupancies of one or more lattice sites are possible. The present work thus incorporates complex formation in the lattice fluid partition function of Guggenheim-Huggins-Miller that avoids this overlap and derives a new EOS containing two mixture parameters – the enthalpy of association or complex formation $\Delta H_a$ and a reference value of the equilibrium constant for complex formation $K_0$. Values of $\Delta H_a$ obtained in the ATR – FTIR studies can be directly incorporated in the new model.

In chapter 3, application of the new EOS to the calculation of $CO_2$ solubility in polymers (sorption) and the extent of swelling of polymers due to $CO_2$ is demonstrated. The new EOS is also extended to the solubility of polymers in $CO_2$ (cloud points) using the same parameters that are obtained from sorption calculations. ATR – FTIR spectroscopy results are presented in Chapter 4. Finally, the new EOS is extended to $CO_2$ + IL systems in Chapter 5, because the same electron donating functional groups also appear in the anion of ILs.

# CHAPTER 2: LITERATURE REVIEW

## 2.1 Introduction

Part of this chapter has been accepted for publication in The Journal of Supercritical Fluids.

### 2.1.1 Application of $CO_2$ in polymer processing

$CO_2$ is widely-used as a solvent and/or reactant during the synthesis of polymers, polymer particle formation, tissue engineering, polymer foaming, and polymer impregnation [27-31]. These applications often rely on the ability of $CO_2$ to manipulate sorption, cloud points, and swelling of polymer systems. In addition, mechanical properties such as the elastic modulus and creep compliance can also be controlled during processing [27, 31, 32]. Figure 2.1 summarizes some of these applications and key thermodynamic properties that influence the use of $CO_2$ in polymer processing. Many of these applications have been reviewed by Duarte et al. [30], Tomasko et al. [32], Kazarian [31], Nalawade et al. [48], Kendall et al. [28], Cooper [27], and Yeo and Kiran [29], among others. Reviews published between 2008 and 2013 are listed in Table 2.1.

### 2.1.2 Phase behavior of $CO_2$ + polymer systems

Five basic types of binary phase diagrams for polymer systems have been proposed by McHugh and Krukonis [2] and are shown in Figure 2.2; however, only Type-III or Type-IV phase diagrams are used to describe the phase behavior of $CO_2$ + polymer systems. These are shown in Figure 2.3. The solubility of $CO_2$ in a polymer (x = mole/weight fraction $CO_2$ dissolved) is generally presented in terms of lines of constant temperature on a x – P diagram, whereas the solubility of a polymer in $CO_2$ is represented in terms of lines of constant weight

fraction of polymer in a P – T diagram. The P – T projections in Figure 2.3 are often called cloud point curves and denote transitions between a homogeneous liquid phase (L) to a demixed system, such as liquid-liquid (LL) or vapor-liquid (VL) [2, 49]. The solid line with negative slope (left) in Figure 2.3 is the UCST (Upper Critical Solution Temperature) curve, while the line with initial positive slope following the negative slope (right) is the LCST (Lower Critical Solution Temperature) curve. The homogeneous region L becomes smaller and moves to higher pressures with increasing MW of the polymer, or with increasing differences in the chemical nature and size of the polymer and solvent. This new positions of the UCST and LCST curve are shown as short dashed lines for the higher MW [2]. Finally, at some point, both the UCST and LCST curves merge to give the so-called U-LCST behavior which is represented by the dashed line (top). The behavior changes (see Figure 2.5) with increasing concentration of polar cosolvent, polymer chain branching, polarity, and polydispersity, since these enhance the solvating power of $CO_2$ [2, 41].

### 2.1.3 Effect of specific interaction on phase behavior in $CO_2$ + polymer systems

Numerous studies have reported that some polymers and copolymers are soluble in $CO_2$ at high pressures and temperatures [3, 50, 51]. Often, such polymers or copolymers contain electron donating functional groups, such as –C=O. Figure 2.5 shows the cloud point curves of poly (vinyl acetate) (PVAc) and poly (methacrylate) (PMA) in $CO_2$ [3]. These two polymers have fairly similar repeat groups in the backbone except for the position of the carbonyl group. The area above the cloud point curve denotes a single phase and the area below the line represents two phases in each case. A higher cloud point pressure means the polymer is more difficult to dissolve in $CO_2$. Note that at 30 ˚C, the cloud point pressure in the $CO_2$ + PMA system (see Figure 2.5) is more than 1500 bar higher compared with that in the $CO_2$ + PVAc

system, despite the fact that the molecular weight of PVAc is four times greater. This type of lowering of the cloud point pressure can also be observed in polymers with other functional groups such as siloxane and fluorine as shown in Figure 2.6. Each of the systems showed in Figures 2.5 and 2.6 exhibits Lewis acid-base interactions between $CO_2$ and the polymer/co-polymer. It can therefore be surmised that the electron donating functional group in the polymer has a significant effect on the phase behavior in such systems. Methods to quantify specific interactions will be reviewed in the following sections.

### 2.2 Interaction in $CO_2$ + polymer systems

Interactions in $CO_2$ + polymer systems can consist of self-interactions between solvent molecules (solvent-solvent), or between polymer segments (segment-segment), as well as cross-interactions between solvent molecules and polymer segments (solvent-segment). The sum of these interactions can be expressed in term of the interchange energy ( $\omega$ ) as [52]:

$$\omega = z\left[\Gamma_{ij}(r,T) - \frac{1}{2}\left(\Gamma_{ii}(r,T) + \Gamma_{jj}(r,T)\right)\right] \tag{2.1}$$

where $z$ is the coordination number and $\Gamma_{ij}(r,T)$ is the intermolecular pair-potential energy. An approximate estimate of the attractive part of the intermolecular potential energy $\Gamma_{ij}(r,T)$ for mixtures of small molecules is given by

$$\Gamma_{ij}(r,T) \approx -\left[C_1\frac{p_i p_j}{r^6} + C_2\frac{\mu_i^2\mu_j^2}{r^6 kT} + C_3\frac{\mu_i^2 Q_j^2}{r^8 kT} + C_4\frac{\mu_j^2 Q_i^2}{r^8 kT} + C_5\frac{Q_i^2 Q_j^2}{r^{10} kT} + Spec.\ Int.\right] \tag{2.2}$$

where $p$, $\mu$, and $Q$ are the polarizability, dipole moment, and quadrupole moment, respectively, and $C_1 - C_5$ are constants. The first five terms in Equation 2.2 represent non-specific interactions in which the dominant terms are the dipole and quadrupole moments. Such interactions are inversely proportional to the temperature. Therefore, configurational alignment

of the polar moment can be disrupted by thermal energy at high temperature and polar molecules behave as non-polar molecules at high temperature. A directional specific interaction such as hydrogen bonding or Lewis acid-base complex formation is also temperature sensitive and contributes to the intermolecular pair potential energy [52]. This contribution can be of the same order of magnitude as other contribution in Equation 2.2 and has significant impact on the phase behavior of $CO_2$ + polymer and polymer + $CO_2$ + cosolvent systems.

### 2.2.1 Non-specific interactions in $CO_2$ + polymer systems

Non-specific interactions can be estimated using the Hildebrand and Scott solubility parameter [53]. This solubility parameter is related to cohesive energy density as follows

$$\delta = \sqrt{\frac{\Delta E_V}{V}} \tag{2.3}$$

where $E$, $\Delta E_V$ and $V$ are the intermolecular attraction energy, molar energy of vaporization, and liquid molar volume, respectively. The Hildebrand solubility parameter is frequently used to calculate the molar energy change of mixing

$$\Delta U_{mix} = \left(x_1 V_1 + x_2 V_2\right)\phi_1\phi_2(\delta_1 - \delta_2)^2 \tag{2.4}$$

where $V_i$, $x_i$ and $\phi_i$ are the molar volume, mole fraction, and volume fraction of component $i$, respectively. Equation 2.4 can be used to estimate the enthalpy of mixing of polymer solutions. This enthalpy is always positive for regular solutions, because all terms in Equation 2.4 are positive [41]. The Scott and Hildebrand approach does not consider polar forces or specific interactions such as hydrogen bonding. Therefore, Hansen proposed an alternative approach that considers three contributions to the attraction energy due to dispersion ($E_d$), dipole-dipole and

dipole-induced dipole forces ($E_p$), and hydrogen bonding or other association such as Lewis acid-base interactions ($E_h$) [54]. Thus:

$$E = E_d + E_p + E_h \tag{2.5}$$

and

$$\delta_T^2 = \delta_d^2 + \delta_p^2 + \delta_h^2 \tag{2.6}$$

Hansen solubility parameters are generally estimated empirically from solubility data and the total solubility parameter $\delta_T$ should be equal to the Hildebrand solubility parameter. The advantage of using Equation 2.6 is that the last term $\delta_h$ can be ignored when there are no specific interactions. Hildebrand et al. [53] suggested that Equation 2.5 is more generally applicable than Equation 2.4 or 2.6.

Giddings et al. [55] reformulated the Hildebrand approach and proposed a corresponding states theory to obtain the solubility parameter as a function of temperature and pressure for supercritical fluids. Their empirical equation for the solubility parameter ($\delta$ in $(\text{cal/cm}^3)^{0.5}$) can be expressed as

$$\delta = 1.25 P_c^{0.5} \left( \frac{\rho_r}{\rho_{r(liquid)}} \right) \tag{2.7}$$

where $\rho_r$ and $\rho_{r(liquid)}$ are the reduced density of the fluid and the reduced density of the liquid phase at its normal boiling point, respectively, and $P_c$ is the critical pressure (atm). Williams et al. [56] proposed that the solubility parameter be obtained from an EOS using

$$\delta^2 = \left( \frac{\Delta E}{V} \right) \approx \left( \frac{\partial E}{\partial V} \right) = T \left( \frac{\partial P}{\partial T} \right)_V - P \tag{2.8}$$

Using this approach, they showed that the solubility parameter of $ScCO_2$ changes from 5 to 15 $MPa^{0.5}$ between 250 K and 20 MPa to 300 K and 60 MPa [56]. In the Compressible Lattice Model (CLM) proposed by Ozkan and Teja [40], the solubility parameter is used to estimate the dispersion interaction parameter ( $\chi_u$ ) via

$$\chi_u = \frac{V_{solvent}\left(\delta_1 - \delta_2\right)^2}{RT(z-2-\alpha)} \tag{2.9}$$

where $\alpha$ is the association ratio (defined as the fraction of associated segments per polymer molecule), $V_{solvent}$ is the volume of the solvent, and $z$ is the coordination number (defined as the number of nearest neighbor in the lattice)

### 2.2.2 Specific interactions in $CO_2$ + polymer systems

Specific interactions include hydrogen bonds as well as EDA complexes between electropositive and electronegative atoms or functional groups. The strength of hydrogen bonds can vary between that of a covalent bond and that of an electrostatic intermolecular interaction – that is between 1 kJ/mol and 162 kJ/mol [41, 57, 58]. The strength of EDA complexes has been shown to lie between -4 kJ/mol and -50 kJ/mol [35, 39]. In the case of polymer systems, the strength of the interactions can be estimated using quantum calculations, molecular dynamics, or spectroscopy. These methods are discussed in the following paragraphs.

#### 2.2.2.1 Quantum calculation

*Ab initio* quantum calculations have often been employed to estimate zero-temperature interaction energies between $CO_2$ and functional groups in polymers. This is because interatomic potentials of atoms can be obtained accurately at 0 K from the ground state total energy of the corresponding electronic system for a given atomic position [59]. In quantum calculations,

gradient-corrected density function is commonly used and it provides accurate estimates of interaction energies in most cases. However, this method does not provide reliable interaction energies for the systems where the van der Waals interactions are dominant and higher-level quantum calculations are therefore necessary [60]. In higher-level quantum calculations, both the level of theory and the basis set need to be corrected with basis set superposition errors [1, 5, 60]. Kim and Kim [61] used MP2 (Second order Møller–Plesset perturbation) level theory together with two different basis sets and basis set superposition error corrections to estimate several $CO_2$ complexes. They also performed high-level quantum mechanical calculations to isolate the stabilization energy of weak hydrogen bonds from the overall binding energy. Their calculations show that the binding energy of $CO_2$ + methyl acrylate is about -3.1 kcal/mol, while it lies between 0.56 kcal/mol and 2.84 kcal/mol for $CO_2$ + acetaldehyde and between 0.80 kcal/mol and 3.84 kcal/mol for $CO_2$ + dimethyl ether complexes for different geometry with cooperative weak hydrogen bonding with α-protons. Kilic et al. [5, 60] also used MP2 level theory using two different basis sets with counterpoise (CP) corrections in their *ab initio* calculations to estimate the binding energies for the C=O…$CO_2$ complex for two different conformation (Figure 2.7 A and B). These two structural orientations of $CO_2$ with respect to the different R groups of the C=O containing molecule lead to quite different solubilities in the polymer. They have reported similar strength of interaction for ether and ester groups (Table 2.2). Note that the strength of interaction in their studies is about three times higher compared to the experimental values of Kazarian et al. [35]. Nelson and Borkman [1] performed *ab initio* calculations using SCF (Self-consistent field) and MP2 level theories to study the binding energy of $CO_2$ and polymer/small molecules with a carbonyl group. The interaction energy varies slightly with the different structures such as $C_s$ and $C_{2v}$ (Figure 2.7 C and D) in SCF level theory. Their results are shown

in Table 2.3. Note that they have preferred $C_s$ symmetry over $C_{2v}$ symmetry since it leads to higher binding energy. Jamroz et al. [39] reported the most general studies using *ab initio* calculations to estimate the energy of EDA complexes between $CO_2$ and electron donating functional groups such as carbonyl, ether, hydroxyl, solphonyl and amine in small molecules. They used parallel and perpendicular geometries, and showed that the binding energy is strongly dependent on the geometry. There are two apparent disadvantages of *ab initio* calculations -- the whole polymer cannot be modeled and finite temperature thermodynamic properties cannot be calculated directly [41]. Therefore, molecular dynamics (MD) calculations are frequently employed to study such interactions in $CO_2$ + polymer systems.

2.2.2.2 Molecular dynamics (MD)

The main disadvantage of *ab initio* quantum calculations is that only a few oligomers can be used in the calculations. Therefore, molecular dynamics simulations are often used to investigate specific interactions between $CO_2$ and solutes such as Ionic Liquids (ILs) [62] and polymers [63-65]. In MD simulation, Newton's equation of motion is integrated over time with an intermolecular force field. Saharay and Balasubramanian [64] used an empirical force field, such as the Vanderbilt ultra-soft pseudo potential, to investigate both the qualitative and quantitative aspects of specific interactions between $CO_2$ and ethanol. They reported that the strength of the EDA complex in $CO_2$ + ethanol is -11.03 kJ/mol. Yuan and Teja [41] used Optimized Potential for Liquid Simulations (OPLS) force field to study specific interactions between $CO_2$ and polymers. Their estimate of the strength of the complex in the $CO_2$ + PVAc system was -10.64 kJ/mol. It should be noted, however, that MD simulations are generally performed on a limited number of molecules. For instance, Saharay and Balasubramanian [64] used one ethanol molecule soaked in a bath of 64 $CO_2$ molecules in a periodic box to perform

their simulations, whereas Yuan and Teja [41] used one polymer molecule with 50 -100 repeat units in 100 molecules of $CO_2$ in their simulation. Therefore, it is preferable to obtain interaction energies by experiment, rather than by MD simulation or *ab initio* methods. FTIR spectroscopy is often considered to be the best technique for such purposes and it will be reviewed in the following section.

2.2.2.3 Infrared spectroscopy

Infrared (IR) radiation is an electromagnetic wave with wavenumbers (reciprocal of wavelength) between 400 $cm^{-1}$ and 4000 $cm^{-1}$. IR radiation contains sufficient energy to interact with a molecule. For instance, IR radiation that is absorbed by a molecule leads to faster rotation or more pronounced vibration of bonds of that molecule. If we treat atoms in a molecule as balls and chemical bonds between the atoms as springs, then the vibration frequency $\nu$ (in wavenumber, $cm^{-1}$) of the harmonic oscillation of a bond can be related by Hooke's law and is given by

$$\nu = \frac{1}{2\pi c}\sqrt{\frac{k}{\mu}} \tag{2.10}$$

where $\mu$, $c$, and $k$ are the reduced mass, velocity of light in a vacuum, and force constant of the spring, respectively. The reduced mass can be expressed as

$$\mu = \frac{m_1 m_2}{m_1 + m_2} \tag{2.11}$$

where $m_1$ and $m_2$ are the masses of the two atoms which form the bond. The frequency (wavenumber in IR spectroscopy) at which the bond absorbs IR radiation can be estimated from the force constant of the chemical bond and the reduced mass of the atoms shown in Equation 2.10 – 2.11. IR bands of different molecular bonds are distinctive and each individual functional

group absorbs IR radiation at a unique wavenumber. These distinguishable IR absorption bands allow the molecular structure of a chemical compound to be determined. It should also be noted that vibrations or rotations in a molecule must change the net dipole moment of the molecule in order to be IR active [66]. Therefore, polar bonds are generally IR – active and non-polar bonds in a symmetrical molecule absorb IR radiation weakly or not at all.

**Attenuated total reflection infrared spectroscopy (ATR-IR)**

In ATR – IR spectroscopy, the incident IR radiation is totally reflected back into the dense medium from the interface and hence it is also known as total internal reflection spectroscopy [66]. There are two necessary conditions that must be satisfied in order to observe total internal reflection: (1) the incident IR beam in the medium with the higher refractive index ($n_2$) must hit the surface that is in contact with the medium of lower refractive index ($n_1$) and (2) the incidence angle of the infrared radiation must be higher than the critical angle $\theta_c = \sin^{-1}\left(n_1 / n_2\right)$.

An evanescent IR beam penetrates into the sample at the interface in the time of internal reflection (see Figure 2.8). The resultant wave in the internal reflection material is formed due to the electromagnetic field created by the superposition of incident and reflective radiation. The penetration distance of the radiation into the sample is influenced by the wavelength ($\lambda$) and by optical properties such as incidence angle of the IR beam ($\theta$) and refractive indices of the sample. The short distance of penetration $d_p$ can be estimated from the following equation [66].

$$d_p = \frac{\lambda}{2\pi n_2 \sqrt{(\sin\theta)^2 - (n_1 / n_2)^2}} \tag{2.12}$$

$d_p$ is about 1 μm for a liquid or polymer sample ($n_1$ = 1.5) in contact with ZnSe ($n_2$ = 2.4) at 45° angle of incidence and at 1700 $cm^{-1}$. Transmission IR is limited by the thickness of the polymer

sample; while ATR – IR is not limited due to the shorter penetration distance. Therefore, ATR – IR spectroscopy is most frequently used in polymers studies [41, 67]. The main advantage of IR spectroscopy is that it can be used for quantitative studies using the Beer-Lambert law:

$$A = \varepsilon L[C] \tag{2.13}$$

where $A$, $\varepsilon$, $L$, and $[C]$ are the absorbance, molar absorptivity, path length, and concentration, respectively. The absorbance can be measured directly from the IR radiation via

$$A = -\log\left(I / I_0\right) \tag{2.14}$$

where $I_0$ and $I$ are the intensity of the background and the intensity of the radiation absorbed by a particular molecular group. Methods for quantifying interactions will be reviewed in the next sections.

**Direct methods to estimate specific interactions with FTIR experiments**

In this method, FTIR data are often used directly to estimate the strength of specific interactions or hydrogen bond formation [38, 68, 69]. Coleman et al. [68] estimated self-association and inter-association constant for polymer blends by fitting of FTIR data (stretching shift of carbonyl). They calculated the enthalpy of specific interaction via the van't Hoff relation. Meredith et al. [69] estimated specific interactions between $CO_2$ and small molecule by considering a reversible reaction between them. FTIR experiments were used to measure the bending mode of $CO_2$ and the data were used to estimate the equilibrium constant from the concentration of associated $CO_2$ and free $CO_2$ in the system. The enthalpy of specific interaction was then calculated via the van't Hoff relation. They have estimated the specific interaction between $CO_2$ and tributyl phosphate was obtained in this way. Recently, Dharmalingam et al. [70] estimated the equilibrium constant for alcohol + ethyl methacrylate from FTIR measurements using Nash's method [71]. They noted that a 1:1 EDA complex is formed between

the alcohol and ethyl methacrylate. However, this approach has not been applied to $CO_2$ + polymer systems.

**Indirect Method to estimate specific interactions with FTIR experiments**

In this method, calorimetric and FTIR results are used to obtain a correlation between the specific interaction and the stretching frequency shift for some systems. Drago and Purcell [72, 73] reported that the hydrogen-bonding enthalpy is linearly related to the OH stretching frequency shift ($\Delta\upsilon_{OH}$) in mixtures containing hydrogen-bonding acids and bases. The general form of the relationship was expressed as

$$-\Delta H_{ab} = m_a \Delta\upsilon_{OH} + n_a \tag{2.15}$$

where $\Delta H_{ab}$ is the enthalpy of the acid-base interaction, and $m_a$ and $n_a$ are two correlation constants which depend on the properties of the acid. However, when a specific base $b$ is mixed with different hydrogen-bonding acids, then Equation 2.15 becomes

$$-\Delta H_{ab} = k_a^b \Delta\upsilon_{OH} \tag{2.16}$$

where $k_a^b$ is a constant. Fowkes et al. [74] obtained a similar correlation for changes in the stretching frequency of the carbonyl group ($\Delta\upsilon_{CO}$) in ethyl acetate mixtures in the presence of various acids. Their expression is given by

$$\Delta H_{ab} = 0.236 \frac{kcal}{mol\ cm^{-1}} \Delta\upsilon_{CO} \tag{2.17}$$

They estimated the enthalpy of acid-base interaction between PMMA and a number of chlorinated hydrocarbons using Equation 2.17. Their approach was adopted by a number of authors to study polymer systems [35, 38, 75]. However, the number of $CO_2$ + polymer systems studied was limited.

## 2.3 Thermodynamic models for $CO_2$ + polymer systems

There are three classes of models commonly used for $CO_2$ + polymer systems: (1) cubic EOS models, (2) perturbation models and (3) models based on the Lattice Fluid (LF) theory [48].

### 2.3.1 Cubic EOS models

Cubic equations of state (EOS) are widely used because of their simplicity and availability in process simulation software. Many of these models, including the van der Waals (vdW) equation, the Soave-Redlich-Kwong-Soave (SRK) equation, and the Peng-Robinson (PR) equation, have achieved some success in interpreting the behavior of specific $CO_2$ + polymer systems [48, 76]. More success has been realized with the Sako-Wu-Prausnitz (SWP) model which is based on the modified van der Waals partition function for chain molecules [77]. As is well-known, the SRK and PR equations incorporate two characteristic pure component parameters ($a$ and $b$), and these are commonly estimated from critical point ($P_c$ or $V_c$ and $T_c$) and vapor pressure data of the substance of interest. The SWP equation takes account of an additional pure component parameter *c*, which is the number of external degrees of freedom of the molecule and accounts for the density dependence of the rotation and vibration of large molecules. When $c$ = 1, the SWP equation turns to the RKS EOS, although c > 1 for large molecules. Finally, classical van der Waals mixing rules are largely used to extend the SRK, PR, and SWP EOS to polymer systems [48, 77-79] and these have proved sufficient for specific $CO_2$ + polymer systems. The SWP EOS, specially, has been used successfully to describe high pressure phase equilibria in the ethylene – polyethylene system and Chen et al. extended this model to calculate the solubility of gases in polymers [79]. However, calculated solubilities were generally not satisfactory for small gases in molten and semi-crystalline polymers [79].

A major drawback of using cubic EOS for polymer systems is that it requires critical point and vapor pressure data to obtain pure component constants. Since this type of information is not often available for polymers, *PVT* data are frequently used to estimate EOS constants [80-83]. Often, these constants must be adjusted by employing binary phase equilibrium data in their estimation [33]. Alternatively, the critical points and acentric factors of some polymers may be calculated by extrapolating vapor pressure and/or *PVT* data for homologous series of substances [78]. Group contribution methods have also been proposed for calculating EOS constants for polymers [84]. A promising method proposed by Ji [76] uses the molecular volume of polymer segments to obtain EOS constants, thus avoiding ambiguities associated with polymer molecular weight as well as polydispersity. None of these methods, however, provide a unique set of polymer characteristic parameters for use with all cubic EOS.

A second drawback of cubic EOS models for polymer systems is the need to incorporate temperature-dependent binary interaction parameters in the calculations [80-82]. This requires extensive data sets and restricts the predictive capability of the models. Nevertheless, cubic EOS models such as SWP remain widely-popular due to their simplicity.

### 2.3.2 Perturbation Models

There are three types of perturbation models for associating polymer systems, such as (i) the Simplified Cubic Plus Association (CPA) model [85], (ii) the Perturbed Hard-Sphere-Chain (PHSC) model [86], and (iii) the Statistical Association Fluid Theory (SAFT) [87] model. The CPA model [88] is consist of two terms related to physical and chemical interactions. The physical contribution is obtained from the SRK EOS [89] and the chemical contribution is obtained from Wertheim's theory of hydrogen bonding [90]. Kontogeorgis et al. [85] extended this approach to evaluate vapor – liquid equilibria (VLE) for different solvent +

polymer/biopolymer systems and this model has already been tested successfully for the non-polymeric hydrogen-bonding systems such as hydrocarbon/water systems [91]. Additional studies are discussed in the following sections.

The Perturbed Hard-Sphere-Chain (PHSC) Theory proposed by Song et al. [86] comprises a van der Waals type perturbation term along with the reference hard sphere chain EOS proposed by Chiew [92]. The PHSC equation is suitable for $CO_2$ + polymer and non-associating + polymer systems [93] but has been superseded some extent by SAFT-based models.

The most popular and successful perturbation model is based on the Statistical Associated Fluid Theory (SAFT) and incorporates four contributions [94] to the residual Helmholtz energy: short range (or hard-sphere) repulsions, long- range dispersion, chemically bonded aggregation and chain formation, and association between different molecules or chain segments. The SAFT equation can be expressed in terms of the compressibility *Z* as follows:

$$Z = \frac{P}{\rho RT} = 1 + Z^{hs} + Z^{chain} + Z^{disp} + Z^{assoc} \tag{2.18}$$

Several versions of this model are available in the literature, depending on the type of expression used for the individual contributions, and some of these are listed in Table 2.4. All SAFT models incorporate three characteristic parameters for pure non-associating substances ($m$, $v^{00}$, *and* $u^0$) and two additional constants ($\varepsilon^{AB}/k$ and $\kappa^{AB}$) for associating substances. Also, application to mixtures requires cross-interaction parameters that incorporate binary interaction parameters as follows:

$$m_{ij} = \frac{m_i + m_j}{2} \tag{2.19}$$

$$u_{ij} = \left(u_{ii} u_{jj}\right)^{1/2} (1 - k_{ij}) \tag{2.20}$$

$$v_{ij}^{0} = \left[ \frac{1}{2} \left[ \left( v_i^0 \right)^{1/3} + \left( v_j^0 \right)^{1/3} \right] \right]^3 \tag{2.21}$$

An advantage of SAFT type molecular models is that pure component parameters have physical meaning, thus facilitating theory-based improvements to individual contributions. This type of extension is not feasible for empirically derived cubic EOS [95]. Therefore, SAFT models are widely used in phase equilibrium calculations for SCFs and polymer systems. However, the SAFT EOS is quite complex, and a large extent of experimental information is necessary to obtain self and cross association parameters. Finally, binary interaction parameters in the equation are often temperature and/or molecular-weight dependent [3, 84, 94, 96].

Pure component parameters in all versions of SAFT can be estimated by regression of experimental vapor pressure and liquid density data [94, 97], even though this can lead to poor vapor pressure predictions for self-associating components [98]. In addition, other approaches have also been employed to estimate polymer parameters. Arce and Aznar proposed the use of experimental or estimated (via group contributions) *PVT* data for polymers to estimate the characteristic parameters of the PC – SAFT EOS [80-82]. *PVT* data for pure polymers and binary phase equilibrium data of $CO_2$ + polymer systems have been used to obtain polymer characteristic parameters of the chain-referenced perturbed hard-sphere-chain (CR-PHSC) [99], SAFT [100], PC – SAFT [50, 100], and simplified PC – SAFT EOS [95]. Stoychev et al. have shown that these pure component parameters do not vary when $CO_2$ is replaced by another solvent [50]. However, Kouskoumvekaki et al. have demonstrated that the use of different sets of binary phase equilibrium data in the regression yields quite different polymer parameters [101]. To overcome these limitations, they used an extrapolation method to estimate unique pure component parameters from *PVT*, vapor pressure and liquid density data of the corresponding monomers. Pure component parameters can also be determined by extrapolating data for

homologous series, as demonstrated in the case of VR – SAFT EOS for LDPE [102]. Finally, it should be noted that most versions of the SAFT equation require the use of temperature dependent binary interaction parameters to describe binary and multicomponent phase equilibria in polymer systems [80-82, 103-105]. In addition, interaction parameters also appear to be the function of MW and/or copolymer composition [50, 105]. This could be due to the MW dependence of pure component data (density, vapor pressures) used to estimate the characteristic parameters of the EOS. Also, characteristic parameters for polymers are sometimes extrapolated from the corresponding homopolymers and may not consider the entanglement, self-interaction, or shielding effects in polymers of different MW [106].

### 2.3.3 Lattice Models

In the lattice theory, polymer segments are distributed on adjacent sites on a lattice, and the remaining sites are assigned to solvent molecules. The number of ways in which this can be arranged then provides an expression for the entropy of mixing, to which is added an empirical contribution for enthalpy of mixing. In some lattice models, holes are introduced to account for the compressibility of the lattice as well as to make the lattice volume temperature dependent. Preferential association between the solvent and polymer segments can also be considered by restricting the sites available to some solvent molecules.

#### 2.3.3.1 Flory-Huggins type models

The most widely used and popular lattice model is that due to Flory and Huggins (FH) which considers a polymer to be a chain of connected segments, with each segment occupying one site on a lattice. Solvent molecules are treated as single segments and distributed randomly on the lattice. This leads to:

$$\frac{\Delta G_{mix}}{NRT} = \phi_A \ln \phi_A + \frac{\phi_B}{r} \ln \phi_B + \phi_A \phi_B \chi_{FH} \tag{2.22}$$

where $N$ is the total number lattice sites, $\chi_{FH}$ is the Flory – Huggins interaction parameter, $r$ is the number of segments in a polymer chain, and $\phi$ is the volume fraction. Although this model is often used to describe the phase behavior of polymer solutions using an adjustable parameter $\chi_{FH}$, the model does not account many important non – combinatorial contributions [107]. Especially, the specific interactions such as Lewis acid – base interactions are not considered, and there is no volume change upon mixing. Coleman and Painter [108-110] is therefore modified the FH model by adding a hydrogen bonding contribution as shown below

$$\frac{\Delta G_{mix}}{RT} = \frac{\phi_A}{M_A} \ln \phi_A + \frac{\phi_B}{M_B} \ln \phi_B + \phi_A \phi_B \chi_{FH} + \frac{\Delta G_H}{RT} \tag{2.23}$$

where $M_A$ and $M_B$ represents the degree of polymerization for component $A$ and $B$, respectively and $\Delta G_H$ represents the free energy for hydrogen bonding. The third term now signifies the enthalpic contribution due to physical interactions and can be obtained from regular solution theory. The final term that describes the free energy contribution due to hydrogen bonding and is estimated from the knowledge of self-association of segments. The polymer solution is assumed to consist of free segments/monomers ($B_1$), dimers ($B_2$) and multimers ($B_m$) that participate in the following reactions:

$$\begin{aligned} B_1 + B_1 &\xrightleftharpoons{K_2} B_2 \\ B_m + B_1 &\xrightleftharpoons{K_B} B_{m+1} \end{aligned} \tag{2.24}$$

In addition, there is cross-association between different molecules or segments:

$$B_m + A \xrightleftharpoons{K_A} B_m A \tag{2.25}$$

These three reactions can be characterized by three equilibrium constants $K_2$, $K_A$, and $K_B$. In the work of Coleman and coworkers [109], $K_2$ (= $K_B$ ) and $K_A$ are estimated using FTIR spectroscopy. The measured values of these equilibrium constants are then used to obtain $\Delta G_H$ and hence the phase behavior of the polymer solutions. Coleman et al. [109-111] used this model to phase equilibria of several hydrogen bonded polymer blends. However, the model did not work satisfactorily for blends of poly(acrylate), poly(acetate), or poly(lactones) with poly(4-vinylphenol) [111], which was attributed to uncertainty in measuring equilibrium constants from FTIR experiments. It should be noted that the Coleman model does not consider compressibility (free volume) effects and therefore is not suitable for $CO_2$ + polymer systems. Ozkan and Teja [40] is therefore modified this approach in their Compressible Lattice Model (CLM).

2.3.3.2 Compressible Lattice Model (CLM)

The Compressible Lattice Model (CLM) is based on the reformulation of the FH model that consider complex formation explicitly [46, 47]. The polymer solution is expected to consist of polymer – solvent complexes, unassociated solvent molecules and unassociated polymer molecules, with polymer – solvent complexes preferentially restricted to specific sites on the lattice. The Gibbs energy of this system is given by

$$\frac{\Delta G_{mix}}{NRT} = \alpha\phi_2\chi_a + \phi_2(\phi_1 - \alpha\phi_2)(z-2-\alpha)\chi_u + \frac{\phi_2}{\xi}\ln\phi_2 + \left(\frac{\phi_1 - \alpha\phi_2}{1+\alpha}\right)\ln\left(\phi_1 - \alpha\phi_2\right) \\ -\phi_1\ln\left(\frac{\phi_1}{\phi_1 - \alpha\phi_2}\right) + \alpha\phi_2\ln\left(\frac{\alpha\phi_2}{\phi_1 - \alpha\phi_2}\right) + \phi_2\left(1-\alpha\right)\ln\left(1-\alpha\right) + \alpha\phi_2\ln\alpha \tag{2.26}$$

where $\chi_a$ is the interaction parameter for association, $\chi_u$ is the interaction parameter for dispersion, $z$ (=10) is the coordination number, $\xi$ is the number of segments, $\alpha$ is the association ratio (defined as the fraction of associated segments per polymer molecule), $N$ is the

total number of sites in the lattice, $\phi_1$ is the volume fraction of the solvent, and $\phi_2$ is the volume fractions of the solute (polymer). The above expression includes enthalpic as well as entropic contributions. There are four characteristic quantities in the model, such as $\chi_a$, $\chi_u$, $\alpha$, and $\xi$. The interaction parameter for dispersion $\chi_u$ can be calculated from the solubility parameters for the solvent ($\delta_1$) and the solute ($\delta_2$) and the relation is mentioned in Equation 2.9. The segments number $\xi$ is expressed by:

$$\xi = \frac{V_2[T,P]}{V_1[T,P]} \tag{2.27}$$

where $V_2[T,P]$ represents the specific volume of solute (polymer) whereas $V_1[T,P]$ represents the specific volume of solvent ($CO_2$) at the temperature *T* and pressure *P* of interest. Note that $\xi$ varies with *T* and *P* in the CLM model, unlike the $\xi$ in Flory-Huggins type models where it is a constant equal to the ratio of liquid molar volumes at ambient conditions. The association interaction parameter $\chi_a$ is related to the enthalpy of association $\Delta H_a$ of the complex formation between a polymer segment $P$ and a solvent molecule $S$ ($P + S \Leftrightarrow PS$) through the following relation:

$$\chi_a = \frac{\Delta H_a}{RT} \tag{2.28}$$

and thereby related to the equilibrium constant *K* of the complex-forming reaction by:

$$\ln \frac{K}{K_0} = -\frac{\Delta H_a}{R}\left(\frac{1}{T} - \frac{1}{T_0}\right) = \chi_a\left(1 - \frac{T}{T_0}\right) \tag{2.29}$$

Here $K_0$ represents the equilibrium constant for association at a reference temperature (say, 298.15 K) and $\Delta H_a$ is assumed to be independent of temperature. In turn, the equilibrium constant for the association $K$ is related to the association ratio $\alpha$ as follows

$$\alpha = \frac{(1+K) - \sqrt{(1+K)^2 - 4\phi_1\phi_2 K(1+K)}}{2\phi_2(1+K)} \tag{2.30}$$

Here, $\alpha$ can now be substituted by expressions containing $K_0$ and $\Delta H_a$ in the model. Therefore, $K_0$ and $\Delta H_a$ are the only binary interaction parameters in the model. Ozkan and Teja showed that the CLM model [40] is capable to correlate many $CO_2$ + polymer phase equilibria using two parameters that are independent of temperature or molecular weight. In addition, they have demonstrated that one of the parameters can be estimated from FTIR measurements [38, 40, 41]. One limitation of the model was that phase equilibria at low-pressures (sorption) could not be correlated simultaneously with cloud points at high pressures using the same set of binary interaction parameters. Kasturirangan and Teja [42] were then able to overcome this limitation by redefining the segment number as follows

$$\xi = \frac{V_2[T,P] - 1.2V_2^{vdw}}{V_1[T,P] - V_1^{vdw}} \tag{2.31}$$

The superscript *vdW* denotes the van der Waals (volume). The modified CLM model was used to correlate cloud point [42] sorption [11] and $T_g$ [100] behavior of several polymer + $CO_2$ systems using the same binary interaction parameters. Yuan and Teja extended the modified CLM model to $CO_2$ + cosolvent + polymer systems successfully [41, 44].

In spite of the success of Gibbs energy models such as the modified CLM model, these models suffer from the shortcoming that they cannot be used directly to determine volumetric properties such as swelling. EOS models are well suited for this purpose and are discussed below.

2.3.3.3 Lattice fluid EOS models

The Sanchez – Lacombe (SL) EOS is probably the most popular Lattice Fluid EOS models. This EOS can be derived from the Guggenheim-Huggins-Miller (GHM) lattice fluid partition function after the introduction of holes into the lattice. This account for the compressibility of the lattice or the free volume into the EOS [45, 112] and leads to:

$$\tilde{\rho}^2 + \tilde{P} + \tilde{T}\left[\ln(1-\tilde{\rho}) + (1-\frac{1}{r})\tilde{\rho}\right] = 0 \tag{2.32}$$

where, $\tilde{T}$, $\tilde{P}$, $\tilde{\rho}$, and $r$ represent the reduced temperature, pressure, density, and average segment number per molecule, respectively. These reduced characteristic parameters can be expressed by

$$\begin{aligned} \tilde{\rho} &= \frac{\rho}{\rho^*} = \frac{\rho r v^*}{M} \\ P &= \frac{P}{P^*} = \frac{P v^*}{\varepsilon^*} \\ \tilde{T} &= \frac{T}{T^*} = \frac{TR}{\varepsilon^*} \end{aligned} \tag{2.33}$$

where $T^*$, $P^*$, $\rho^*$, $rv^*$, and $\varepsilon^*$ are the characteristic temperature, pressure, density, closed pack molar volume, interaction energy in each mer, respectively and $M$ represnts the molecular weight. The equation can be extended to mixtures using the following mixing rules:

$$\begin{aligned} T^*_{mix} &= \frac{\varepsilon^*_{mix}}{R} \\ \varepsilon^*_{mix} &= \frac{\sum_i \sum_j \phi_i \phi_j \varepsilon^*_{ij} v^*_{ij}}{v^*_{mix}} \\ v^*_{mix} &= \sum_i \sum_j \phi_i \phi_j v^*_{ij} \\ \frac{1}{\hat{r}} &= \sum_i \left(\frac{\phi_i}{r_i}\right) \end{aligned} \tag{2.34}$$

where $\phi_i$ and $\phi_j$ are the volume fraction of component $i$ and $j$ respectively, $\hat{r}$ is the average segment number, and cross terms are expressed by the following equations

$$\varepsilon_{ij}^{*} = (\varepsilon_{ii}^{*}\varepsilon_{jj}^{*})^{1/2}(1-k_{ij})$$
$$v_{ij}^{*} = \frac{1}{2}(v_{ii}^{*}+v_{jj}^{*})(1-\eta_{ij}) \tag{2.35}$$

Here $k_{ij}$ and $\eta_{ij}$ are binary interaction parameters. In most cases $\eta_{ij}$ is set equal to zero [100, 113], but $k_{ij}$ is temperature dependent. The SL EOS has been widely used for investigating the phase behavior in associating systems, although it does not explicitly consider specific interactions per se [45, 100, 112, 113].

Panayiotou et al. [114, 115] proposed a Nonrandom Hydrogen Bonding (NRHB) lattice theory by incorporating the combinatorial term from the generalized Staverman expression [116], with nonrandom corrections from Guggenheim's quasi-chemical theory [117] and the hydrogen bonding contribution of Panayiotou and Sanchez [118, 119]. The model was then extended to mixtures [115] using the following expression:

$$\tilde{P}+\tilde{T}\left[\ln(1-\tilde{\rho})-\tilde{\rho}\left(\sum_{i=1}\varphi_i\frac{l_i}{r_i}-v_H\right)-\frac{z}{2}\ln\left(1-\tilde{\rho}+\frac{q}{r}\tilde{\rho}\right)+\frac{z}{2}\ln\Gamma_{00}\right]=0 \tag{2.36}$$

where $\varphi_i$ is the segment fraction, $zq$ is the number of external contacts per molecule, $\Gamma_{00}$ is the nonrandom factor between holes, $r$ is the segment number per molecule. $q$ can be obtained from UNIFAC group contributions [114]. The parameter $l_i$ can be estimated as follows:

$$l_i = \frac{z}{2}(r_i-q_i)-(r_i-1) \tag{2.37}$$

where $l_i$ is equal to zero for SL and ALF EOS. $v_H$ is the average number of hydrogen bonds per segment that can be expressed as

$$v_H = \sum_i \sum_j \frac{N_{ij,H}}{rN} \tag{2.38}$$

where $N_{ij,H}$ represents the total number of hydrogen bonds between a donor of type $i$ and an acceptor of type $j$, and $N$ is the total number of molecules in the system. Mixing rules are similar for corresponding parameters in the SL, ALF, and NRHB EOS, the exception being the mixing rule for the characteristic energy parameter in the NRHB EOS which is expressed by:

$$\begin{aligned} \varepsilon^* &= \sum_i \sum_j \theta_i \theta_j \varepsilon_{ij}^* \\ \varepsilon_{ij}^* &= (1-k_{ij})\sqrt{(\varepsilon_i^* \varepsilon_j^*)} \end{aligned} \tag{2.39}$$

where, $\theta_i$ and $\theta_j$ are surface (contact) fractions for component $i$ and $j$, respectively, and $k_{ij}$ refers to a temperature dependent binary interaction parameter. The Nonrandom Hydrogen Bonding (NRHB) lattice theory accounts for strong interactions explicitly between a solvent and a polymer and has found substantial success in describing phase equilibrium behavior of solvent + polymer/organic liquid systems [8, 114, 115, 120]. Unfortunately, three lattice fluid scaling parameters, as well as a shape factor, are necessary to apply this model for non – associating systems. Also, there are three additional hydrogen bonding pure component parameters for associating systems, along with a temperature dependent binary interaction parameter.

As in the case of other EOS models, the main disadvantage of lattice fluid EOS models is that characteristic parameters for polymers must often be obtained by fitting experimental phase equilibrium data for mixtures. The physical meaning of polymer characteristic parameters is then lost somewhat. In addition, mixing rules incorporate more adjustable (binary) parameters in the

mixture calculations. Successes and limitations of these models will be discussed further in the following sections

## 2.4 Application of thermodynamic models

### 2.4.1 Solubility of $CO_2$ in polymers

Table 2.5 includes recent studies (2000-2013) of $CO_2$ sorption in different polymers together with the model applied to correlate the data. A comparative study of the performance of several models (PR, SL, and PC-SAFT) has been presented by Arce and Aznar, who correlated the solubility of $CO_2$ in polymers and polymer blends [80, 121]. They concluded that the PR EOS calculations require a binary interaction parameter that is a strong function of temperature and MW, while the binary parameters required in the PC – SAFT and SL EOS were only weakly dependent on temperature. Shin et al. [33] also used the PR and SAFT models to correlate the solubility of $CO_2$ in several polymers (HPDE, PS, PVAc, and PBMA) and suggested that a combination of the SAFT association contribution and the PR attraction/repulsion contributions led to substantial improvement in the correlation. Weiron [76] extended the SRK EOS to interpret *PVT* data and phase behavior of polymer melts. The motivation of this study, however, was on the characterization of polymer melts focusing on polymer segments instead of polymer molecules, thereby avoiding the problem of molecular weight and its distribution on the calculations.

Table 2.6 includes recent modeling studies of the swelling behavior of $CO_2$ + polymer mixtures. In general, SAFT-based models performed better in correlating the swelling behavior of amorphous polymers, while this is not true in the case of glassy polymers [122]. The latter may possibly be due to the assumption made in the calculations that gas molecules absorb only

in the amorphous regions of a polymer. This is a poor assumption for small gas molecules such as $H_2$ [102]. Nonetheless its effect on larger molecules such as $CO_2$ is not clear.

The SL EOS was found to work satisfactorily for estimating the swelling behavior of non-associating polymer systems such as $CO_2$+PS, but poorly for associating polymer systems such as $CO_2$+PVAc system in which there is evidence for association between $CO_2$ and the carbonyl group of PVAc [7, 12, 123, 124]. Hossain et al. [6] showed that the ALF EOS performed better compare to the SL EOS in correlating the swelling of several associating polymers by $CO_2$. As noted in chapter 3, the ALF equation requires two binary parameters ($\Delta H_a$ and $K_0$) to correlate both phase equilibria and volumetric properties of $CO_2$ + polymer mixtures. A typical calculation for $CO_2$ solubility in PVAc, and the extent of swelling of PVAc due to $CO_2$, using the ALF equation with $K_0$ = 0.10 and $\Delta H_a$ = - 9.3 kJ mol$^{-1}$ is illustrated in Figure 2.9. The lines represent calculations using the ALF model [6] and the points represent the experimental measurements [7] in the figure. Note that the value of $\Delta H_a$ was estimated from spectroscopic measurements.

Pantoula et al. [8, 120] were able to correlate the extent of swelling of PS and PMMA due to $CO_2$ using the NRHB model considering the non-equilibrium character of the glassy state. Gutiérrez et al. [125] calculated the solubility of $CO_2$ + PS and Limonene + PS systems via the SL EOS with one temperature dependent binary interaction parameter. They were able to predict the phase boundaries of the $CO_2$ + Limonene + PS ternary system without any additional parameters. Aionicesei et al. [126] applied both the SL and SAFT EOS to correlate the solubility of $CO_2$ in solid and molten PEG. They showed that the SAFT EOS performed better compare to the SL EOS for molten PEG + $CO_2$ mixtures, which is consistent with what has been suggested by others [79].

Recent studies of $CO_2$ + cosolvent + polymer systems are listed in Table 2.7. Galia et al. [127] used the SL EOS to investigate the solubility of $CO_2$ in $CO_2$ + VDF + PVDF. However, it is difficult to draw general conclusions from their work due to the significant scatter that can be observed in the data that were used in their calculations. The phase behavior of several $CO_2$ + cosolvent + polymer systems has been investigated using the PHSC and SL EOS by Favari et al. [128] and Lotfollahi et al. [129]. They concluded that both the PHSC and SL EOS were suitable for correlating the transition of LCST to UCST behavior with pressure [129], but expressed a preference for the SL EOS because of its simplicity. It should be noted that both models made use of temperature dependent binary interaction parameters to correlate data.

### 2.4.2 Solubility of polymers in $CO_2$

Models used to correlate the cloud point behavior of binary and multicomponent $CO_2$ + polymer systems are listed in Table 2.8 and Table 2.9. Byun et al. [51, 130, 131] used PR EOS to study the LLE behavior of $CO_2$ + polymer systems as well as the influence of cosolvent on polymer miscibility in these systems. The PR EOS was shown to interpret successfully the transition of LCST to U-LCST and U-LCST to UCST upon increasing the concentration of the cosolvent. However, two temperature dependent binary interaction parameters were necessary to correlate the binary cloud point behavior of the systems. Moreover, agreement was qualitative in the mixture critical region. Similar conclusions have been drawn by a number of authors [49, 81, 84, 132]. Arce and Aznar [121] showed that the correlation of both the UCST and LCST also be governed by on the molecular weight. Stoychev et al. [50] study the cloud point behavior of $CO_2$ + PEO, $CO_2$ + PPO, and $CO_2$ + block copolymer (PEO-PPO-PEO or Pluronics L/R) using the PC – SAFT EOS. This model successfully describes the cloud point behavior as a function of MW (cloud point pressure increases with MW), but requires one temperature independent

interaction parameter for each binary system. Nevertheless, the agreement was only qualitative for some systems. In addition, the binary parameter was dependent on structure of the copolymer. Similar results have been showed by Walker et al. [133] who investigated the miscibility behavior of PDMS/PEMS blends in the presence of high pressure $CO_2$. The miscibility behavior is governed by competing effects of hydrostatic pressure and $CO_2$ plasticization. The UCST type cloud point curve of this blend exhibit a negative change in volume upon mixing so that the miscibility of this blend increases (and cloud point temperature decreases) with increasing hydrostatic pressure. However, in the presence of high-pressure $CO_2$, substantial swelling occurs in both homopolymers and miscibility decreases. Walker et al. [133] have successfully captured both affects using the SL EOS, although agreement with experiment was unsatisfactory in the PEMS rich phase. In addition, their binary interaction parameter is a function of both temperature and pressure. Becker et al. [134] successfully correlated cloud point curves using the PC-SAFT EOS, although three binary parameters were necessary in their calculations. However, these parameters are not a function of temperature, pressure or polymer molecular weight.

Haruki et al. [135, 136] studied the phase behavior of binary and ternary systems involving PE with using the SL EOS with one temperature dependent binary interaction parameter. They infer that phase separation pressure increases with MW and temperature, which is consistent with the investigation of Gwon et al. [83]. The SL EOS also was capable to predict the upper critical solution pressure, except at high weight fractions of PE.

Several authors have used lattice models to describe the cloud point behavior of $CO_2$ + polymer and $CO_2$ + cosolvent + polymer systems. For example, Kasturirangan and Teja used the modified CLM model to interpret the experimental cloud point data [42] for biopolymer + $CO_2$

systems. The model was then extended to $CO_2$ + cosolvent + polymer systems by Yuan and Teja [44] and its performance was found to be comparable to that of the PC – SAFT EOS [51]. In addition, the two binary interaction parameters used in the calculations were found to be independent of temperature. Moreover, one of the parameters could be obtained from FTIR measurements.

### 2.4.3 Perspectives and future directions

(i) Since there is a scarcity of experimental data on sorption, swelling, and cloud point behavior of $CO_2$ + polymer systems, thermodynamic models have a vital role to play in process calculations.

(ii) Industry continues to adopt simple models based on cubic equations of state such as the SWP EOS. However, complex formation must frequently be taken into account in $CO_2$ + polymer systems, and it is not clear whether empirical modifications that are necessary to use cubic EOS models for $CO_2$ + polymer systems offer predictive capabilities.

(iii) Molecular models, such as the several versions of SAFT are ideally suited to take into account all types of intermolecular contributions. PC – SAFT is the most popular molecular model among the all SAFT versions and is often used in process calculations. However, the SAFT model is quite complex and requires a large amount of experimental information to estimate pure polymer and mixture parameters.

**(iv)** Lattice fluid models provide a practical compromise between cubic EOS and SAFT approaches. Models such as the SL and ALF EOS have demonstrated their versatility in correlating different types of polymer phase equilibria using a minimum number of binary interaction parameters. In addition, because of their fundamental basis, it has proved possible to estimate one or more binary parameters from independent

(spectroscopic) measurements. However, only a limited number of these measurements have been reported on $CO_2$ + polymer systems. Additional work on these, as well as NMR measurements and quantum calculations, to obtain EOS parameters is likely to prove useful.

### 2.5 $CO_2$ + Ionic liquid (IL) systems

$CO_2$ possesses relatively high solubility in ILs [18], whereas the solubilities of ILs in $CO_2$ are immeasurably low [137]. As a consequence, ILs are promising solvents for carbon dioxide capture from flue gases, and for separation of organic solutes using supercritical carbon dioxide ($ScCO_2$). Brennecke and coworkers have reported that organic solutes can be extracted from an IL using supercritical $CO_2$ without cross contamination [21, 138, 139]. The high pressure solubility behavior of $CO_2$ + IL systems is therefore of considerable practical interest. This behavior is strongly influenced by Lewis acid-base interactions between $CO_2$ and the anion of ILs [14, 16-19, 21, 140-142].

Several authors have used the classical Peng-Robinson (PR) [143-145] and Redlich–Kwong (RK) EOS [18, 146, 147] to correlate IL + $CO_2$ phase behavior. However, in order to obtain agreement between calculated and experimental values, they included up to four binary temperature-dependent interaction parameters in the models, which limits their predictive power. In addition, the approach did not consider the structure of the ILs or association effects explicitly [148]. Other authors have used the UNIQUAC and UNIFAC activity coefficient models [149-152] for IL + $CO_2$/alkane phase behavior. However, the activity coefficient models require a large amount of experimental data since group interaction parameters are temperature dependent. In addition, volume and surface parameters for ILs are also needed in the calculations. Karakastani et al. used the tPC-SAFT equation to correlate $CO_2$ solubility in imidazolium based

ILs. Although this approach proved successful in describing the phase behavior of associating $CO_2$+ILs [153], the tPC-SAFT model is complex and requires a large number of physical and cross-association parameters. Therefore, it is desired to develop a thermodynamic model for $CO_2$ + IL systems with lower number of physically meaningful parameters that considered association explicitly.

## 2.6 Summary

In summary, molecular models such as the SAFT EOS are useful for calculating the properties of complex systems because they take into account many types of intermolecular contributions. The PC – SAFT EOS is the most commonly used version of the SAFT model in process simulations since this model is capable of interpreting phase behavior of non-associating mixtures using temperature independent binary parameters. However, all versions of the SAFT EOS are complex and require significant amount of experimental information to obtain pure and mixture parameters. On the other hand, lattice models offer a practical compromise between cubic EOS and SAFT approaches. However, in most cases lattice models require two temperature and/or molecular weight (Mw) dependent mixture parameters to correlate experiment data over a range of temperatures, pressures, and molecular weights of the polymer. The CLM model appears to be a promising model for calculating phase equilibria of associating $CO_2$ + polymer systems because interaction parameters in this model can be obtained from independent measurements such as FTIR spectra. However, the CLM model is an activity coefficient model and is incapable of calculating volumetric properties such as swelling. Consequently, an EOS model which considers specific interactions explicitly and incorporates one or two temperature-independent binary interaction parameters is of practical interest.

Mohammad Z. Hossain and Amyn S. Teja, Modeling Phase Equilibria in $CO_2$ + Polymer Systems, Journal of Supercritical Fluids, (Accepted, August 2014)

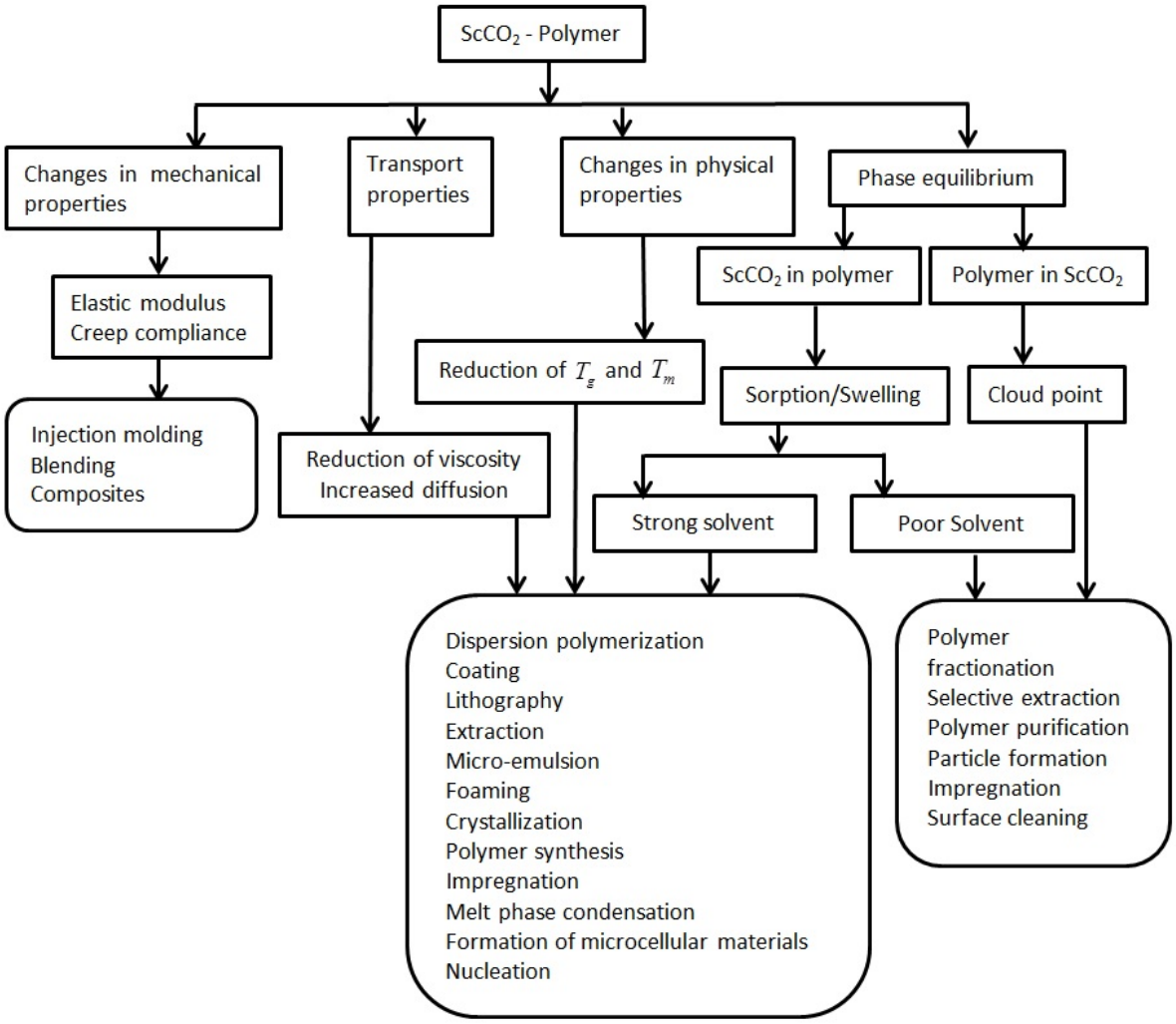


**Figure 2.1** Polymer property changes in the presence of $ScCO_2$ and applications that exploit these changes.

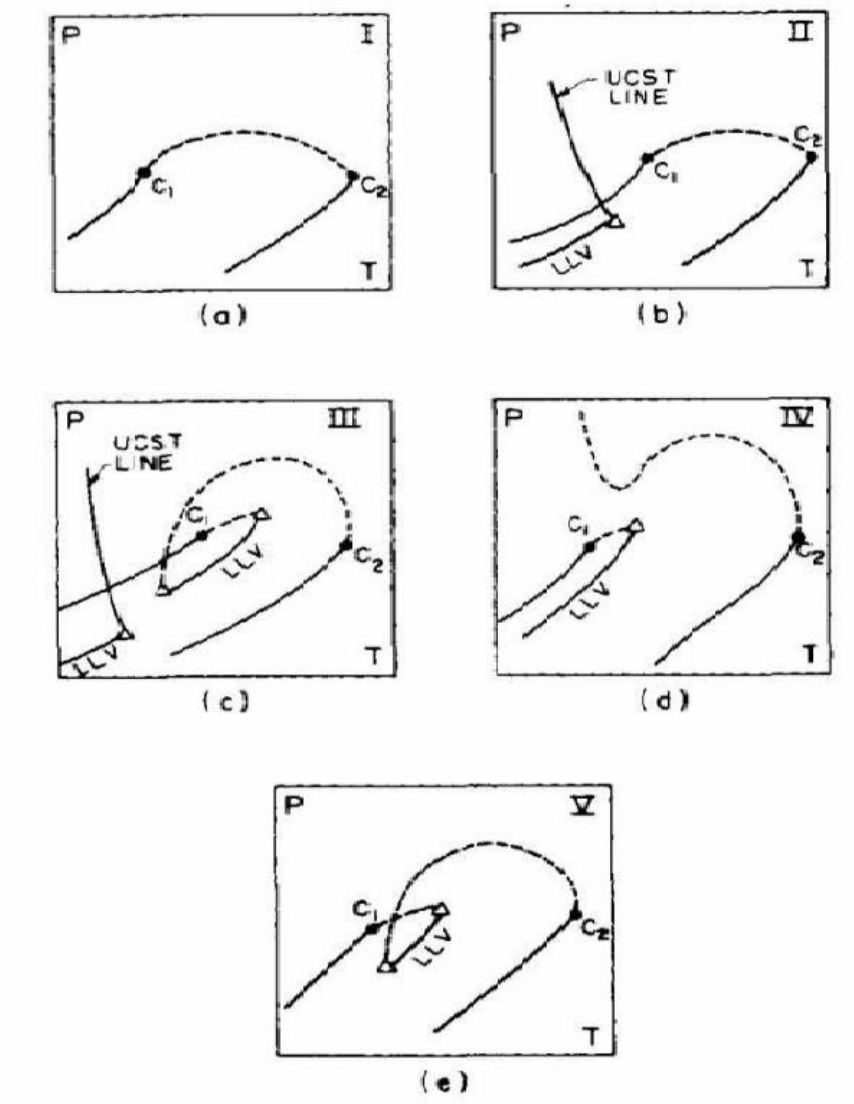


**Figure 2.2** Typical binary phase diagrams for polymer systems; C1 and C2 are the critical points of component 1 and 2, respectively; the dashed lines are the critical mixture curves and the open triangles are critical end points [2].

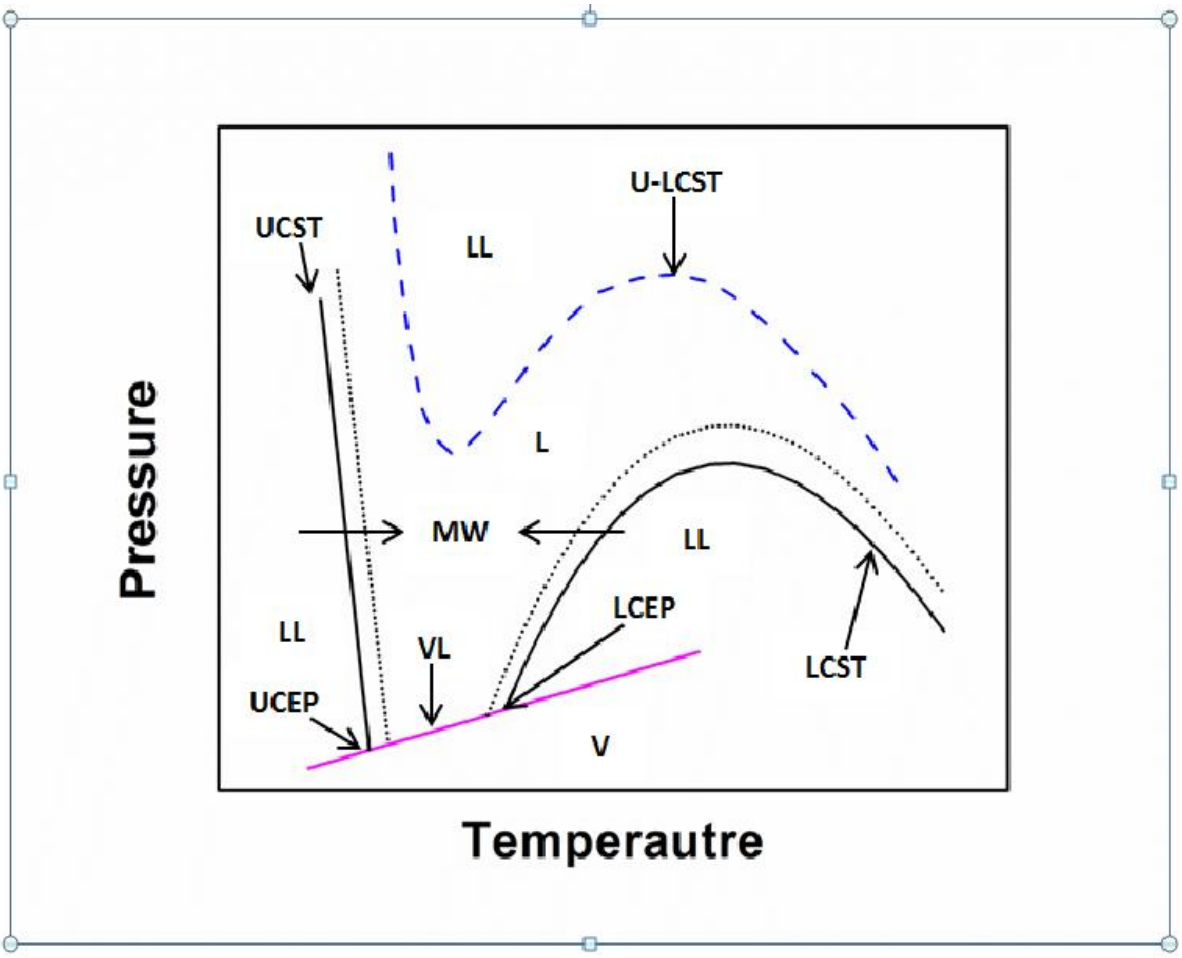


**Figure 2.3** Typical P-T diagrams for SCF + polymer systems

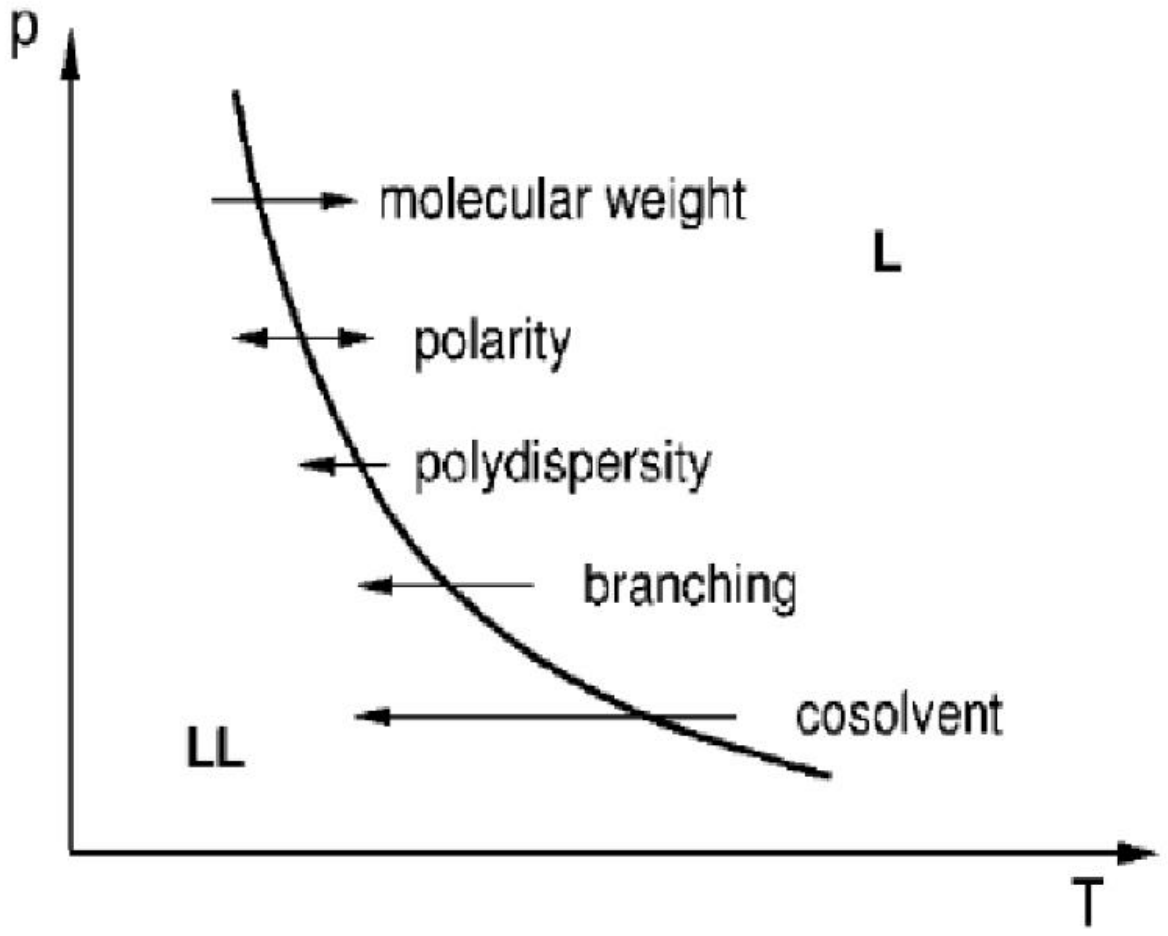


**Figure 2.4** Impact of various properties in the solubility of polymer in $CO_2$ [2].

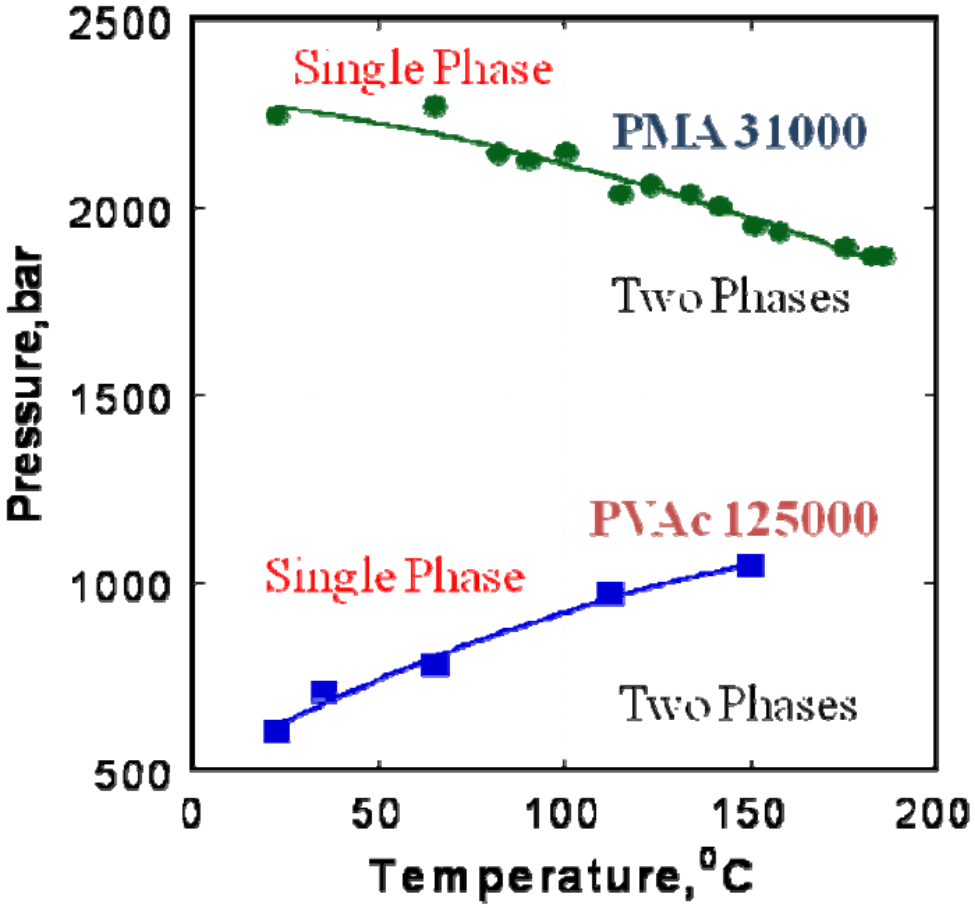


**Figure 2.5** Cloud point of $CO_2$ + poly (methyl acrylate) (PMA) and $CO_2$ +poly (vinyl acetate) (PVAc) systems [3].

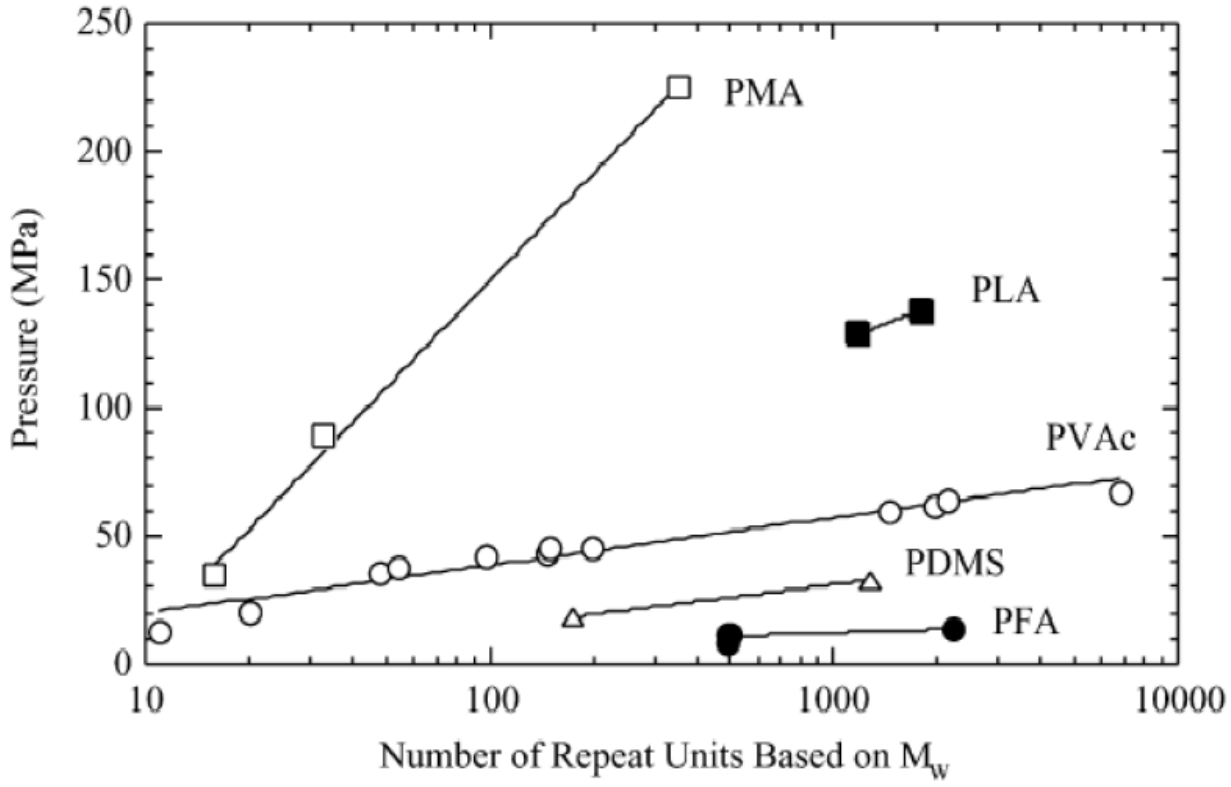


**Figure 2.6** Cloud-point pressures for polymers at ~5 wt. % (PMA, PLA, PVAc, PDMS, and PFA) in $CO_2$ versus the number of repeat units of polymer based on Mw at 298 K [4].

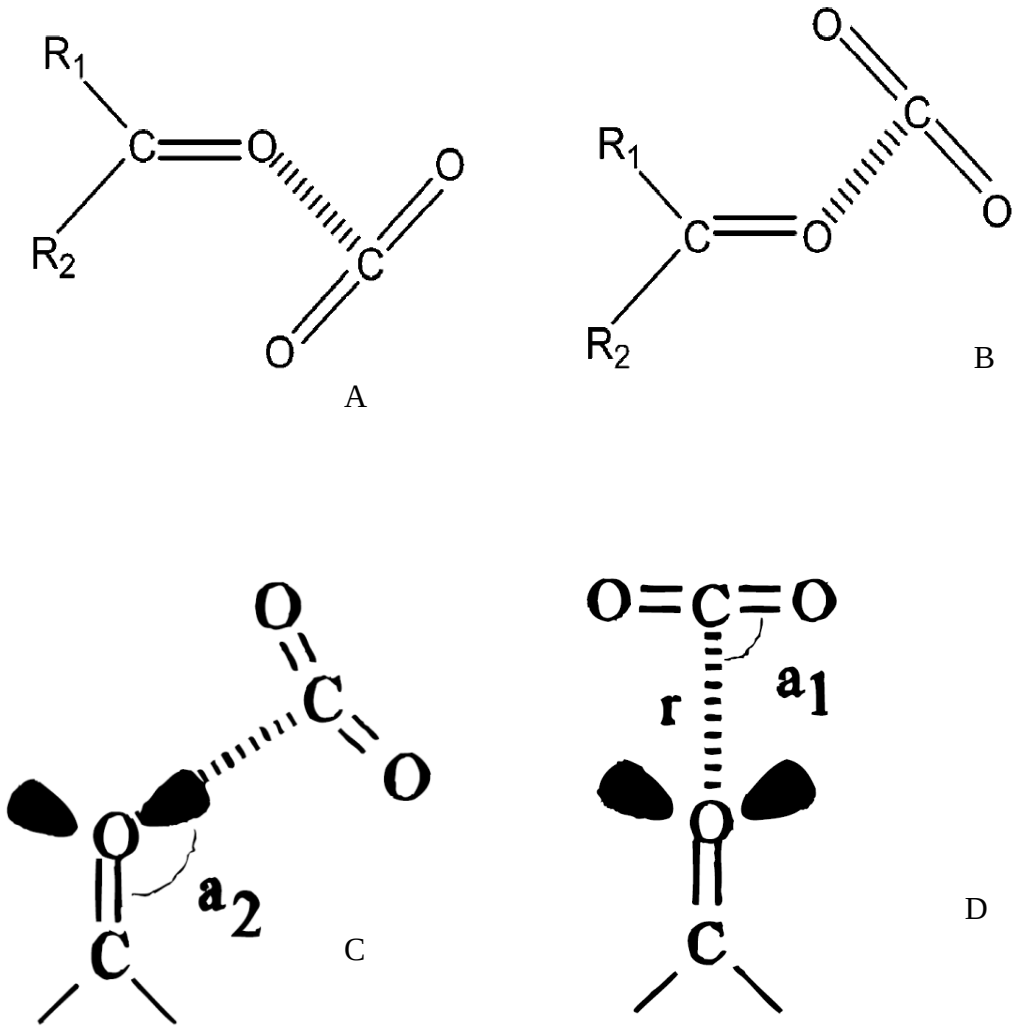


**Figure 2.7** Different conformations of C=O…$CO_2$ interactions [1, 5]; A and B are the different conformations, C = $C_s$ symmetry, and D = $C_{2v}$ symmetry.

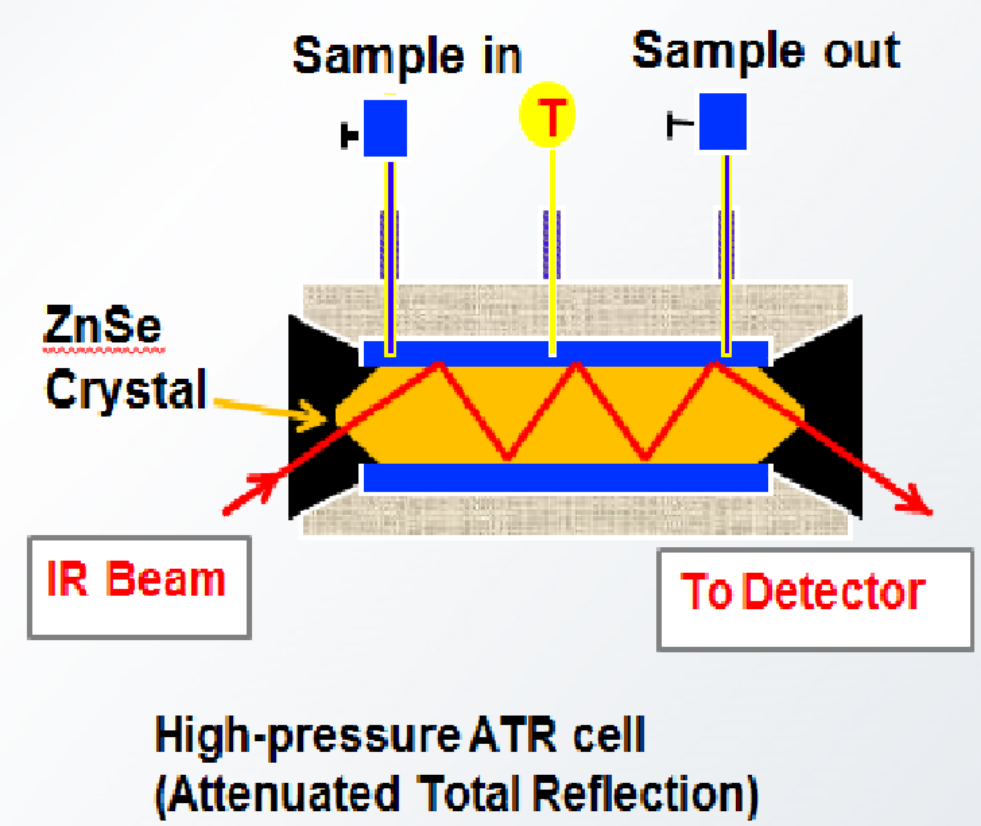


**Figure 2.8** Schematic of ATR – IR cell containing ZnSe crystal with multiple reflections.

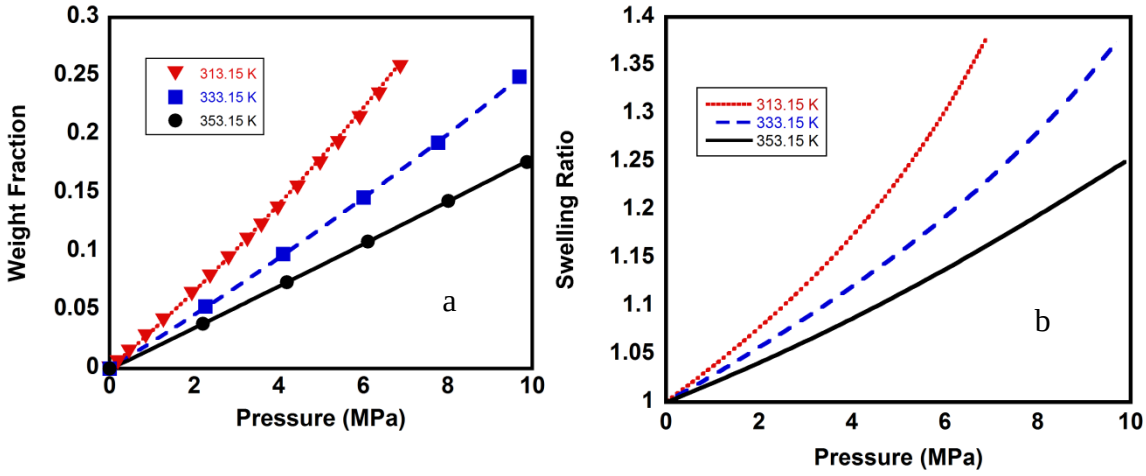


**Figure 2.9** (a) $CO_2$ solubility in PVAc and (b) swelling of PVAc due to $CO_2$ calculated using the ALF EOS with $K_0$ = 0.10 and $\Delta H_a$ = 9.3 kJ $mol^{-1}$. Lines represent calculated values using ALF model [6] and the points represent experimental values [7])

**Table 2.1** Review papers published in 2008-2013 dealing with $CO_2$ + polymer systems

| Area | Reference |
|---|---|
| Tissue engineering | [30, 154-156] |
| Polymer purification | [157] |
| Particle formation | [158-161] |
| Membrane separation | [162-164] |
| Fuel cells | [165] |
| Nano-composites | [166, 167] |
| Catalytic reaction | [168] |
| Drug delivery | [169-172] |
| Phase equilibrium measurements | [34, 173, 174] |
| Polymer processing | [175-177] |
| Foaming | [178] |
| Polymer synthesis | [179] |
| Thermodynamic modeling | [180] |
| Formation of micro-emulsions | [181] |

**Table 2.2** Interaction energies between $CO_2$ and molecule with carbonyl and ether groups for two different conformations in Figure 2.6 [5]

| Molecules | Interaction energies / - kJ·mol$^{-1}$ | | |
|---|---|---|---|
| | $CO_2$/Ether oxygen | $CO_2$/Carbonyl oxygen (A) | $CO_2$/Carbonyl oxygen (B) |
| IPA | 14.8 | 14.2 | 15.9 |
| MIE | 18.0 | - | - |
| EIE | 18.6 | - | - |
| IBA | 15.1 | 14.1 | 14.3 |
| MIK | - | 13.6 | 16.0 |

IPA = isopropyl acetate; MIE = methyl isopropyl ether; EIE = ethyl isopropyl ether; IBA = isobutyl acetate; MIK = methyl isobutyl ketone.

**Table 2.3** Interaction energies between $CO_2$ and molecules with carbonyl groups for two different symmetries in Figure 2.6 [1]

| Level with 6-31G basis set | Molecule | Symmetry | Binding energy / -kJ·mol$^{-1}$ |
|---|---|---|---|
| SCF | Acetone | $C_{2v}$ | 16.04 |
| | | $C_s$ | 18.38 |
| | Acetaldehyde | $C_{2v}$ | 17.47 |
| | | $C_s$ | 20.98 |
| | Formaldehyde | $C_{2v}$ | 12.86 |
| | | $C_s$ | 16.29 |
| | Acetic acid | $C_{2v}$ | 15.85 |
| | | $C_s$ | 22.04 |
| | Methyl acetate (ester side attack) | $C_{2v}$ | 18.34 |
| | Methyl acetate (methyl side attack) | $C_s$ | 20.92 |
| | | $C_s$ | 21.86 |
| MP2 | Acetone | $C_{2v}$ | 10.55 |
| | | $C_s$ | 16.80 |
| | Acetaldehyde | $C_{2v}$ | 9.67 |
| | | $C_s$ | 17.02 |
| | Formaldehyde | $C_{2v}$ | 8.88 |
| | | $C_s$ | 14.31 |
| | Acetic acid | $C_{2v}$ | 10.79 |
| | | $C_s$ | 17.83 |
| | Methyl acetate (ester side attack) | $C_{2v}$ | 13.22 |
| | Methyl acetate (methyl side attack) | $C_s$ | 16.70 |
| | | $C_s$ | 17.42 |

MP2: Second order Møller–Plesset perturbation theory and SCF: Self-consistent field theory

**Table 2.4** Differences among various version of the SAFT

| SAFT Model | Reference | Dispersion | Association |
|---|---|---|---|
| Chapman et al. [87] | Hard sphere [87, 182] | Mean field approx. with LJ fluid | Wertheim 1st order principle [90] |
| Huang and Radosz [94] | Hard sphere [87, 182] | Mean field approx. with square-well fluid | Wertheim 1st order principle [90] |
| PC – SAFT [96] | Hard sphere chain [87, 182] | Baker and Henderson 2nd order pert. theory [183] | Wertheim 1st order principle [90] |
| S – SAFT [184] | Hard sphere [87, 182] | Simplified square well fluid of Lee et al. [185] | Wertheim 1st order principle [90] |
| VR – SAFT [186] | Hard sphere (flexible chain) [87, 182] | van der Waals attractive term [186] | Wertheim 1st order principle [90] |

**Table 2.5** Models used to correlate sorption data of $CO_2$ + polymer systems

| Polymer | Temperature / K | Pressure / MPa | Model | Ref. |
|---|---|---|---|---|
| PLA, PLGA | 308 – 323 | 10 – 30 | SL, PC – SAFT | [187] |
| PMMA, PTFPME, PTFE, PVDF | 313 – 353 | 25 | SL, SAFT | [122] |
| LDPE, HDPE, PMMA, PIB, PBMA, PVAC, PS, PP, PTFE, PVDF, PBS | 298 – 483 | 62 | SL, SWP, PC – SAFT | [79] |
| PS | 373 – 473 | 20 | PC – SAFT | [103] |
| PEG1500, PEG4000 | 298, 323 | 7 – 25 | SL, SAFT | [126] |
| PLGA | 313 | 1 – 4 | PHSC | [188] |
| PVDF | 323 | 35 | SL | [127] |
| PS | 298 – 313 | 15 | SL | [125] |
| PP | 453 – 493 | 35 | SL, PC – SAFT | [104] |
| PBMA | 313 – 353 | - | SRK | [76] |
| PVAc | 333 – 373 | - | SRK | [76] |
| PS | 373 – 453 | - | SRK | [76] |
| PS | 373 – 453 | 2 – 20 | PR, SL, PC – SAFT | [82] |
| PS, PVME | 293 – 313 | 2 | SL, PC – SAFT | [121] |
| LDPE, HDPE, i-PP, PVAC, PS, PMMA, PBMA, PDMS, PC, PBS, PBSA | 293 – 473 | 40 | PR, PC – SAFT | [80] |

**Table 2.5** Continued

| | | | | |
|---|---|---|---|---|
| PEG300, EVA40, PVAc, PBS, PBSA, PLA, PLGA50, PMMA, PBMA | 303 – 393 | 1 – 40 | ALF | [6] |
| PP | 313 – 484 | 25 | SL | [189] |
| PS, PMMA | 323 – 453 | 25 | PC – SAFT | [190] |
| HPDE, PS, PVAc, PBMA | 313 – 473 | 20 | PR + SAFT | [33] |
| HPDE, PA-11, PVDF | 298 – 393 | 5 | PC – SAFT | [95] |
| PVAc | 313 – 353 | 10 | CLM | [40] |
| PVAc, PLA, PLGA15, PLGA15, PLGA35 | 313 – 353 | 10 | CLM | [11] |
| PMMA | 303 – 333 | 15 | SL | [191] |
| PBS, PBSA | 323 – 473 | 20 | SL | [12] |
| PS, PVAc | 313 – 473 | 20 | SL | [7] |
| PS, PMMA | 308 – 405 | 50 | NRHB | [8] |
| PS, PMMA | 324 – 405 | 45 | NRHB | [120] |
| PS, PPO, PPO/PS50, PPO/PS50 | 373 – 473 | 20 | SL | [124] |
| i-PP | 373 – 423 | 15 | SL | [192] |
| PLA15k, PLA52k, PLGA85, PLGA75, PLGA65, PLGA50 | 308 | 20 | SL | [193] |
| PLA, PLGA75, PLGA50 | 303 – 333 | 10 | SL | [10] |
| PET | 383 – 403 | 30 | SL | [194] |
| PS | 373 – 453 | 10 | PHSC | [128] |

**Table 2.6** Models used to correlate swelling data of $CO_2$ + polymer systems

| Polymer | Temperature / K | Pressure / MPa | Model | Ref. |
|---|---|---|---|---|
| PLA, PLGA | 308 – 323 | 10 – 30 | SL, PC – SAFT | [187] |
| PMMA, PTFPME, PTFE, PVDF | 313 – 353 | 25 | SL, SAFT | [122] |
| PP | 313 – 484 | 25 | SL | [189] |
| PMMA | 313 – 433 | 10 | SL | [191] |
| PS, PMMA | 324 – 405 | 45 | NRHB | [120] |
| PS, PPO, PPO/PS50, PPO/PS50 | 373 – 473 | 20 | SL | [124] |
| EVA40 | 323 – 348 | 30 | SL | [123] |
| PMMA, PBMA | 308 – 354 | 40 | ALF | [6] |
| PLA15k, PLA52k, PLGA85, PLGA75, PLGA65, PLGA50 | 308 | 20 | SL | [193] |
| PLA, PLGA75, PLGA50 | 303– 333 | 10 | SL | [10] |

**Table 2.7** Models used to correlate sorption data for $CO_2$ + cosolvent + polymer systems

| Cosolvent | Polymer | Temperature / K | Pressure / MPa | Model | Ref. |
|---|---|---|---|---|---|
| pentane | PS | 363 | 1 | PC – SAFT | [103] |
| VDF | PVDF | 323 | 35 | SL | [127] |
| n-butane | PE | 400 – 460 | 120 | SL, PHSC | [129] |
| n-pentane | PP | 400 – 460 | 70 | SL, PHSC | [129] |
| cyclohexane | PS | 400 – 460 | 10 | SL, PHSC | [129] |
| cyclohexane | PS | 443 – 468 | 10 | PHSC | [128] |

**Table 2.8** Models used to correlate cloud point or bubble point data of $CO_2$ + polymer systems

| Polymer | Temperature / K | Pressure / MPa | Model | Ref. |
|---|---|---|---|---|
| PEO, PPO2k, PPO4k, L61, L81, L62, 17R2, 17R4, 25R2 | 293– 338 | 10 – 40 | PC – SAFT | [50] |
| PDMS/PEMS | 303 – 433 | 35 | SL | [133] |
| PVAc, PBMA, PMA, PEA, PBA, PEHA, PODA | 423 | 300 | CLM | [40] |
| PLA, PLGA15, PLGA25, PLGA35, PVC, PVA, PMMA, PHMA, POMA, PDMA, PFHMA, PFOMA, PFDMA | 423 | 300 | CLM | [42] |
| PCL, PIPA, PIDA | 393 – 513 | 300 | CLM | [44] |
| PCHA, PCHMA | 303 – 473 | 250 | PR | [130] |
| PIPA, PPA | 313 – 513 | 300 | PR | [51] |
| PIDA, PDA, PIPA | 413 – 493 | 250 | PR | [195] |
| PP50k, PP95k | 400 – 460 | 35 | PR, SL, PC – SAFT | [81] |
| PDDMA | 473 | 248 | | [132] |
| PLGA | 310 – 370 | 310 | PR, SL, PC – SAFT | [84] |
| PCL | 310 -335 | 15 | PC – SAFT | [196] |

**Table 2.9** Models used to correlate cloud point or bubble point data of $CO_2$ + cosolvent + polymer systems

| Cosolvent | Polymer | Temperature / K | Pressure / MPa | Model | Ref. |
|---|---|---|---|---|---|
| Ethanol | PEG1k, PEG6k, PEG20k | 301 – 325 | 20 | SL | [113] |
| MMA | PMMA | 338 – 353 | 10 – 15 | PC – SAFT | [197] |
| $CH_2Cl_2$ | PLA | 313 – 363 | 30 | PR+PC – SAFT | [83] |
| DDMA | PDDMA | 473 | 248 | PR | [132] |
| DME | PDDMA | 473 | 248 | PR | [132] |
| n-pentane | PP50k, PP95k | 400 – 460 | 35 | PR, SL, PC – SAFT | [81] |
| CFC-22 | PLA | 300 – 400 | 50 | PR + SAFT | [33] |
| DME | PCL, PIPA, PIDA | 323 – 513 | 300 | CLM | [44] |
| CHA, CHMA | PCHA, PCHMA | 303 – 473 | 250 | PR | [130] |
| IPA, DME, IPMA | PIPA, PIPA, PIPMA | 313 – 513 | 300 | PR | [51] |
| IDA, DME | PIDA, PIDA | 313 – 473 | 250 | PR | [195] |
| Ethylene | EVA | 393 – 493 | 110 – 130 | PC – SAFT | [49] |

# CHAPTER 3: A LATTICE FLUID EQUATION OF STATE FOR ASSOCIATING $CO_2$ + POLYMER SYSTEMS

In this chapter, a new Associated Lattice-Fluid (ALF) Equation of State (EOS) is derived by incorporating complex-formation in the Guggenheim-Huggins-Miller (GHM) lattice fluid partition function for $CO_2$ + polymer systems. The contents of this chapter have been published in Industrial & Engineering Chemistry Research 2013, 52, 12654 – 12660.

## 3.1 Introduction

The phase behavior of $CO_2$ + polymer systems is of practical interest in polymer synthesis [27], in membrane separation of flue and natural gases [162, 163], and in the fabrication of porous scaffolds for tissue engineering [30, 198]. It is also of interest in the fabrication of micro- and nanoparticles of biodegradable polymers using supercritical $CO_2$ in controlled drug delivery [29, 199-201]. Both theoretical arguments and experimental evidence suggests that $CO_2$ is able to interact with electron donating functional (e.g. carbonyl) groups in polymers to form weak Lewis acid-base complexes [1, 35, 41, 69]. These interactions have measurable effect on the phase behavior of $CO_2$ + polymer systems [3, 41, 43]. However, few thermodynamic models consider specific Lewis acid-base interactions explicitly, and hence are restricted in their ability to interpret the behavior of associating $CO_2$ + polymer solutions.

Several versions of the Statistical Association Fluid Theory (SAFT) [94, 96, 153, 202], and several lattice fluid equations of state (EOS) [45, 112, 203], [115] have been employed successfully for the calculation of phase behavior and volumetric properties of associating polymer solutions. However, these models generally require self and cross-asssociation parameters that depend on temperature or molecular-weight [84, 94, 96]. Excess Gibbs energy models, such as that of Coleman and co-workers, [109-111], are not suitable for the calculation

of volumetric properties. The Compressible Lattice Model (CLM) proposed by Ozkan and Teja [40] and extended by Kasturirangan et al. [11, 42] and Yuan and Teja [44] successfully accounts for association between $CO_2$ and polymers with one adjustable parameter per binary system. However, the CLM model is not directly applicable to volumetric properties such as swelling since it is also an excess Gibbs energy model.

In this study, a new Associated Lattice Fluid (ALF) Equation of State (EOS) is proposed by combining the Guggenheim-Huggins-Miller lattice partition function [117] with the partition function for association used in the CLM model [46, 47]. The association contribution contains physically meaningful parameters which are independent of temperature or pressure. Furthermore, as illustrated in the CLM model, one of the parameters can be obtained using *in situ* ATR-FTIR measurements [38, 43].

The utility of the new EOS is demonstrated by correlating the solubility of $CO_2$ in polymers such as poly(vinyl acetate) (PVAc), poly(lactide) (PLA), poly(lactide-co-glycolide 50:50) (PLGA50), poly(methyl methacrylate) (PMMA), poly(ethylene-co-vinyl acetate) (EVA40), poly(butylene succinate) (PBS), poly(butylene succinate-co-adipate) (PBSA), poly(n-butyl methacrylate) (PBMA), poly (carbonate) (PC), poly (styrene) (PS), poly (propylene) (PP), Poly (ethylene) (PE), and poly(ethylene glycol) (PEG 300). In addition, the new EOS is also used to predict swelling and cloud points in $CO_2$+ polymer systems, with the parameters that are obtained by correlating solubility.

### 3.2 Development of the ALF EOS for associating systems

Consider a lattice with a coordination number $z$ that contains $N_1$ solvent molecules (each consisting of $r_1$ segments) and $N_2$ polymer molecules (each consisting of $r_2$ segments),

with all segments arranged randomly on the lattice. The Guggenheim-Huggins-Miller partition function for this system can be written as follows:

$$\Omega_R = \left(\frac{\tau}{\sigma}\right)^{N_2} \frac{(r_1 N_1 + r_2 N_2)!}{N_1! N_2!} \left(\frac{(r_1 N_1 + q N_2)!}{(r_1 N_1 + r_2 N_2)!}\right)^{\frac{z}{2}} \tag{3.1}$$

where $\sigma$, $\tau$, and $zq$ are the symmetry number, flexibility parameter, and the number of non-bonded segment pairs around each polymer molecule, respectively. Also

$$zq = (r_2 - 2)(z-2) + 2(z-1) = r(z-2) + 2 \tag{3.2}$$

If we distribute $N_0$ holes and $\hat{r}\hat{N}$ (polymer and solvent) segments randomly on this lattice, then the partition function becomes:

$$\Omega_R = \left(\frac{\tau}{\sigma}\right)^{\hat{N}} \frac{N_r!}{N_0! \hat{N}!} \left(\frac{N_q!}{N_r!}\right)^{\frac{z}{2}} \tag{3.3}$$

where $N_q = N_0 + q\hat{N}$, $N_r = N_0 + \hat{r}\hat{N}$, and $N = \hat{r}\hat{N} = r_1 N_1 + r_2 N_2$. The total number of non-bonded pairs $N_q z / 2$ is now can be expressed as:

$$\frac{N_q z}{2} = \frac{N_r z}{2} - \hat{N}(\hat{r} - 1) = \frac{N_r z}{2} - \hat{r}\hat{N} + \hat{N} \tag{3.4}$$

The partition function in Equation 3.3 can now be simplified using the Sterling ($\ln N! = N \ln N - N$) and Flory ($\hat{r}/q \to 1$) approximations [204] to give:

$$\Omega_R = \left(\frac{\hat{r}\tau}{\sigma}\right)^{\hat{N}} \left(\frac{N_r}{N_0}\right)^{N_0} \left(\frac{N_r}{\hat{r}\hat{N}}\right)^{\hat{N}} \tag{3.5}$$

If some solvent segments are restricted to specific sites on the lattice because of association with polymer segments, then the contribution to the partition function due to association is given by [46, 47]

$$\Omega_{Complex} = \frac{1}{N_2!}\left[\frac{(z-1)^{N_2(r_2-1)}}{N^{N_2(r_2-1)}}\right]\left(\frac{r_2!}{(r_2-\alpha r_2)!(\alpha r_2)!}\right)^{N_2}\left[r_2(1+\alpha)\right]^{r_2 N_2} \times\left[\left(\frac{N}{r_2(1+\alpha)}\right)!\Big/\left(\frac{N}{r_2(1+\alpha)}-N_2\right)!\right]^{r_2}\left(\frac{(r_1N_1)!}{(\alpha r_2 N_2)!(r_1N_1-\alpha r_2 N_2)!}\right) \tag{3.6}$$

where $\alpha$ represents the association ratio. In this work, it is assumed that the polymer and solvent associate with a binding ratio of 1:1 to form a chemical complex. The association ratio α is therefore related to the equilibrium constant $K$ of the complexation reaction that can be expresses via:

$$\alpha = \frac{(1+K)-\sqrt{(1+K)^2-4\phi_1\phi_2K(1+K)}}{2\phi_2(1+K)} \tag{3.7}$$

where $\phi_1$ and $\phi_2$ are volume fractions of the solvent and polymer. The final form of the associated lattice fluid partition function can then be obtained by combining the random and complex contributions according to:

$$Q = \Omega_R\Omega_{complex}\exp\left(-\frac{E}{RT}\right) \tag{3.8}$$

where $E$ is the energy and $V$ is the volume of the lattice that has $N_0$ unoccupied sites (holes) and $N$ occupied sites as illustrated in Figure 3.1. The Gibbs energy can be obtained by differentiation of the partition function according to:

$$G = -RT\left[\ln Q-\left(\frac{\partial \ln Q}{\partial V}\right)_{T,N}\right] = -RT\ln Q + PV \tag{3.9}$$

The final expression for the Gibbs energy is then:

$$\frac{G}{NRT}=\frac{E}{NRT}+\frac{PV}{NRT}-\frac{1}{\hat{r}}\ln\left(\frac{\hat{r}\tau}{\sigma}\right)+\left(\frac{f_0}{1-f_0}\right)\ln f_0+\frac{1}{\hat{r}}\ln(1-f_0)-\left(\phi_2-\frac{\phi_2}{r_2}\right)\ln(z-1)$$
$$+\frac{\phi_2}{r_2}\ln\frac{\phi_2}{r_2}-\frac{\phi_2}{r_2}+\phi_2+(\frac{\phi_1-\alpha\phi_2}{1+\alpha})\ln(\phi_1-\alpha\phi_2)-\phi_1\ln\left(\frac{\phi_1}{\phi_1-\alpha\phi_2}\right)+\alpha\phi_2\ln\left(\frac{\alpha\phi_2}{\phi_1-\alpha\phi_2}\right) \quad (3.10)$$
$$+\phi_2(1-\alpha)\ln(1-\alpha)+\alpha\phi_2\ln\alpha$$

where $f_0$ is the fraction of holes in the lattice and is given by:

$$f_0=\frac{N_0}{N_0+\hat{r}\hat{N}}=1-\frac{\hat{r}\hat{N}}{N_0+\hat{r}\hat{N}}=1-\hat{\rho} \quad (3.11)$$

Since the third term of equation 3.10 does not contribute to the pressure [205], we can write [6]:

$$G=\hat{r}\hat{N}\left\{\begin{array}{l}-\tilde{\rho}\varepsilon^*+P\tilde{v}v^*+RT\left[\left(\frac{f_0}{1-f_0}\right)\ln f_0+\frac{1}{\hat{r}}\ln(1-f_0)\right]\\ +RT\left[\begin{array}{l}-\left(\phi_2-\frac{\phi_2}{r_2}\right)\ln(z-1)+\frac{\phi_2}{r_2}\ln\frac{\phi_2}{r_2}-\frac{\phi_2}{r_2}+\phi_2+(\frac{\phi_1-\alpha\phi_2}{1+\alpha})\ln(\phi_1-\alpha\phi_2)\\ -\phi_1\ln\left(\frac{\phi_1}{\phi_1-\alpha\phi_2}\right)+\alpha\phi_2\ln\left(\frac{\alpha\phi_2}{\phi_1-\alpha\phi_2}\right)+\phi_2(1-\alpha)\ln(1-\alpha)+\alpha\phi_2\ln\alpha\end{array}\right]\end{array}\right\} \quad (3.12)$$

where $V=\hat{r}\hat{N}\tilde{v}v^*$, $\hat{r}\hat{N}=N$, and $E=-\varepsilon^*\tilde{\rho}$. The equation of state can now be derived using

$$\left(\frac{\partial G}{\partial f_0}\right)_{T,P,N_i}=0 \quad (3.13)$$

and is given by:

$$\tilde{\rho}^2+\tilde{P}+\tilde{T}\left[\ln(1-\tilde{\rho})+(1-\frac{1}{\hat{r}})\tilde{\rho}\right]=0 \quad (3.14)$$

with

$$\tilde{\rho} = \frac{\rho}{\rho^*} = \frac{\rho \hat{r} v^*}{M} \qquad P = \frac{P}{P^*} = \frac{P v^*}{\varepsilon^*}$$

$$\tilde{T} = \frac{T}{T^*} = \frac{TR}{\varepsilon^*} \qquad \tilde{v} = \frac{1}{\tilde{\rho}} = \frac{1}{1 - f_0} = \frac{V}{V^*} = \frac{V}{\hat{r} \hat{N} v^*}$$

Note that this EOS is of the same form as the Sanchez Lacombe (SL) EOS, but with the average lattice energy per segment given by:

$$\varepsilon^* = \phi_1 \varepsilon_1^* + \phi_2 \varepsilon_2^* + \Delta\varepsilon_{ex} \tag{3.15}$$

$$\Delta\varepsilon_{ex} = -\frac{\Delta H_{mix}}{N} = -\left[\alpha \phi_2 \chi_a + \phi_2 (\phi_1 - \alpha \phi_2)(z - 2 - \alpha)\chi_u\right] RT \tag{3.16}$$

$$\chi_u = \frac{\chi_u^*}{(z - 2 - \alpha)} = \frac{\left(\varepsilon_1^* + \varepsilon_2^* - 2\varepsilon_{12}^*\right)}{RT(z - 2 - \alpha)} \tag{3.17}$$

with,

$$\chi_u^* = \frac{\left(\varepsilon_1^* + \varepsilon_2^* - 2\varepsilon_{12}^*\right)}{RT} \tag{3.18}$$

$$\chi_a = \frac{\Delta H_a}{RT} \tag{3.19}$$

The enthalpy of complex formation ($\Delta H_a$) is related to the equilibrium constant for the complex reaction via the van't Hoff relationship:

$$\ln \frac{K}{K_0} = \frac{\Delta H_a}{RT}\left(\frac{1}{T} - \frac{1}{T_0}\right) \tag{3.20}$$

In Equation 3.20, $T_0$ is some arbitrary reference temperature (298.15 K in this work), so that three parameters are required to apply the equation of state derived above -- namely, $\Delta H_a$, $K_0$ and $\varepsilon_{12}$. We may express $\varepsilon_{12}$ as follows:

$$\varepsilon_{12}^* = (1 - k_{ij})\sqrt{(\varepsilon_1^* \varepsilon_2^*)} \tag{3.21}$$

From Table 3.1, we can see that the dispersion interactions that are obtained from ALF parameters are very similar to those calculated using the experimental Flory parameter. Therefore it is reasonable to assume $k_{ij}$ = 0 for simplicity in the following discussion (reducing the number of binary interaction parameters to 2, namely $\Delta H_a$ and $K_0$). Note that, $k_{ij}$ represents non –Regular Solution behavior excluding association. Therefore, Equation 3.18 becomes

$$\chi_u^* = \frac{\left(\sqrt{\varepsilon_1^*} - \sqrt{\varepsilon_2^*}\right)^2}{RT} \tag{3.22}$$

The characteristic volume and segment number can be expressed using

$$v^* = \phi_1 v_1^* + \phi_2 v_2^* \tag{3.23}$$

$$\frac{1}{\hat{r}} = \frac{\phi_1}{r_1} + \frac{\phi_2}{r_2(1+\alpha)} \tag{3.24}$$

then the chemical potential of pure $CO_2$ (assuming no polymer dissolved in gas phase) and of $CO_2$ (1) dissolved in a polymer (2) can be obtained from the Gibbs free energy and written as:

$$\frac{\mu_1^{G,pure}}{RT} = \frac{r_1}{RT}\left[-\tilde{\rho}_1\varepsilon_1^* + \frac{Pv_1^*}{\tilde{\rho}_1}\right] + r_1\left[\left(\frac{1-\tilde{\rho}_1}{\tilde{\rho}_1}\right)\ln(1-\tilde{\rho}_1) + \frac{1}{\hat{r}}\ln\tilde{\rho}_1\right] \tag{3.25}$$

$$\begin{aligned}\frac{\mu_1^L}{RT} &= \frac{1}{RT}\left(\frac{\partial G}{\partial N_1}\right)_{T,P,N_{j\neq 1}} = \frac{Pr_1}{RT\tilde{\rho}}\left[-f_0 v^* + v_1^*\right] - r_1 f_0 + \frac{r_1}{\hat{r}} f_0 + \ln(1-f_0) \\ &-\frac{1}{RT}\left[r_1\tilde{\rho}(1-\tilde{\rho})\varepsilon^* + r_1\varepsilon_1^*\tilde{\rho}\right] + \left(\beta_1\phi_2\chi_a + \phi_2\left[\left\{-\beta_1\phi_2 + \phi_2(1+\alpha)\right\}(z-2-\alpha) - \beta_1(\phi_1 - \alpha\phi_2)\right]\chi_u\right)\tilde{\rho} \\ &-\frac{r_1\phi_2}{r_2} + \left[\frac{1}{1+\alpha} - \frac{\beta_1}{(1+\alpha)^2}\right]\ln(\phi_1 - \alpha\phi_2) + \frac{\phi_1 - \alpha\phi_2}{1+\alpha}\left(\frac{1-\phi_2\beta_1}{\phi_1 - \alpha\phi_2} - 1\right) - \ln\left(\frac{\phi_1}{\phi_1 - \alpha\phi_2}\right) - 1 + \phi_1\left(\frac{1-\phi_2\beta_1}{\phi_1 - \alpha\phi_2}\right) \\ &+\beta_1\phi_2\ln\left(\frac{\alpha\phi_2}{\phi_1 - \alpha\phi_2}\right) + \alpha\phi_2\left(\frac{\beta_1}{\alpha} - \frac{1-\phi_2\beta_1}{\phi_1 - \alpha\phi_2}\right) + \beta_1\phi_2\ln\frac{\alpha}{1-\alpha}\end{aligned} \tag{3.26}$$

with, $\beta_1 = \partial\alpha/\partial N_1 = \dfrac{\alpha(1+K) - K}{(1+K)(2\alpha\phi_2 - 1)}$

Equation 3.25 - 3.26 can then be used to calculate the solubility of $CO_2$ (1) in polymers (2) by equating the chemical potential of pure $CO_2$ in the gas phase to the chemical potential of $CO_2$ dissolved in the polymer. The extent of swelling of polymers due to $CO_2$ can be estimated using

$$S_w = \frac{V}{V_0} \times 100\ \% \tag{3.27}$$

where $V_0$ and $V$ are the volume of the dry polymer and the $CO_2$ + polymer solution, respectively.

### 3.3 Results and Discussion

In order to apply the new EOS to mixtures, it is first necessary to obtain the characteristic constants $P^*$, $T^*$, $\rho^*$ (or $\varepsilon_i^*$, $v_i^*$, $r_i$) for the pure components of interest. These constants are obtained by fitting PVT data and listed in Table 3.2. Table 3.2 also lists the constants of the SL EOS from literature for many of the same polymers, as well as constants for $CO_2$ reported by Condo et al. [206] . As can be seen in Table 3.2, SL and ALF constants for many polymers are almost identical. Any differences in values can probably be attributed to the use of different sets of PVT data in fitting the two models, or to differences in the molecular weights of the polymers considered. Therefore, it appears reasonable to use literature values of SL characteristic constants for polymers when ALF constants are not available.

For mixture calculations, it is also necessary to estimate binary parameters $K_0$ and $\Delta H_a$. The enthalpy of association $\Delta H_a$ can be estimated from FTIR measurements, quantum calculations, or via molecular modeling [1, 38, 69]. The results of our calculations of sorption equilibria for four $CO_2$ + polymer systems using the ALF EOS are shown in Table 3.3. In these

calculations, $\Delta H_a$ values were estimated from FTIR spectra reported in the literature [38] and $K_0$ was treated as an adjustable parameter. Average absolute deviations (AAD) between calculated and experimental values, the values of $K_0$ obtained by fitting sorption equilibria using the ALF EOS, and the corresponding values of $k_{ij}$ obtained using the SL EOS are also listed in Table 3.3. Note that the values of $k_{ij}$ in the SL EOS calculations are temperature dependent, while the values of $K_0$ in the ALF EOS are temperature independent.

The results of our calculations of sorption equilibria in several $CO_2$ + polymer systems using the ALF EOS are shown in Table 3.4. Table 3.4 includes Average Absolute Deviations (AAD) between calculated and experimental solubilities of $CO_2$ in each polymer, the values of $\Delta H_a$, and the corresponding values of $K_0$ used in the calculations. The values of $\Delta H_a$ were estimated from FTIR spectra reported in the literature [38] or were set equal to the reported values of $\Delta H_a$ for polymers with a similar functional group. Thus, the value of $\Delta H_a$ for $CO_2$ + PVAc was assumed to be the same as that for EVA40 + $CO_2$, since both PVAc and EVA40 contain the interacting vinyl ester group in their structures. The value of $\Delta H_a$ for $CO_2$ + PC was also assumed to be the same as that for $CO_2$ + PVAc due to the similar the functional group in their structures even though PC is not a vinyl ester. Similarly, the same value of $\Delta H_a$ was assumed to be valid for $CO_2$ + polymers with an aliphatic ester, such as PLA, PBS or PBSA. This was also the case for $CO_2$ + acrylate polymers such as PMMA and PBMA. Nelson and Borkman [1] showed that there is a some association occurs even in between neutral benzene ring and $CO_2$ and they have reported the value of that binding energy is around -4 kJ/mol.

Therefore, we have assumed this value for all the $CO_2$ + neutral polymer (PS, i-PP, PE) systems we have studied.

The following trends can be ascertained from the values reported in Table 3.4:

(i) For polymers containing the same electron donating functional group in their structures, greater accessibility of the functional group to $CO_2$ leads to higher values of $K_0$. Hence, $K_0$(= 0.18) for $CO_2$ + PBMA is larger than $K_0$(= 0.16) for $CO_2$ + PMMA. This is because the mobility of the PBMA side chain allows its acrylate group to be more accessible to $CO_2$. Parts a and b of Figure 3.2 show sorption results for $CO_2$ + PMMA and $CO_2$ + PBMA systems. One isotherm in each system was used to obtain the value of $K_0$.

(ii) Higher values of $K_0$ were obtained for $CO_2$ + polymer systems compared with the corresponding $CO_2$ + copolymer systems. For example, $K_0$ = 0.09 in the case of $CO_2$ + PLGA system while $K_0$ = 0.20 in the case of $CO_2$ + PLA. The associating group of PLA may be more accessible to $CO_2$ compared with the same group in PLGA, leading to higher $CO_2$ solubility in PLA than in PLGA. Sorption equilibria for $CO_2$ + PLA and $CO_2$ + PLGA50 systems are illustrated in parts a, and b of Figure 3.4. Similar results were observed in the case of $CO_2$ + PVAc and $CO_2$ + EVA40 (see Table 3.4).

(iii) The value of $K_0$ (0.21) obtained by fitting sorption data for $CO_2$ + amorphous PBSA is nearly the same as the value of $K_0$ (0.22) obtained for $CO_2$ + PBS. $T_g$ values (236.0 K for PBSA and 239.5 K for PBS), and $CO_2$ solubility in the two polymers are also very similar. This could be due to the fact that the lower value of $K_0$ for the associating group in PBSA is balanced by the higher dispersion interaction between $CO_2$ and PBSA.

Figures 3.5 a and b illustrate the sorption behavior of $CO_2$ + PBS and $CO_2$ + amorphous PBSA.

(iv) As expected, the value of $K_0$ (0.21) obtained by fitting sorption data for $CO_2$ + amorphous PBSA is greater than the value of $K_0$ (0.17) in the $CO_2$ + crystalline PBSA system, since the solubility of $CO_2$ is higher in amorphous PBSA than in crystalline PBSA. Figure 3.5c demonstrates this point.

(v) For neutral polymers, the values of $K_0$ and the $CO_2$ solubility in these polymers follow the opposite trend. For instance, the value of $K_0$ increased in the order of PS<i-PP$\approx$PE, however the $CO_2$ solubility is increased in opposite order.

The extent of swelling can be predicted using the same binary interaction parameters that were obtained by fitting sorption data. Figure 3.3 a-b illustrate this in the case of PMMA and PBMA using $K_0$ values from solubility data correlation. So, the ALF EOS is capable to predict the swelling behavior of polymer/copolymer only from one isotherm of the sorption data. The ALF EOS is also capable of predicting the cloud point behavior of $CO_2$ + polymer systems using the parameters listed in Table 3.4. Figure 3.6 demonstrates such prediction in the case of $CO_2$ + PBMA, $CO_2$ + $PLA_L$ (low MW), $CO_2$ + $PLA_H$ (high MW), $CO_2$ + $PLGA_{50}$, and $CO_2$ + PVAc. As seen from Figure 3.6, both LCST and UCST type behavior can be predicted using ALF EOS. LCST type phase behavior can be observed in $CO_2$ + PBMA, whereas $CO_2$ + $PLGA_{50}$ (MW = 69.6 kg/mol), $CO_2$ + $PLA_L$ (low MW), $CO_2$ + $PLA_H$ (high MW), and $CO_2$ + PVAc display UCST type behavior. As expected from Figure 2.2, the cloud point pressure increases with the Mw as demonstrated for PLA ($PLA_L$, MW = 84.5 kg/mol; $PLA_H$, MW = 128.5 kg/mol). The predicted cloud point pressure is 132 MPa for $CO_2$ + $PLA_L$ (low MW) while it is 141 MPa for $CO_2$ + $PLA_H$ (high MW) at 300 K.

## 3.4 Conclusions

A new Associated Lattice-Fluid Equation of State has been derived for $CO_2$ + polymer systems by combining the Guggenheim-Huggins-Miller (GHM) lattice fluid partition function with the complex contribution from the CLM model. The new EOS contains two mixture parameters – the enthalpy of association $\Delta H_a$ and the equilibrium constant at a reference temperature $K_0$. These parameters do not depend on temperature, pressure or molecular weight. The new EOS was used to correlate $CO_2$ solubility in a number of polymers over a wide range of pressures and temperatures, using $\Delta H_a$ from FTIR experiments and $K_0$ as an adjustable parameter. Only one value of $K_0$ was required to correlate solubility data within experimental error (maximum AAD of ~ 4%). In addition, swelling and cloud point behavior of $CO_2$ + polymer systems could be predicted (maximum AAD of ~ 6.6 %) without any additional adjustable parameters. Both LCST and UCST type cloud point behavior could be predicted using this EOS. Therefore, the ALF EOS shows considerable promise in the calculating sorption, cloud point, and volumetric data of $CO_2$ + polymer systems.

Mohammad Z. Hossain, Yanhui Yuan, and Amyn S. Teja, A Lattice Fluid Equation of State for Associating $CO_2$ + Polymer Systems, Industrial & Engineering Chemistry Research 2013, 52, 12654 – 12660

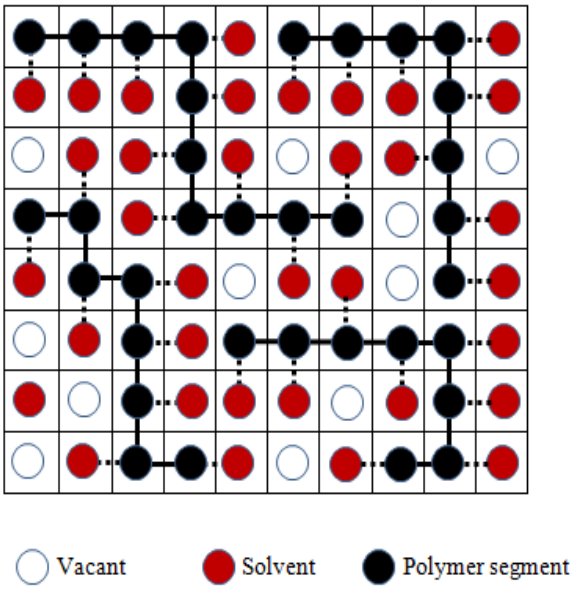


**Figure 3.1** Associated Lattice

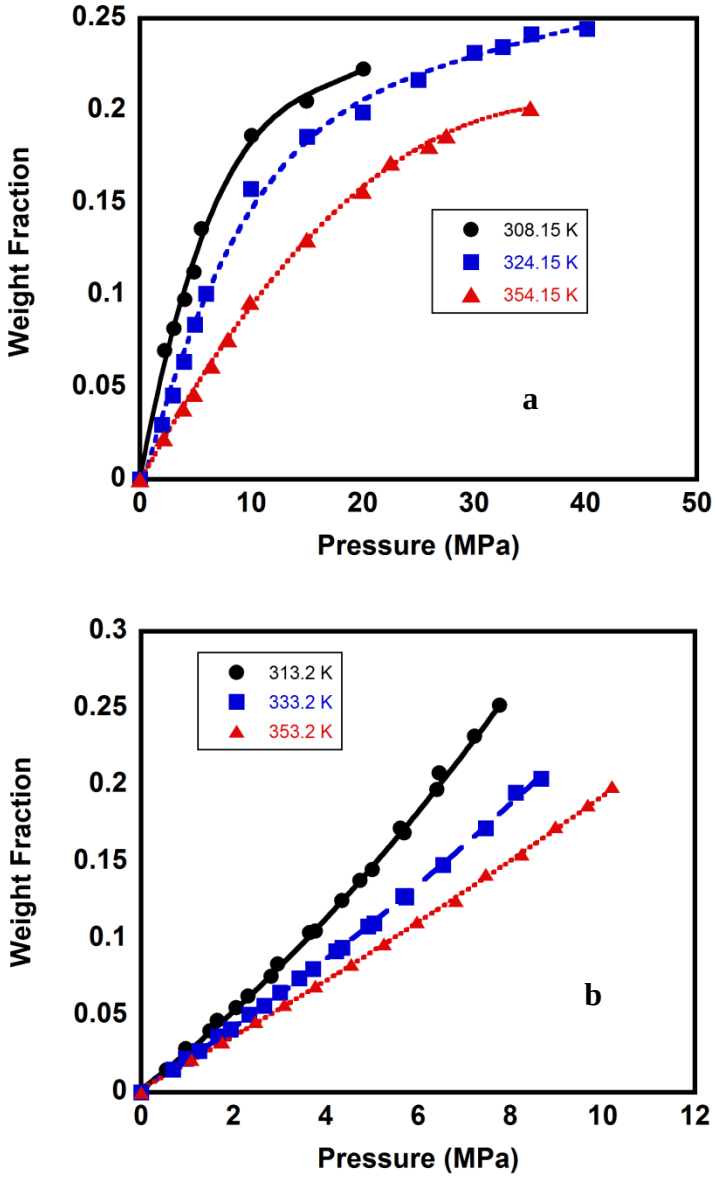


**Figure 3.2** Solubility of $CO_2$ in (a) PMMA and (b) PBMA; lines are calculated from the model and points are the experimental results [8, 9].

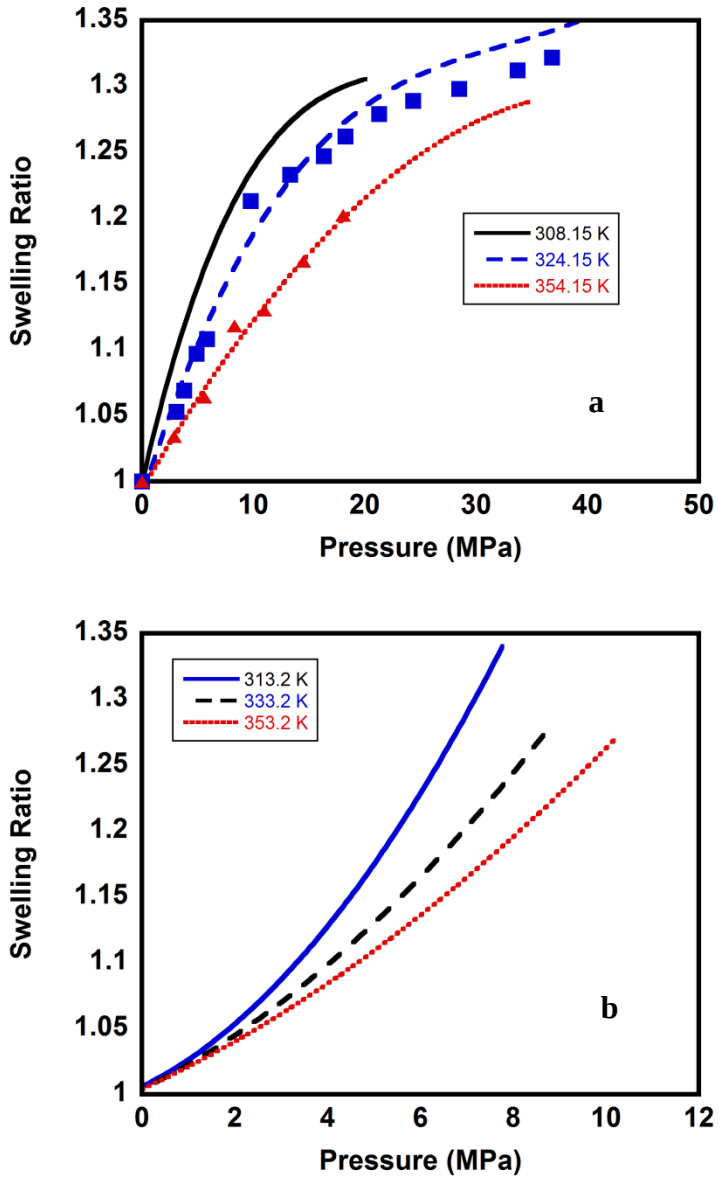


**Figure 3.3** Swelling of (a) PMMA and (b) PBMA due to $CO_2$; lines are calculated from the model and points are the experimental results [8].

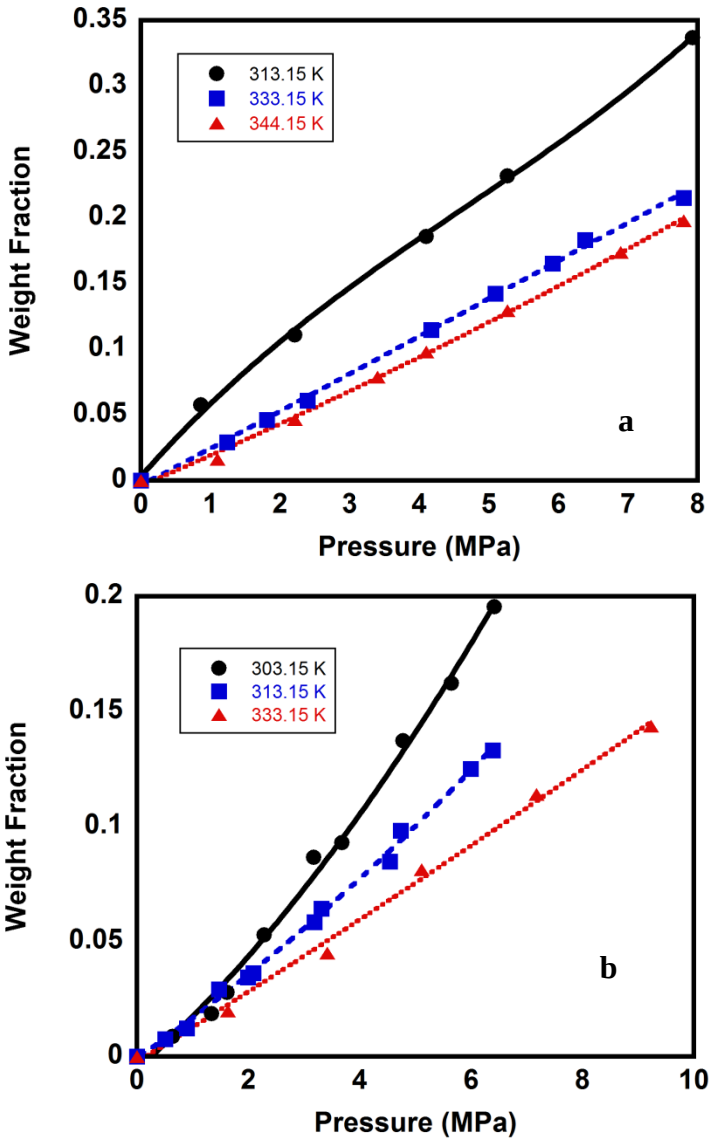


**Figure 3.4** Solubility of $CO_2$ in (a) PLA and (b) PLGA50; lines are calculated from the model and points are the experimental results [10, 11].

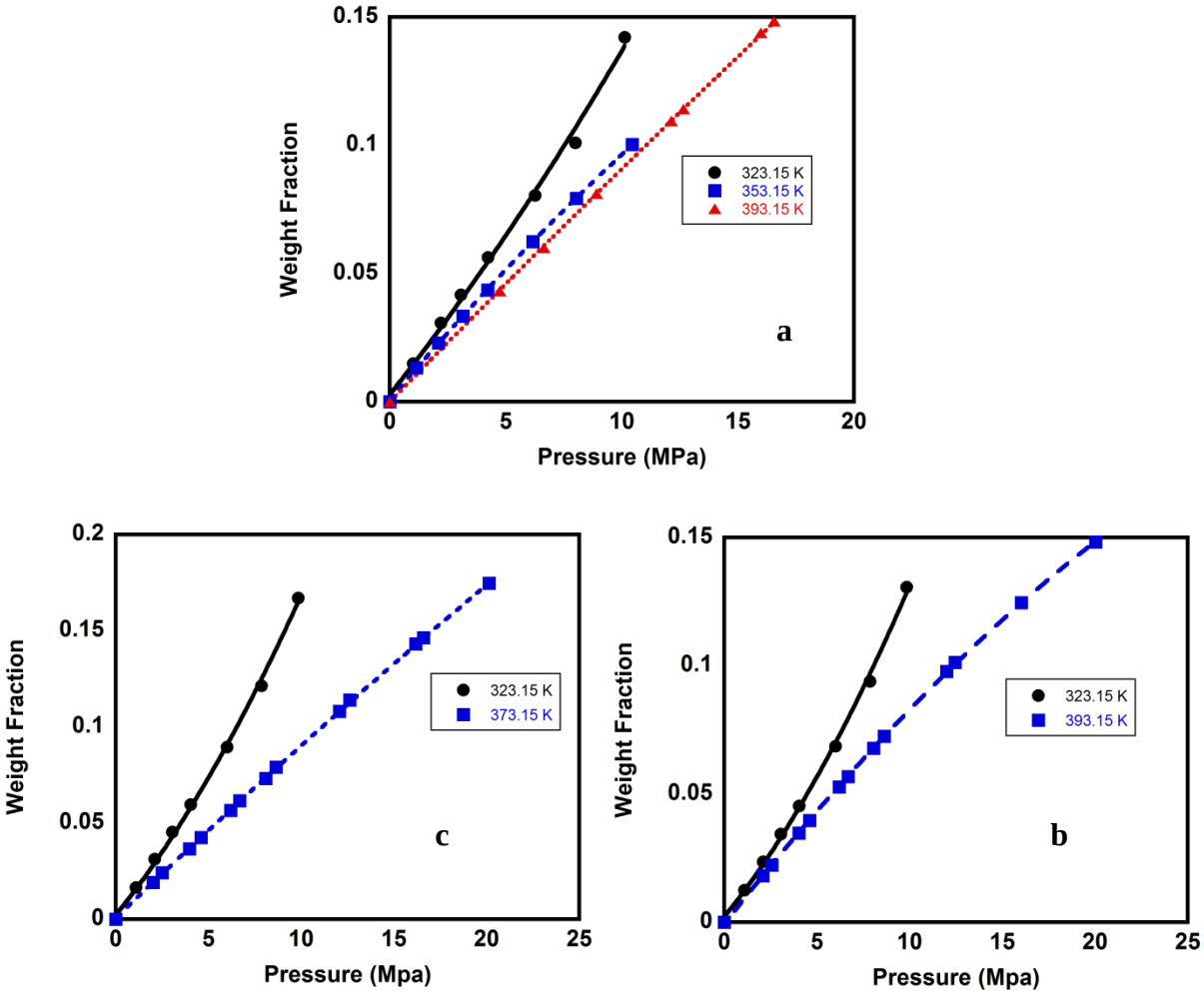


**Figure 3.5** Solubility of $CO_2$ in (a) PBS, (b) amorphous PBSA and (c) crystalline PBSA; lines are calculated from the model and points are the experimental results [12].

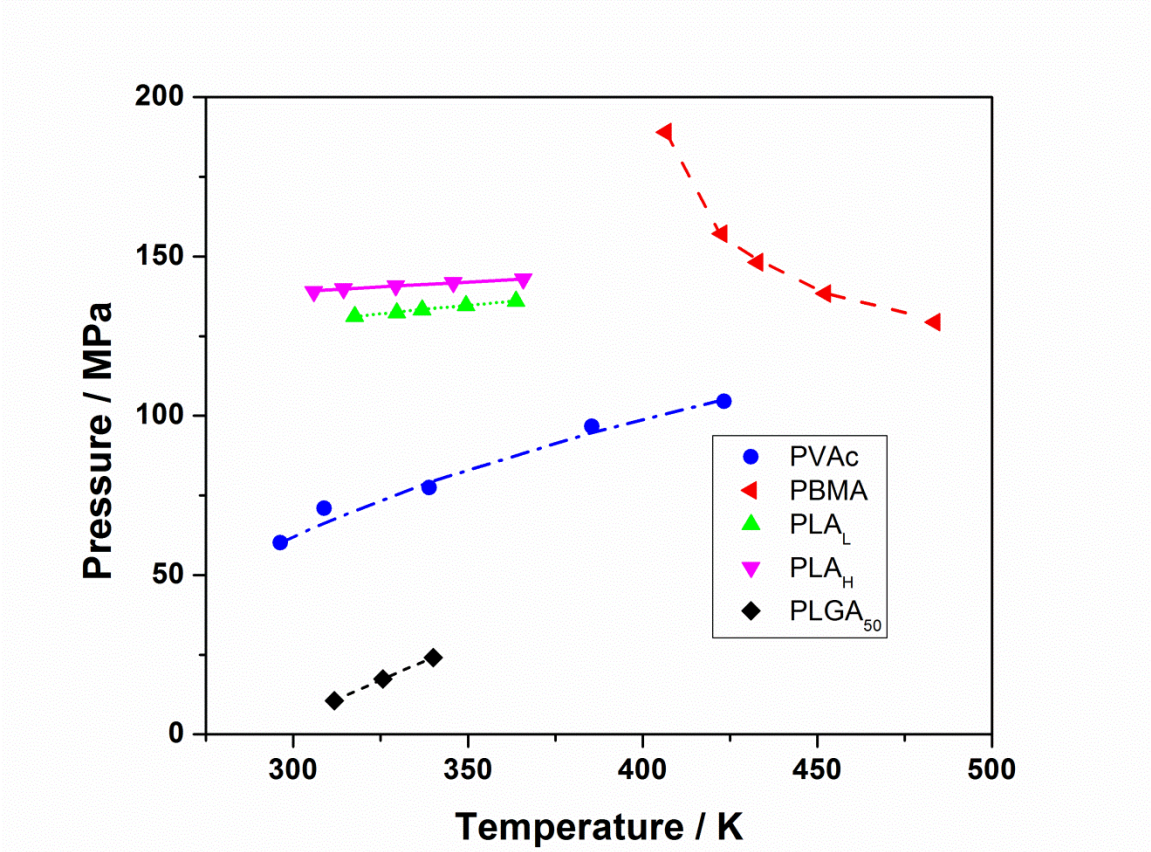


**Figure 3.6** Cloud-point pressures in $CO_2$ + PBMA, $CO_2$ + $PLA_L$, $CO_2$ + $PLA_H$ , $CO_2$ + $PLGA_{50}$ and $CO_2$ + PVAc systems ; lines are calculated using the ALF EOS with binary parameters from Table 3.4 and points represent experimental results [3, 13]. Polymer wt. fractions are ~5 % in each case.

**Table 3.1** Comparison of the dispersion interaction of the ALF EOS with experimental Flory parameter for solvent + poly (ethylene adipate) (PEA) systems at 303.15 K.

| Solvent | $\delta_{i-ALF} = \sqrt{\frac{\varepsilon_i^*}{v_i^*}}$ / (MPa)$^{0.5}$ | Dispersion interaction calculated using ALF EOS, $\chi_u^*$ | Exp. Flory parameter for solution, $\chi_{FH}$ |
|---|---|---|---|
| Benzene | 18.69 | 0.155 | 0.146 – 0.166 [207] |
| Chloroform | 18.05 | 0.178 | 0.153 – 0.173 [207] |
| Acetone | 17.52 | 0.204 | 0.182 – 0.202 [207] |
| PEA | 25.71 | - | - |

$\chi_u^* = \frac{v^* \left(\delta_{solvent} - \delta_{pol}\right)^2}{RT}$; PVT data for solvents were taken from Dortmund data bank; PVT data for PEA [208]; solution - solvent + polymer.

**Table 3.2** Characteristic constants of the ALF and SL equations for pure components.

| Polymer | $T^*$ / K | $P^*$ / MPa | $\rho^*$ / kg·m$^{-3}$ | Ref | Data Ref |
|---|---|---|---|---|---|
| PEG300 | 728.9 | 544.8 | 1169.5 | This work | [208] |
| EV40 | 618.9 | 500.5 | 1023.7 | This work | [209] |
| | 613.0 | 495.6 | 1020.0 | [123] | - |
| PVAC | 592.0 | 504.2 | 1282.7 | This work | [7] |
| | 592.0 | 504.2 | 1282.0 | [210] | - |
| PBS | 717.8 | 523.6 | 1263.5 | This work | [211] |
| | 717.8 | 523.5 | 1263 | [12] | - |
| PBSA | 691.7 | 570.1 | 1257.2 | This work | [211] |
| | 691.8 | 570.1 | 1235 | [12] | - |
| PLA | 641.6 | 547.7 | 1330.1 | This work | [211] |
| | 631.0 | 559.2 | 1333.0 | [10] | - |
| PLGA50 | 638.0 | 536.6 | 1458.5 | This work | [10] |
| | 649.6 | 572.7 | 1451.6 | [10] | - |
| PMMA | 698.6 | 467.1 | 1265.3 | This work | [212] |
| | 742.0 | 488.3 | 1249.8 | [210] | - |
| PBMA | 624.3 | 409.6 | 1124.8 | This work | [212] |
| | 627.0 | 431.0 | 1125.0 | [9] | - |
| PC | 787.4 | 538.9 | 1262.3 | This work | [209] |
| PS | 784.4 | 312.2 | 1088.6 | This work | [213] |
| | 773.0 | 366.9 | 1092.8 | [210] | - |
| i-PP | 666.4 | 293.4 | 944.0 | This work | [208] |
| | 692.0 | 297.5 | 882.8 | [214] | - |
| PE | 675.0 | 288.0 | 886.3 | This work | [215] |
| | 736.0 | 288.7 | 867.0 | [210] | |
| $CO_2$ | 308.6 | 574 | 1505.0 | [206] | - |

**Table 3.3** Adjustable parameters used in fitting sorption equilibria in $CO_2$ + polymer systems using the ALF and SL EOS.

| System | SL EOS | | | ALF EOS (This work) | |
|---|---|---|---|---|---|
| | $k_{ij}(T)$ | AAD % | References | $K_0$ | AAD % |
| PVAC + $CO_2$ | 0.1158 - 0.00055*T | 3.60 | [7] | 0.10 | 2.90 |
| PBS + $CO_2$ | 0.310 - 0.00104*T | 1.90 | [12] | 0.22 | 0.42 |
| PBSA (am) + $CO_2$ | 0.261 -0.00885*T | 2.20 | [12] | 0.21 | 0.73 |
| PLGA50 + $CO_2$ | -0.0273 - 0.00007*T | 8.03 | [10] | 0.09 | 1.00 |

am – amorphous

**Table 3.4** Binary parameters for $CO_2$ sorption in polymer X

| X | $K_0$ | $\Delta H_a$ / kJ·mol$^{-1}$ | AAD % | Data Ref |
|---|---|---|---|---|
| PEG300 | 0.16 | -11.5 [b] | 4.07 | [216] |
| EVA40 | 0.08 | -9.3 [a] | 3.30 | [123] |
| PVAC | 0.10 | -9.3 [b] | 2.90 | [7] |
| PBS | 0.22 | -8.8 [a] | 0.42 | [12] |
| PBSA(am) | 0.21 | -8.8 [a] | 0.73 | [12] |
| PBSA (cr) | 0.17 | -8.8 [a] | 0.69 | [12] |
| PLA | 0.20 | -8.8 [b] | 0.39 | [11] |
| PLGA50 | 0.09 | -8.5 [b] | 1.00 | [10] |
| PMMA | 0.16 | -8 [b] | 0.34 | [8] |
| PBMA | 0.18 | -8 [a] | 0.81 | [9] |
| PC | 0.29 | -9.3 [a] | 2.76 | [217] |
| PS | 0.22 | -4 [a] | 0.28 | [8] |
| i-PP | 0.09 | -4 [a] | 0.28 | [192] |
| PE | 0.09 | -4 [a] | 0.43 | [218] |

a - assumed; b - [41]; am – amorphous; and cr – crystalline

# CHAPTER 4: QUANTITATIVE STUDY OF SPECIFIC INTERMOLECULAR INTERACTIONS BETWEEN $CO_2$ AND $CO_2$ – PHILIC POLYMERS USING *in situ* ATR – FTIR SPECTROSCOPY

Although the existence of Lewis acid-base interactions between $CO_2$ and electron donating functional groups in polymers can be determined from the vibrational spectra of polymers, only a few quantitative estimates of such interactions have been reported. This chapter therefore reports the results of ATR – FTIR studies of association between $CO_2$ and $CO_2$-philic functional groups in polymers using the bending vibrations of $CO_2$. This chapter also attempts to relate the strength of these interactions to the structure of the polymer. The contents of this chapter have been submitted for publication in The Journal of Supercritical Fluids in August 2014.

## 4.1 Introduction

Spectroscopic **s**tudies and *ab initio* calculations have both shown that $CO_2$ readily forms electron donor-acceptor (EDA) complexes with electron donating functional groups in polymers [1, 38, 39, 69]. These complexes can have a significant effect on the swelling [6, 35, 219], plasticization [219, 220], viscosity [36], and glass transition properties [43, 219, 220] of polymers and thereby affect polymer processing [27], membrane technology [163], and drug delivery [199].

The strength of EDA complexes in $CO_2$ – polymer systems can be determined from (i) the stretching vibration of the electron donating functional groups (e.g. carbonyl), (ii) the anti-symmetric stretching vibration ($v_3$) of $CO_2$, or (iii) the bending mode ($v_2$) of $CO_2$ in presence of a polymer. The carbonyl stretching band has been used

by Fowkes and Tischler [74], as well as Kolling [221], to study interactions between ethyl acetate (EA) and poly(methyl methacrylate) (PMMA) in presence of several solvents. Also, Fried and Li [222] have studied such shifts in order to determine interactions between $CO_2$ and cellulose acetate (CA) or PMMA. On the other hand, Kazarian et al. [35] and Higuchi and Nakagawa [223] have noted that changes in the antisymmetric stretching vibration of $CO_2$ in the presence of PMMA does not provide sufficient information to calculate Lewis acid-base interactions between the carbonyl group in poly (methyl methacrylate) (PMMA) and $CO_2$. Finally, *ab initio* calculations [1, 39, 224] and experimentally determined FTIR and Raman spectra [36-38, 69, 225] have been employed to show that the bending mode ($v_2$) of $CO_2$ can be used to obtain quantitative information on specific interactions between $CO_2$ and electron donating groups. Kazarian el al. [35] noted that the degeneracy of the bending mode of $CO_2$ diminishes in the presence of a polymer with carbonyl groups. This was confirmed in the case of poly (methyl methacrylate) (PMMA), poly (vinyl acetate) (PVAc), poly (carbonate) (PC), poly (phenylene oxide) (PPO), poly (ethylene glycol) (PEG), poly (lactide – co – glycolide) (PLGA), and poly (lactide) (PLA) and several poly(esters) [36-38]. Although most of these studies were qualitative in nature, a few quantitative results have also been published [1, 5, 35, 39, 69, 74]. Unfortunately, enthalpies of interaction obtained from these studies differ significantly from their *ab initio* estimates.

The Drago correlation [226] also provides a measure of Lewis acid-base interactions via the expression $-\Delta H_a = C_A C_B + E_A E_B$. Here, $C_A$ and $E_A$ are estimates of the acidity, and $C_B$ and $E_B$ are estimates of the basicity of small molecule. Unfortunately, these values are not available for $CO_2$ or for many polymers, and therefore

the Drago correlation is therefore not very useful for the determination of $CO_2$ – polymer interactions. Instead, shifts in the stretching frequency of electron donating functional groups such as carbonyl or hydroxyl have often been used to determine such interactions [72, 74]. Fowkes and Tischler [74] derived a relationship between the strength of these interactions and the carbonyl shift, and this relationship was used by Kazarian et al. [35] to obtain the enthalpy of association between $CO_2$ and PMMA. However, the Fowkes and Tischler relationship was developed for small organic solutes in the liquid phase and its validity for $CO_2$ – polymer systems has yet to be confirmed. In addition, the enthalpy of association for the carbonyl group…$CO_2$ interaction (-4.0 kJ/mol) estimated by Kazarian et al. [35] is not in agreement with the value of -15.0 kJ/mol estimated by Kilic et al. [5] using *ab initio* methods. Meredith et al. [69] did not use the Fowkes and Tischler relationship, but instead obtained the enthalpies of association between $CO_2$ and small organic molecules from a van't Hoff plot of equilibrium constants for the association reactions. Their method was used by Yanhui and Teja [38] to estimate specific interactions between $CO_2$ and carbonyl polymers using ATR – FTIR spectroscopy. In the present work, this method has been extended to more $CO_2$ + polymer systems to relate the strength of these interactions to the structure of the polymer.

## 4.2 Experiment

Poly (styrene-co-methyl methacrylate 40:60) (PS-co-PMMA, Mw = 100 – 150 kg/mol, and $T_g$ = 101 °C), poly (ethylene glycol) (PEG, Mw = 100 kg/mol, and $T_g$ = -67 °C), poly (butyl methacrylate) (PBMA, Mw = 337 kg/mol, and $T_g$ = 15 °C), and poly (ethylene-co-vinyl acetate 60:40) (EVA40, and $T_g$ = -40 to -30 °C) were purchased from Aldrich Chemical Co. (St. Louis, MO); Poly(sulfone) (PSF) was supplied by Solvay

Advanced Polymers. All polymers were used as received. Research grade $CO_2$ gas (99.999 mol %) was purchased from Airgas Inc. (Radnor, PA) and also used as received.

A Nicolet 550 Fourier Transform Spectrometer with a DTGS detector was used to collect FTIR spectra of each polymer sample at a resolution of 2 $cm^{-1}$. Each polymer was coated on the surface of a ZnSe crystal that is held by a Teflon O-ring in a cylindrical high-pressure ATR cell. The cell was made by Axiom Analytical, Inc (Irvine, CA, USA) and had a volume of 2 mL. Spectra were measured in the range of 4000 – 400 $cm^{-1}$ wavenumber with a scanning rate of 64. The angle of the incident IR beam was 45 ° and 10 specimen-sensing reflections were obtained on the surface of the ZnSe crystal. The temperature in the cell was controlled within ± 0.1 K using an Omega CN9000A controller, whereas pressure in the cell was kept constant within ± 0.2 bar using a $CO_2$ syringe pump. A pressure gauge (Heise, Model 710A) was used to monitor the pressure.

A coating of each polymer on the surface of the ZnSe crystal was obtained by injecting a 3-5 wt. % solution of the polymer in toluene into the cell at ambient conditions, and stripping the solvent with a gentle flow of nitrogen into the cell for 1 – 2 h. Most of the toluene evaporated during this process, leaving a coating of the polymer on the ZnSe crystal. Any residual solvent was removed by maintaining the cell under vacuum at 353 K for 10-12 h. The cell was then pressurized with $CO_2$ and kept at a fixed temperature and pressure for 12 – 24 h. Equilibrium conditions were deemed to have been achieved when consecutive measurements of ATR – FTIR spectra of the $CO_2$ - polymer system exhibited no changes with time. An additional 3 – 5 spectra were then collected for analysis, together with a reference spectrum under vacuum.

## 4.3 Results and discussions

Figure 4.1 shows ATR – FTIR spectra of EVA40 under vacuum and EVA40 under $CO_2$ pressure of 10 bar, both at 298 K. The carbonyl stretching band of EVA40 at 1736.0 $cm^{-1}$ can be easily identified in the figure, as well as the bending mode of $CO_2$ at ~ 660.0 $cm^{-1}$ and the anti-symmetric stretching band of $CO_2$ at 2336.4 $cm^{-1}$. Other characteristic bands are also visible in the range of wavenumbers from 400 – 4000 $cm^{-1}$. However, these are not relevant to the present work and are not discussed further. Instead, changes in the three vibrational modes that have been used by other researchers to quantify specific interactions in $CO_2$ – polymer systems are emphasized.

Several authors [35, 74, 221] have quantified specific interactions between a solvent and a solute with an electron donating functional group (e.g. C=O, P=O, S=O, or $-NH_2$) via the shift in the stretching frequency of the electron donating functional group. Table 4.1 lists such shifts in the stretching vibration of the carbonyl group in polymers before and after $CO_2$ exposure at various pressures. Normalized results for PBMA at 318.15 K under vacuum and at 10 bar $CO_2$ pressure are shown in Figure 4.2, which shows a shift in the carbonyl stretching frequency of PBMA from a wavenumber of 1726.0 $cm^{-1}$ at vacuum conditions to 1727.0 $cm^{-1}$ in the presence of $CO_2$ at 10 bar. Similar shifts to higher wavenumbers have also been observed in other carbonyl polymers and are listed in Table 4.1. However, quantum calculations [227] suggest that the carbonyl peak of small molecules should shift to a lower wavenumber for Lewis acid-base complex formation. This apparent discrepancy can be explained by invoking the Kirkwood–Bauer–Magat (KBM) equation as follows [38, 221, 228]:

$$\frac{\nu_0 - \nu_s}{\nu_0} = \frac{C(\varepsilon - 1)}{2\varepsilon + 1} + k\ AN \tag{4.1}$$

In this equation, $v_0$ and $v_s$ are wavenumbers of the peaks for carbonyl stretching in the gas and solution phases, $\varepsilon$ is the dielectric constant of the solvent, $AN$ is the Gutmann acceptor number of the solvent, and C and $k$ are constants. The first term on the right hand side of Equation 4.1 represents the carbonyl shift due to dispersion forces and the second term represents the shift due to solute – solvent interactions. These terms are of opposite sign [228] so that the carbonyl stretching shift can be to lower wavenumbers (if the second term of Equation 4.1 dominates), or to higher wavenumbers (if the first term dominates) [38]. Our experimental results imply that the dispersion contribution to the carbonyl shift is greater than the association contribution, so that only shifts to higher wavenumbers can be seen in Table 4.1 and Figure 4.2. We therefore conclude that shifts in the carbonyl stretching mode are not useful for quantifying specific interactions in $CO_2$ – polymer systems [38].

### 4.3.1 Anti-symmetric stretching mode of $CO_2$

Figure 4.3 (a) shows absorbance peaks of the anti-symmetric stretching mode of $CO_2$ in the EVA40 + $CO_2$ system at different pressures. Although the peak area increases with pressure, the position of the peak remains unchanged at 2336.38 $cm^{-1}$ at all pressures. Increasing the temperature results a decrease in the peak area, as can be seen in Figure 4.3 (b). However, the position of the peak did not change with temperature. The peak area can be used to estimate the concentration of $CO_2$ in polymers, as discussed by Kazarian [67]. However, the position of the peak cannot provide a measure of Lewis acid – base interactions in $CO_2$ – polymer systems because the peak position in insensitive to these interactions [35, 223].

### 4.3.2 Bending mode of $CO_2$

As discussed previously, both spectroscopic experiments [35-38, 69] and quantum calculations [1, 39] indicate that the bending mode ($v_2$) of $CO_2$ changes significantly when $CO_2$ is in contact with electron donating polymers. Indeed, several experimental studies have employed such changes for quantitative estimation of the strength of complex formation between $CO_2$ and polymers [38, 69].

Figure 4.4 shows the FTIR spectrum of $CO_2$ at 10 bar and 298 K in the region of the $CO_2$ bending mode in the $CO_2$ + PBMA system. The solid circles in the figure represent experimental data, the solid line represents a curve fit of the experiments, and dashed lines represent deconvoluted peaks. Pure $CO_2$ exhibits only one peak at around 667.0 $cm^{-1}$ at these conditions [35, 38]. On the other hand, Figure 4.4 shows that there are three (deconvoluted) peaks at 667.6 ±0.6 $cm^{-1}$, 661.6 ± 0.4 $cm^{-1}$, and 654.2 ± 0.3 $cm^{-1}$ in the $CO_2$ spectrum in presence of PBMA. Hence, splitting of the $CO_2$ bending mode occurs in presence of the Lewis base polymer and therefore the double degeneracy of the $CO_2$ bending mode is removed due to Lewis acid – base interactions [1, 38, 39, 69]. The order of the bending frequencies is as follows: in-plane bending of associated $CO_2$ < free $CO_2$ < out-of-plane bending of associated $CO_2$ [1, 35, 38]. The lowest frequency peak in Figure 4.4 near 654.0 $cm^{-1}$ can therefore be assigned to in-plane bending of associated $CO_2$ [35, 38, 69], whereas the peak near 662.0 $cm^{-1}$ can be assigned to free $CO_2$ that is dissolved in the polymer but not associated with electron donating functional groups (e.g. C=O). The peak near 662.0 $cm^{-1}$ is also observed in the $CO_2$ + PS system where there is no complex formation [35]. The third peak in Figure 4.4 near 667.0 $cm^{-1}$ is due to pure $CO_2$ in the gaseous state [35, 38]. At higher pressures, this peak and the peak at 662.0 $cm^{-}$

[1] (for unassociated $CO_2$ in the polymer) become more pronounced with respect to the peak at 654cm$^{-1}$ since the amounts of free and gas phase $CO_2$ increase with pressure.

An unambiguous peak cannot be identified for the out-of-plane bending mode of $CO_2$ in Figure 4.4, which is consistent with the studies of Meredith et al. [69], Kazarian et al. [35], and Yuan and Teja [38]. This could be because the out-of-plane bending mode of $CO_2$ overlaps with the free $CO_2$ band near 662.0 cm$^{-1}$. Nelson and Borkman [1] reported that the out-of-plane bending peak occurs near 664.3 cm$^{-1}$ in the $CO_2$ + acetone system. Moreover, *ab initio* calculations of Park suggest that it occurs at a much lower wavenumber than the in-plane bending peak of associated $CO_2$ [229]. Most importantly, Park also suggested that the absorbance of the in-plane bending mode is three times that of the out-of-plane mode for associated $CO_2$. At the same time, it is reasonable to assume that the free $CO_2$ peak is not affected by the out-of-plane bending mode of associated $CO_2$. These observations allow the $CO_2$ spectra to be deconvoluted and the strength of the associated complex to be determined as described in the following section.

### 4.3.3 Enthalpy of association determination and discussion

To calculate the enthalpy of association, we start with the assumption that the formation of EDA complexes between $CO_2$ and an electron donating functional group can be described by a reversible chemical reaction as follows:

$$P + CO_2 \Leftrightarrow P...CO_2 \tag{4.2}$$

The equilibrium constant for this association reaction is given by

$$K_c = \frac{[P...CO_2]}{[P][CO_2]} \tag{4.3}$$

where $[P...CO_2]$, $[P]$, and $[CO_2]$ are the concentrations of the associated complex, free polymer, and free $CO_2$, respectively. As discussed by Yuan and Teja [38], this reduces to:

$$K_c = \text{constant} \times \frac{A_{[CO_2]_A}}{A_{[CO_2]_F}} \tag{4.4}$$

where $A_{[CO_2]_A}$ and $A_{[CO_2]_F}$ are absorbances of the associated and free $CO_2$. These absorbances can be obtained from areas of the respective peaks in the FTIR spectra. In the case of $CO_2$ + PBMA shown in Figure 4.4, $A_{[CO_2]_F}$ is obtained from the area under the curve at 661.6 ± 0.4 $cm^{-1}$ and $A_{[CO_2]_A}$ is obtained from the area under the curve at 654.2 ± 0.3 $cm^{-1}$. $K_c$ at various temperatures can be estimated using this approach and the enthalpy of association ($\Delta H_a$) obtained from the slope of the van't Hoff plot. Figure 4.5 illustrates such a plot for $CO_2$ + PS-co-PMMA. The enthalpies of association and their uncertainties for this and other systems obtained using this approach are presented in Table 4.2 together with results from the literature. Table 4.2 also includes values of FWHM (the Full Width at Half Max) which represents a measure of the strength of the complex.

Table 4.2 shows that the highest negative value of the enthalpy of association is obtained in the case of $CO_2$ + PEG, which indicates that the interaction between $CO_2$ and an ether (C–O–C) group is stronger than that between $CO_2$ and any other functional group listed in the Table. Furthermore, the value of FWHM for $CO_2$ + PEG is also greater than that for the other systems listed in Table 4.2, which suggests that the solubility of $CO_2$ in PEG is likely to be higher than in the other polymers listed in the table. We have observed that higher negative values of $\Delta H_a$ are associated with higher values of FWHM

for the same electron donating functional group in polymers regardless of the position of the functional groups. Kazarian et al. [35] and Yuan and Teja [38] also reported similar conclusion for several $CO_2$ + polymer systems. Table 4.2 also shows that values of negative $\Delta H_a$ and FWHM are higher when the carbonyl group is in end of the side chain than when it is in near the backbone of the polymer. Thus, negative $\Delta H_a$ and FWHM are larger in the order of: $CO_2$ + PS-co-PMMA < $CO_2$ + PMMA <$CO_2$ + PBMA < $CO_2$ + PVAc < $CO_2$ + EVA40 in which these polymers contain same carbonyl functional group. This could be due to the fact that the carbonyl group in EVA40 is more accessible to $CO_2$ than the carbonyl group in PS-co-PMMA, PMMA, PBMA, and PVAc.

The addition of an alkyl group to the main or to side chain of a $CO_2$-philic polymer leads to stronger interactions with $CO_2$ while it is weaker for the addition of an aromatic group. Thus, the value of the enthalpy of association for $CO_2$ + PBMA system (-8.3 kJ/mol) is more negative than that for $CO_2$ + PMMA (-8.0 kJ/mol). On the other hand, the PS comonomer in PS-co-PMMA has (-$C_8H_8$-) one benzene ring along with ethylene group and strength of the enthalpy of association is weaker for $CO_2$ + PS-co-PMMA system (-7.3 kJ/mol) compare to the $CO_2$ + PMMA system (-8.0 kJ/mol). The benzene ring in PS-co-PMMA may provide stiffness to the segments and reduce the accessibility of the functional group to $CO_2$. Similar analogy holds true for $CO_2$ + PVAc, and $CO_2$ + EVA40 systems. EVA40 is the copolymer of the PVAc and PE and ethylene group in the main chain may increase the mobility of the EVA40 segments compare to the PVAc. Meanwhile, we have observed higher negative $\Delta H_a$ value for $CO_2$ + EVA40 system (-9.6 kJ/mol) compare to the $CO_2$ + PVAc system (-9.3 kJ/mol). We did not observe any regular trend for the value of the $\Delta H_a$ between $CO_2$ + polymer and its

constituent co-polymer system. For example, the value of the negative $\Delta H_a$ increases in the order of $CO_2$ + PMMA (polymer) > $CO_2$ + PS-co-PMMA (co-polymer of PMMA) systems while it is reverse order for $CO_2$ + PVAc < $CO_2$ + EVA40 (co-polymer of PVAc). The value of the $\Delta H_a$ for the interaction between $CO_2$ and PSF (O=S=O) is -8.5 kJ/mol and it is in between the value of the $CO_2$ + acrylic polymer ((O=C)-O) systems (-7.3 – -8.3 kJ/mol) and $CO_2$ + vinyl ester polymer O-(C=O) systems (-9.3 – -9.6 kJ/mol). PSF is much stiffer (higher glass transition temperature) compare to the other polymer studied here since it has several benzene blocks in its repeat unit. However, it has sulfonyl functional group with two oxygen atoms. In addition, it contains ether group in it. Meanwhile, the value of the $\Delta H_a$ in $CO_2$ + PSF system may be dependent on the competing effect between the sulfonyl + ether group and the stiffness offered by the several aromatic rings in the main chain.

## 4.4 Conclusions

A general method that employs *in situ* ATR-IR spectroscopy to obtain enthalpies of interaction between $CO_2$ and carbonyl polymers is extended to other $CO_2$-philic functional groups in this work. Enthalpies of association $\Delta H_a$ were found to become more negative in the following order: $CO_2$ + PS-co-PMMA < $CO_2$ + PMMA < $CO_2$ + PBMA < $CO_2$ + PSF < $CO_2$ + PVAc < $CO_2$ + EVA40 < $CO_2$ + PEG, which implies that interactions between $CO_2$ and the polymer are stronger in the $CO_2$ + PEG system than in the $CO_2$ + PS-co-PMMA system. This suggests that $CO_2$ solubility in the polymers studied would be highest in PEG and lowest in PS-co-PMMA.

Mohammad Z. Hossain, Yanhui Yuan, and Amyn S. Teja, Measurement of Specific Intermolecular Interactions between $CO_2$ and Polymers via *in situ* ATR-FTIR Spectroscopy, The Journal of Supercritical Fluids (Submitted, August 2014)

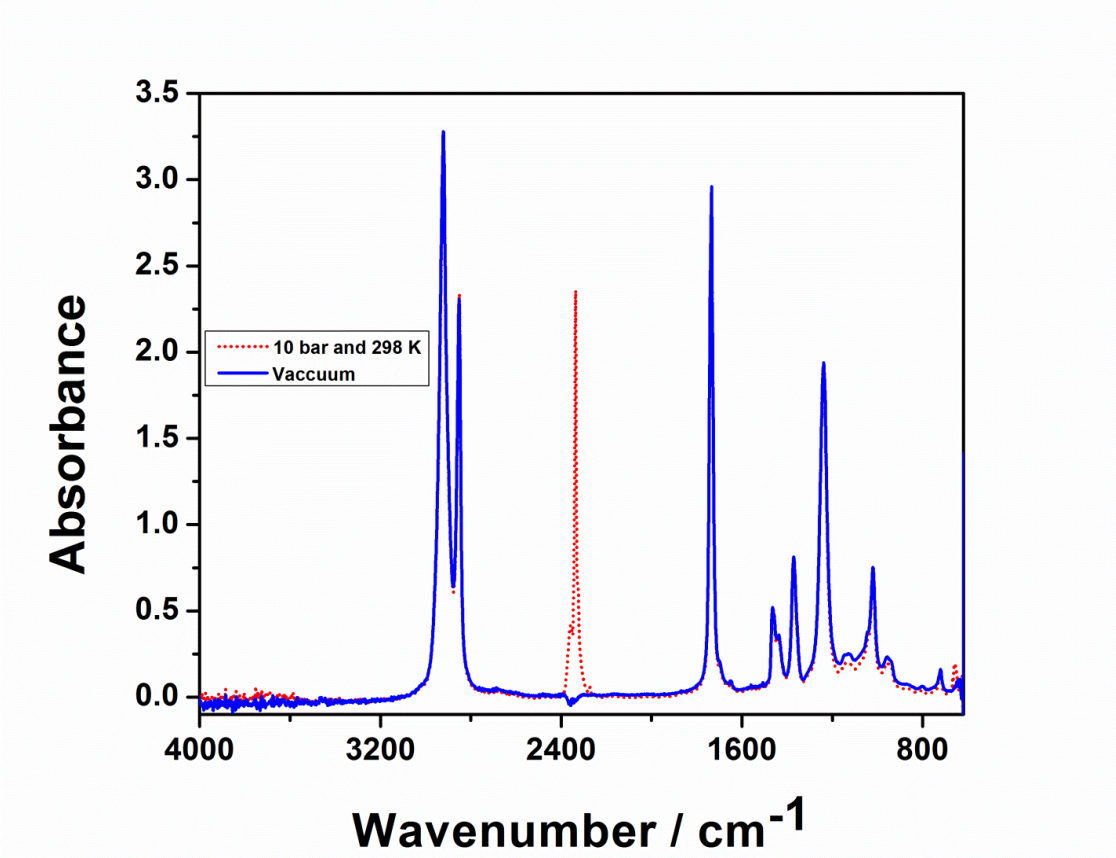


**Figure 4.1** IR spectra of EVA40 before (blue solid line) and after (red dotted line) exposure to 10 bar $CO_2$ at 298 K

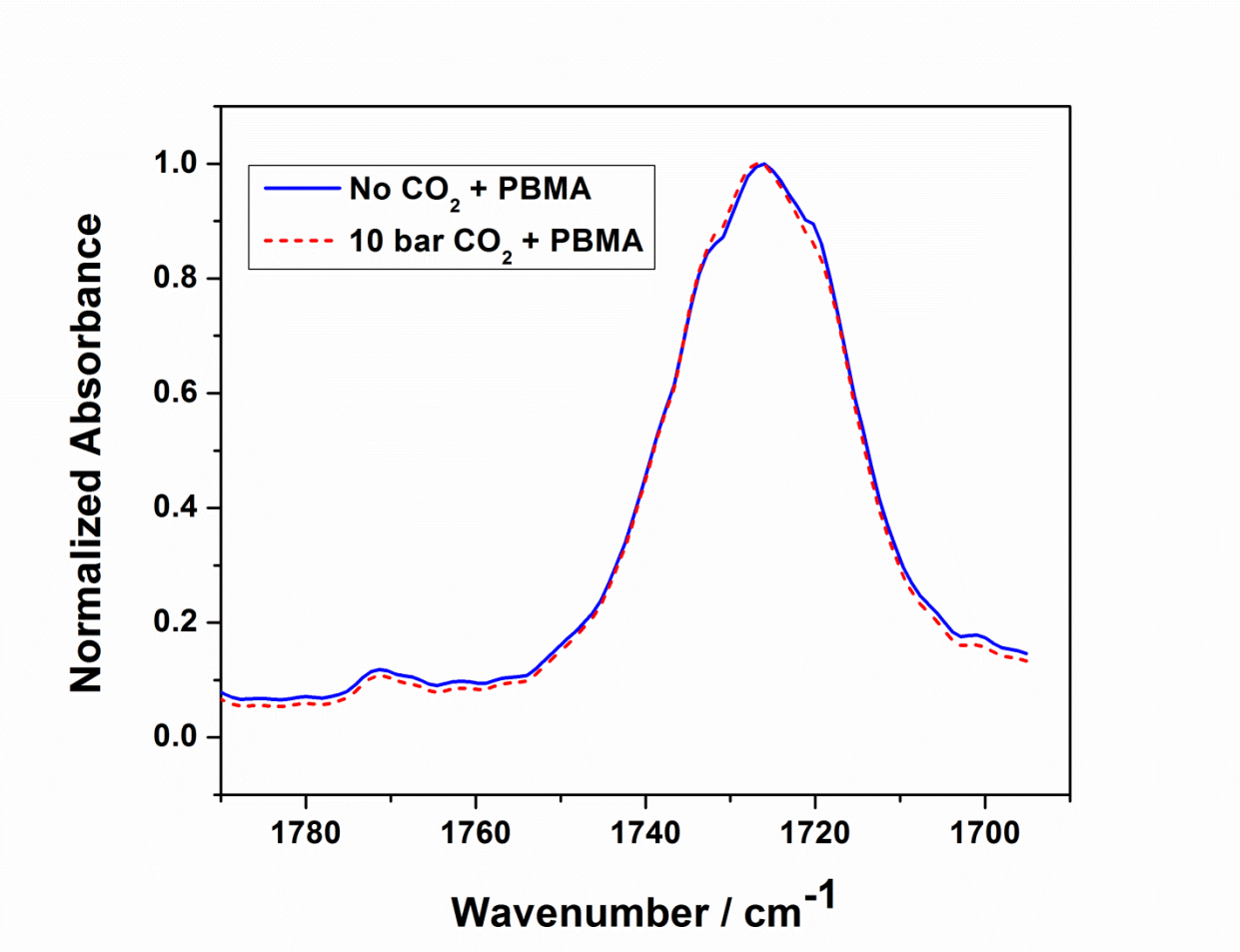


**Figure 4.2** Normalized C=O stretching spectrum in PBMA before and after $CO_2$ exposure at 318 K

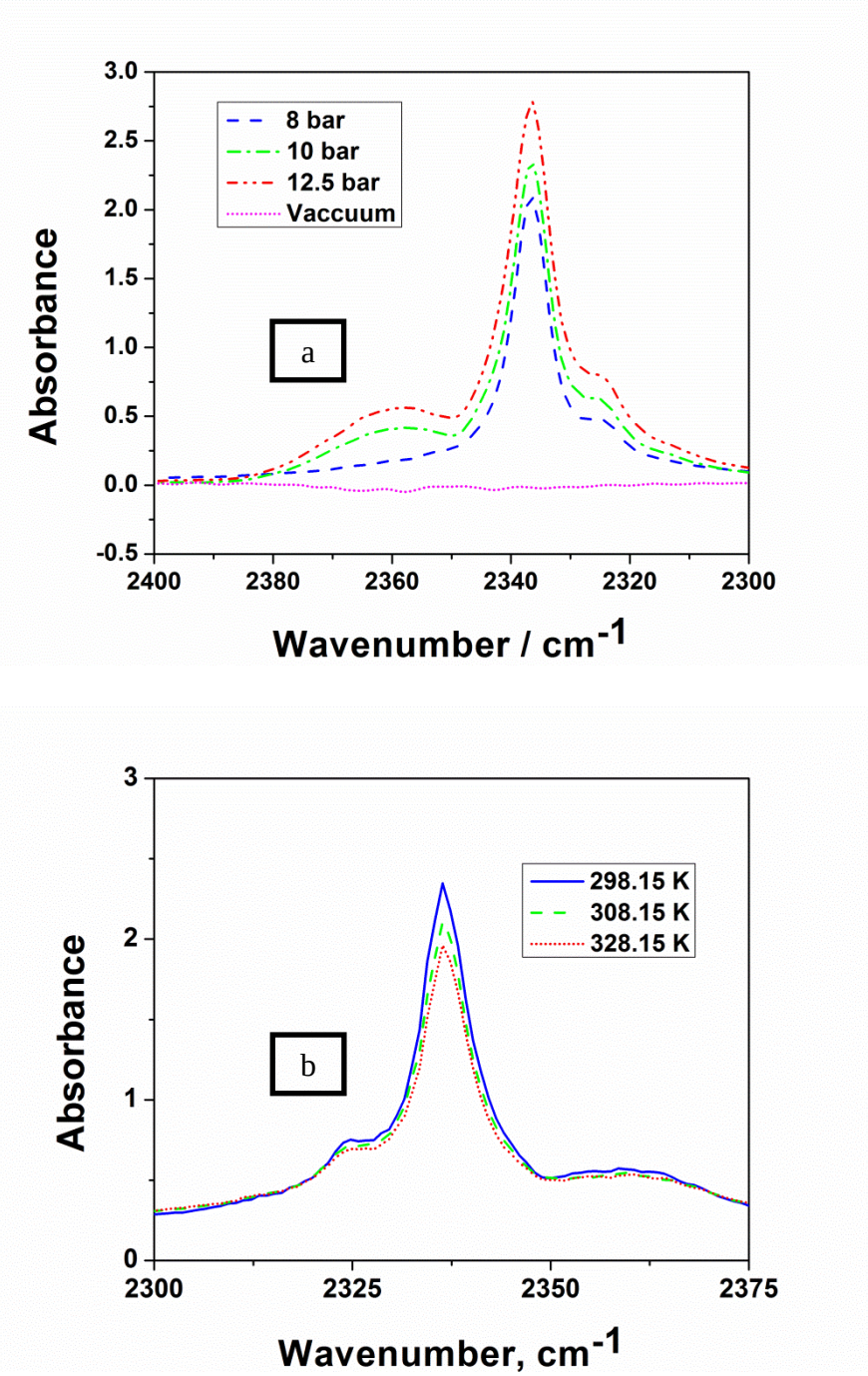


**Figure 4.3** Anti-symmetric stretching frequencies of EVA40 + $CO_2$ at different pressures (a) and temperatures (b).

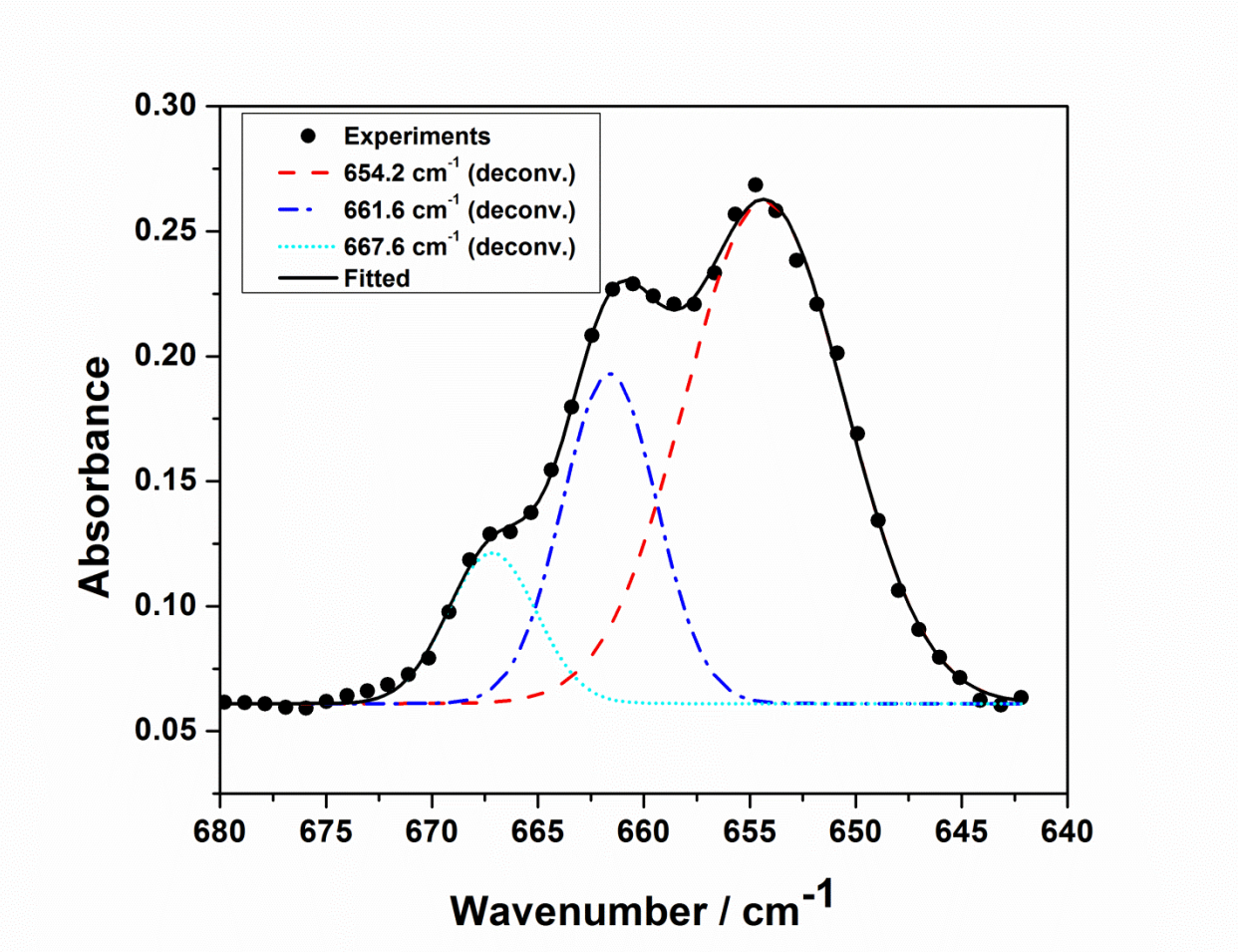


**Figure 4.4** Bending mode of $CO_2$ in the IR spectrum of $CO_2$ + PBMA at 10 bar and 298 K; solid circles represent experimental data; the solid line represents curve fit of the experiments; and the dashed lines are deconvoluted peaks. Gas phase $CO_2$ peak is at 668 $cm^{-1}$, impregnated $CO_2$ peak is at 662 $cm^{-1}$, and 654 $cm^{-1}$.

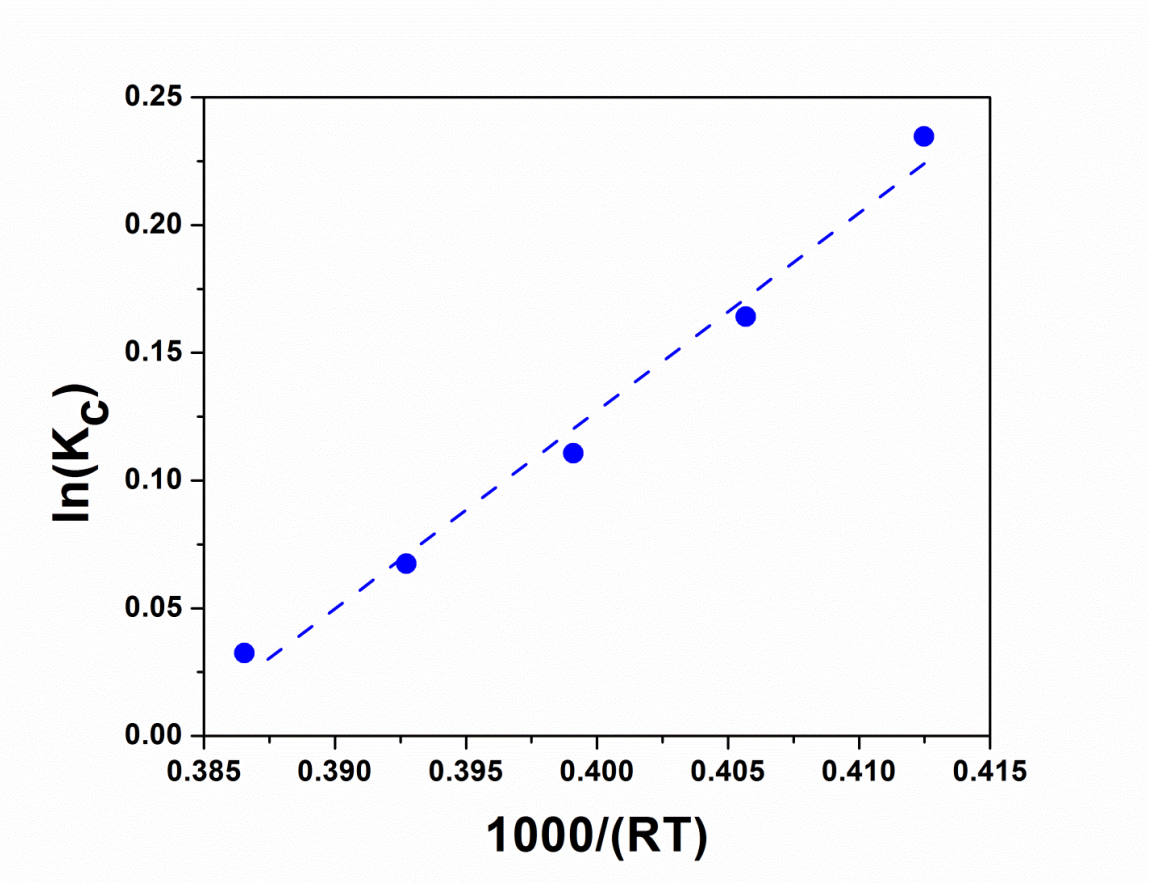


**Figure 4.5** van't Hoff plot for $CO_2$ – PS-co-PMMA system at 298 K to 318 K and 10 bar $CO_2$ pressure ($R^2$ = 0.98); line represents a least squares fit of data.

**Table 4.1** Wavenumber of C=O stretching peaks for different polymers in vacuum and under $CO_2$ pressure

| C=O stretching | Solid polymer | Polymer + 8 bar $CO_2$ | Polymer + 10 bar $CO_2$ | Polymer + 40 bar $CO_2$ | Reference |
|---|---|---|---|---|---|
| PMMA | 1728.2 | - | 1728.3 | 1729.6 | [38][a] |
| PS-co-PMMA | 1726.0 | - | 1727.9 | - | This work[a] |
| PBMA | 1726.0 | - | 1727.0 | - | This work[b] |
| PVAc | 1734.5 | - | 1735.0 | 1735.5 | [38][a] |
| EVA40 | 1734.7 | - | 1736 | - | This work[b] |
| P120 | 1716.8 | 1720.5 | - | - | [36][c] |
| P130 | 1717.9 | 1719.9 | - | - | [36][c] |

Note: a – 298.15 K; b – 318.15 K; c – 313.15 K; P120 – Propoxy based polyester; P120 – Ethoxy based polyester.

**Table 4.2** Strength of specific interactions and the full width at half max of the bending mode of $CO_2$ in polymers with different functional groups.

| Polymer | Functional group | $\Delta H_a$ / kJ·mol$^{-1}$ | $\Delta \nu_{1/2}$ / cm$^{-1}$ | Reference |
|---|---|---|---|---|
| PS-co-PMMA | (O=C)-O | 7.3 ± 0.3 | 14.5 | This work |
| PMMA | (O=C)-O | 8.0 ± 0.2 | 15.0 | [38] |
| PBMA | (O=C)-O | 8.3 ± 0.1 | 15.5 | This work |
| PVAc | O-(C=O) | 9.3 ± 0.3 | 16.0 | [38] |
| EVA40 | O-(C=O) | 9.6 ± 0.4 | 17.5 | This work |
| PEG | C-O-C | 11.5 ± 0.3 | 22.0 | [38] |
| PSF | O=S=O | 8.5 ± 0.3 | 13.0 | [38] |

# CHAPTER 5: EXTENSION OF THE ALF EQUATION OF STATE TO $CO_2$ + IONIC LIQUID SYSTEMS

In this chapter, the Associated Lattice – Fluid (ALF) Equation of State (EOS) is used for correlating / predicting the volumetric and phase behavior of $CO_2$ + imidazolium-based ionic liquids (ILs) over a wide range of pressures and temperatures. The contents of this chapter have been published in the Journal of Chemical & Engineering Data, 59 (2013) 1038-1044.

## 5.1 Introduction

The use of $CO_2$ + IL systems has been proposed in numerous applications such as $CO_2$ capture from flue gases [230], separation of organic solutes using $CO_2$ [137-139], and biphasic catalytic reactions [231-234]. These applications need fundamental data related to the volumetric and phase behavior of $CO_2$ + IL systems. Such data must either be measured or calculated from thermodynamic models. There is evidence [14, 142] to suggest that specific interactions between $CO_2$ and the anion of an IL have measurable effect on the phase behavior of some of these systems. However, very few thermodynamic models consider specific interactions explicitly.

Conventional EOS models such as the Peng–Robinson (PR) [144, 145] and Redlich–Kwong (RK) EOS [18, 146, 147] have been successfully used in describing the phase behavior of $CO_2$ + IL systems. However, these cubic EOS models are limited in their predictive capability, since they require three or more temperature – dependent binary interaction parameters to correlate phase equilibrium data. Excess Gibbs energy models have also been applied to the calculation of alkane/alkene + IL phase behavior

[149, 151]. However, activity coefficient models such as the UNIFAC equation require volume and surface parameters for the ILs, along with two or more binary parameters. In addition, activity coefficient models also have limited predictive capabilities and they are not capable of providing volumetric data. The truncated perturbed chain – polar statistical associating fluid theory (tPC-PSAFT) of Karakastani et al. [153, 235], the soft-SAFT model of Andreu and Vega [236, 237], and the Sanchez and Lacombe (SL) EOS extensions of Tome et al. [238] and Machida et al. [239] have also been used successfully to correlate phase equilibria in $CO_2$ + IL systems. However, these models incorporate binary interaction parameters that are temperature and/or molecular weight-dependent.

In this study, the Associated Lattice-Fluid (ALF) Equation of State (EOS) [6] is extended to $CO_2$ + imidazolium based IL systems [240]. The ALF EOS was derived by incorporating the GHM lattice partition function [117] with a contribution for association [46, 47] used in the compressible lattice (CLM) model as shown in chapter 3. The association contribution of the model contains physically meaningful parameters which do not depend on pressure or temperature.

The application of the ALF EOS is demonstrated for the calculation of the $CO_2$ solubility in several homologous series of ILs with a common anion. The ILs investigated include 1-n-alkyl-3-methylimidazolium bis(trifluoromethylsulfonyl)imide ([$C_n$mim][$Tf_2$N]), 1-n-alkyl-3-methylimidazolium tetrafluoroborate ([$C_n$mim][$BF_4$]), 1-n-alkyl-3-methylimidazolium hexafluorophosphate ([$C_n$mim][$PF_6$]), and 1- n-alkyl -3-methylimidazolium trifluoroacetate ([$C_n$mim][ TFA]) with *n* ranging from 1 to 10. It is noted that there are 10, 6, 4, and 4 $CO_2$ – philic groups in the $Tf_2$N, $PF_6$, $BF_4$, and TFA anions ($Tf_2$N has six fluorine and four sulfonyl groups, $PF_6$ has six fluorine groups, $BF_4$

has four fluorine groups, and TFA contains three fluorine groups and one carbonyl group). It should therefore be possible to determine the effect of these groups on the binary parameters of the ALF EOS. Finally, it should also be possible to predict volumetric properties such as swelling using values of the binary parameters obtained by fitting solubility data.

## 5.2 Associated Lattice Fluid (ALF) Model

The detail derivation of the ALF EOS is described in chapter 3. We have used Equation 3.25 to Equation 3.26 to calculate the solubility of $CO_2$ (1) in an IL (2) by equating the chemical potential of pure $CO_2$ in the gas phase to the chemical potential of $CO_2$ dissolved in the IL. Equation 3.14 and 3.27 are used to calculate the extent of swelling $S_w$ due to $CO_2$ dissolution in the IL at a given $P$ and $T$. Mixing rules contain two mixture parameters, such as $K_0$ and $\Delta H_a$ shown in Equation 3.15 to 3.24. The following section illustrates the method for estimating the pure component as well as mixture parameters in the solubility and swelling calculations.

## 5.3 Results and discussion

To calculate phase equilibrium in $CO_2$ + IL systems, it is first necessary to obtain the characteristic constants $P^*$, $T^*$, $\rho^*$ (or $\varepsilon_i^*$, $v_i^*$, $r_i$) for the pure ILs. These constants are obtained by non-linear least squares fit of *PVT* data of each IL and are listed in Table 5.1. Characteristic constants of the SL EOS for some of the ILs from the literature are also listed in Table 5.1. The two sets of pure component constants are almost identical, especially the closed packed volume ($v^*r$). Minor differences in values can be attributed to the use of different sets of *PVT* data during fitting of the two models. This suggests

that it is possible to use SL EOS constants when ALF EOS constants are not available. Table 5.1 also includes the characteristic constants for pure $CO_2$ from the work of Condo et al. [206].

As mentioned above, the ALF EOS requires two binary parameters ( $K_0$ and $\Delta H_a$ ) in calculations involving mixtures. One is the enthalpy of association $\Delta H_a$ that can be obtained from FTIR measurements, quantum calculations, or via molecular modeling [1, 6, 38, 69]. Unfortunately, no values of $\Delta H_a$ for $CO_2$ + IL systems have been reported. On the other hand, enthalpies of absorption are available for several $CO_2$ + IL systems [14, 15, 140, 141, 241]. Therefore, this work assumes that enthalpies of absorption provide reasonable estimates of $\Delta H_a$, or that both $\Delta H_a$ and the enthalpy of absorption exhibit similar trends within a series of ILs with a common ion. At worst, it is expected that relative values of both properties remain constant within a series. This leaves $K_0$ as an adjustable parameter to account for differences between the enthalpy of absorption and $\Delta H_a$ values, as well as for limitations of the theory.

The results of our calculations using the ALF EOS are demonstrated in Table 5.2 for each $CO_2$ + IL system studied. The Table includes the $\Delta H_a$ value used in our calculations, the source of the $\Delta H_a$ value (literature value or estimate), and the value of $K_0$ obtained by fitting solubility data using the ALF EOS, the average absolute deviations (AAD) between calculated and experimental $CO_2$ solubilities in each IL, and the solubility data references. Literature citations for the value of the enthalpy of absorption are listed in Table 5.2 when these values are available. In cases where literature values are not available, the values of the enthalpies of absorption are estimated

based on the assumption that ILs with a common anion exhibit regular trends within a series. Figure 5.1 demonstrates our procedure. Figure 5.1a confirms that the enthalpy of absorption of $CO_2$ + [$C_n$mim][$TF_2N$] mixtures with $n$ = 2, 4, 6 increases linearly with $n$. Therefore, the value when $n$ = 8 is easily estimated. The same type of interpolation/extrapolation is demonstrated in Figure 5.1b for the enthalpy of absorption of $CO_2$ + [$C_n$mim][$BF_4$] mixtures. Only one enthalpy of absorption value is available for $CO_2$ + [$C_n$mim][$PF_6$] mixture with $n$ = 4 and for $CO_2$ + [$C_n$mim][TFA] mixture with $n$ = 2. In such cases, we have assumed that ILs with organic fluorinated anions such as [$Tf_2N$] and [TFA] display similar trends, as do ILs with inorganic fluorinated anions such as [$PF_6$] and [$BF_4$]. Figure 5.1 demonstrates these extrapolations.

Table 5.2 shows the ALF EOS performance for $CO_2$ + IL systems. In general, solubility data for such systems can be correlated with AADs between 1-6 % over a range of temperatures and pressures. Figure 5.2 illustrates the fit for the $CO_2$ + [$C_n$mim][$Tf_2N$] series, while Figure 5.3 demonstrates the fit for $CO_2$ + [$C_4$mim][Tf2N], $CO_2$ + [$C_4$mim][$PF_6$], $CO_2$ + [$C_4$mim][TFA] and $CO_2$ + [$C_4$mim][$BF_4$] systems. Moreover, the values of $K_0$ exhibit regular trends with increasing size of the cation within an IL series with a common anion. Consequently, the values of $K_0$ decreases with the size of the cation in the three series $CO_2$ + [$C_n$mim][$TF_2N$], $CO_2$ + [$C_n$mim][$PF_6$], and $CO_2$ + [$C_n$mim][TFA] reflecting decreasing solubility of $CO_2$ with the size of the cation. The strength of association decreases with size of the cation (- $\Delta H_a$ decreases with $n$) which is a result of decreasing $CO_2$ solubility. Note that free volume increases with size of the cation and should lead to increasing $CO_2$ solubility. Finally, as presented in Table 5.3 for [$C_n$mim][$Tf_2N$] ILs, differences in solubility parameters between $CO_2$ and ILs decrease

with size of the cation within a series, suggesting that $CO_2$ solubility should increase with size of the cation. As a result, it would seem that free volume as well as dispersion effects dominate in the three series $CO_2$ + [$C_n$mim][$TF_2N$], $CO_2$ + [$C_n$mim][$PF_6$], and $CO_2$ + [$C_n$mim][TFA].

The values of $K_0$ in $CO_2$ + [$C_n$mim][$BF_4$] systems do not follow a decreasing trend with the size of the cation. However, the values of $K_0$ appear to be strongly influenced by the experimental data used in the correlation. Thus the solubility data of Kroon et al. [19] yield a value of $K_0$ of 0.109, while the data of Aki et al. [16] for $CO_2$ + [$C_4$mim][$BF_4$] systems yield a value of $K_0$ of 0.075. Therefore, it is not possible to say whether association, dispersion, or free volume forces govern the phase equilibrium in these systems.

Figure 5.4 illustrated the results of swelling calculations in $CO_2$ + ILs mixtures in the case of $CO_2$ + $C_4$mim][$PF_6$] system. Swelling ratios were predicted using parameters that were estimated by fitting solubility data, so that no additional adjustable parameters were incorporated in the model. The calculated swelling ratios agree with measured values within experimental error which is shown in Figure 5.4.

## 5.4 Conclusions

The extension of the Associated Lattice Fluid Equation of State model has been described to the calculation of volumetric and phase behavior of $CO_2$ + imidazolium-based IL systems. Although two binary parameters are necessary in the calculations, these parameters are independent of temperature, or pressure. Moreover, we have shown that one of the parameters can be estimated from enthalpy of absorption measurements.

Thus, only one adjustable parameter has been used to correlate the solubilities of $CO_2$ in a number of ILs over a wide range of temperatures and pressures. The calculated $K_0$ values follow regular trends with the size of the cation in an IL series with a common anion. The value of $K_0$ also allows us to conclude whether association, or dispersion and free volume effects influence phase equilibria in an IL system. Finally, the swelling behavior of these ILs in $CO_2$ + IL systems was predicted without any additional adjustable parameters. The ALF EOS therefore demonstrates substantial promise in calculating both phase equilibrium and volumetric data of $CO_2$ + IL systems.

Mohammad Z. Hossain, Amyn S. Teja, Extension of an Associated Lattice–Fluid Equation of State to $CO_2$ + Ionic Liquid Systems, Journal of Chemical & Engineering Data, 59 (2013) 1038-1044

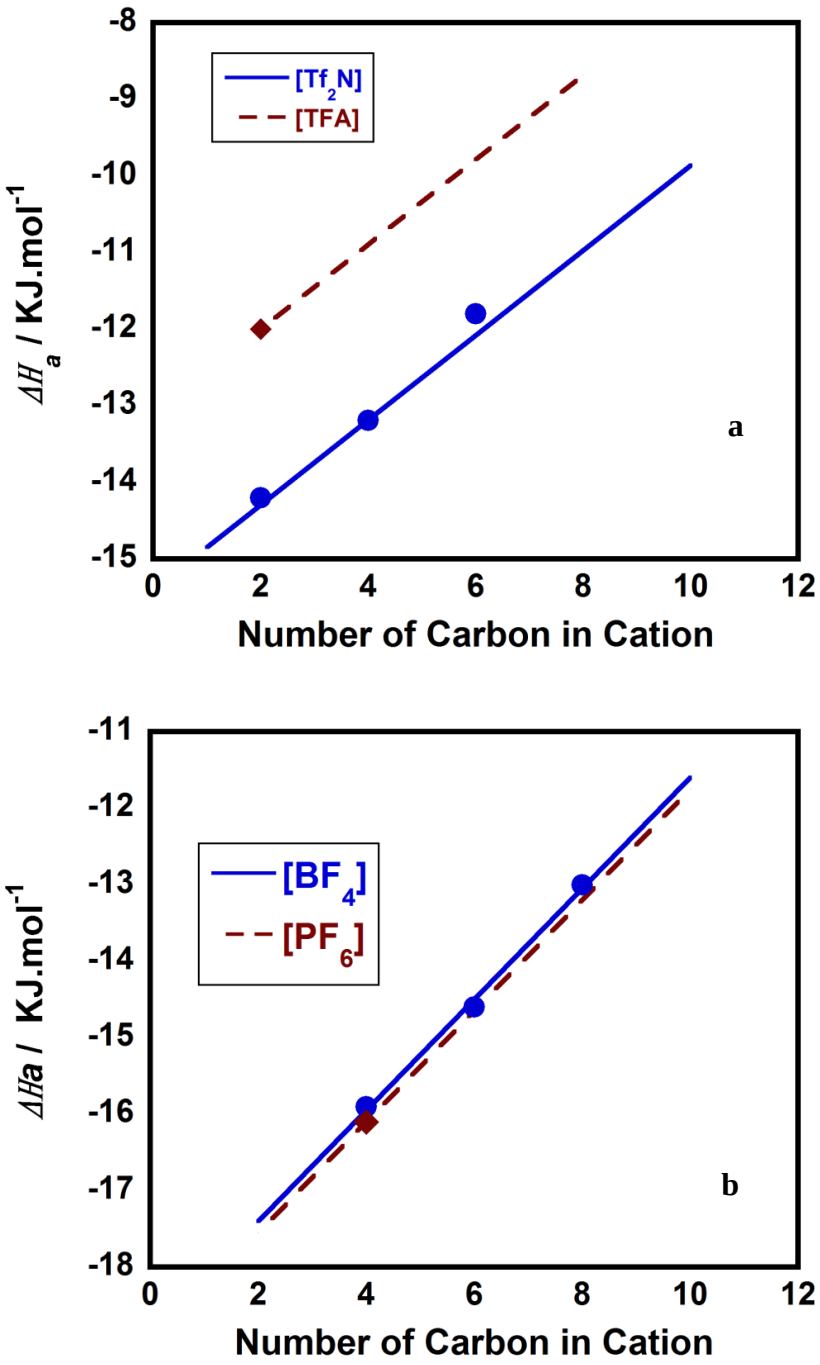


**Figure 5.1** Enthalpy of absorption versus number of alkyl groups *n* for (a) $CO_2$ + [$C_n$mim][$Tf_2N$] and $CO_2$ + [$C_n$mim][TFA] (b) $CO_2$ + [$C_n$mim][$BF_4$] and $CO_2$ + [$C_n$mim][$PF_6$]; lines are fitted and points represent literature data [14-16].

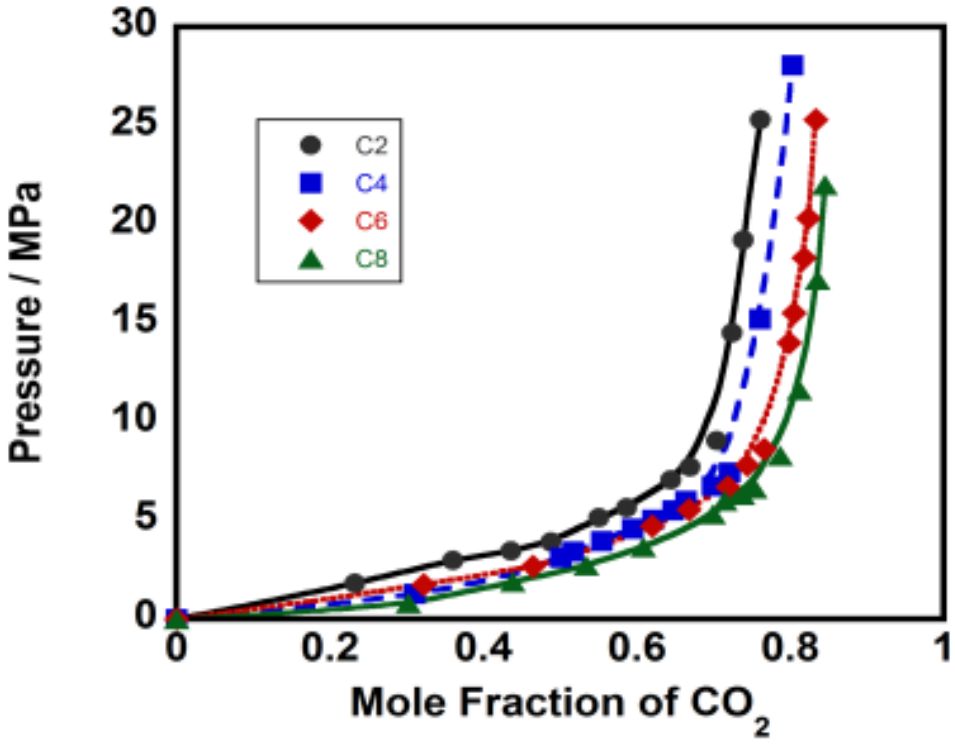


**Figure 5.2** Solubility of $CO_2$ in $[C_2mim][Tf_2N]$, $[C_4mim][Tf_2N]$, $[C_6mim][Tf_2N]$, and $[C_8mim][Tf_2N]$ at 314.15 K; lines are calculated from the model and points are experimental results [17].

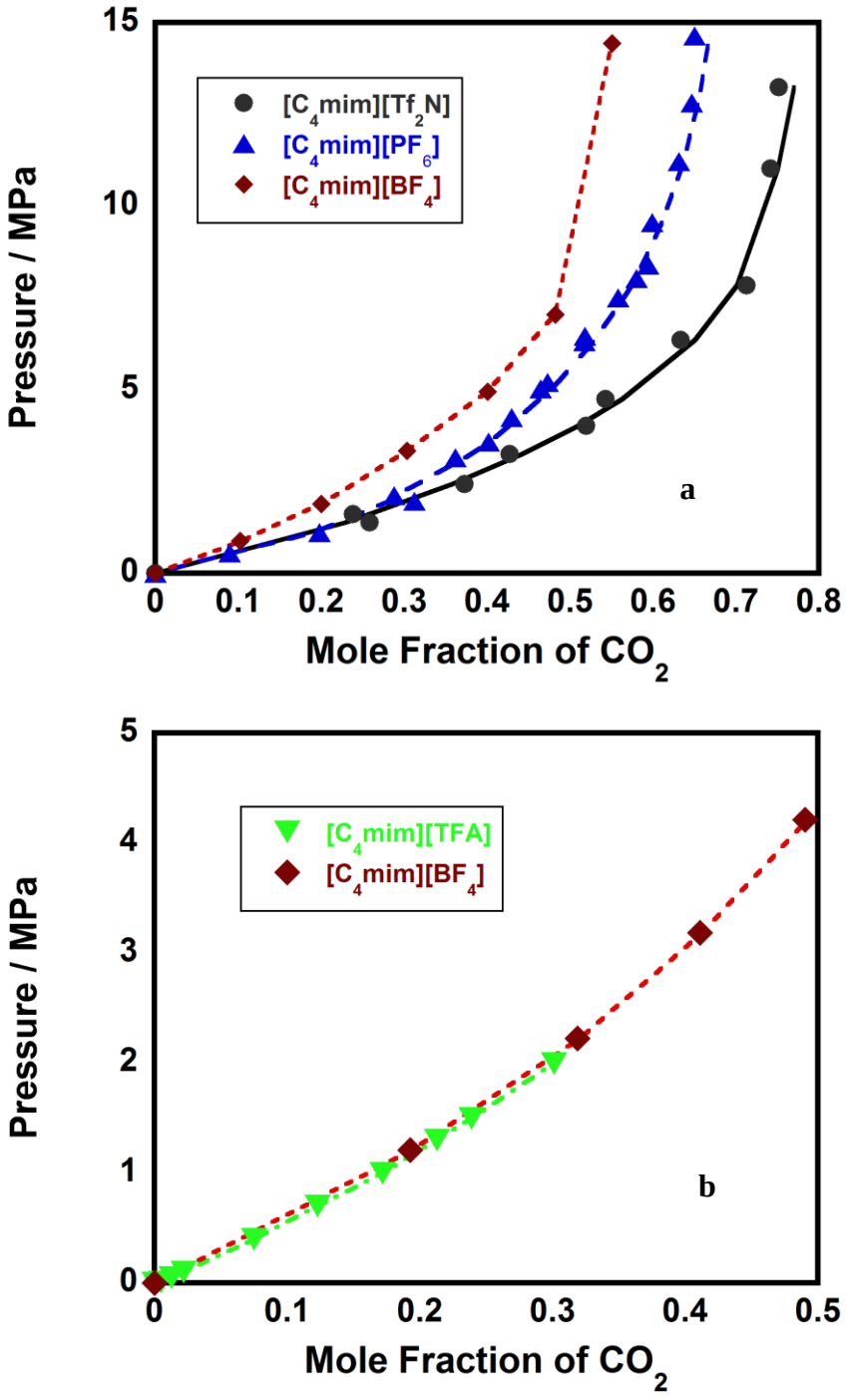


**Figure 5.3** Solubility of $CO_2$ in (a) [$C_4$mim][Tf2N], [$C_4$mim][$PF_6$], and [$C_4$mim][$BF_4$] at 313.2 K and (b) [$C_4$mim][$BF_4$] and [$C_4$mim][TFA] at 298.2 K; lines are calculated from the model and points are experimental results [16, 18, 19].

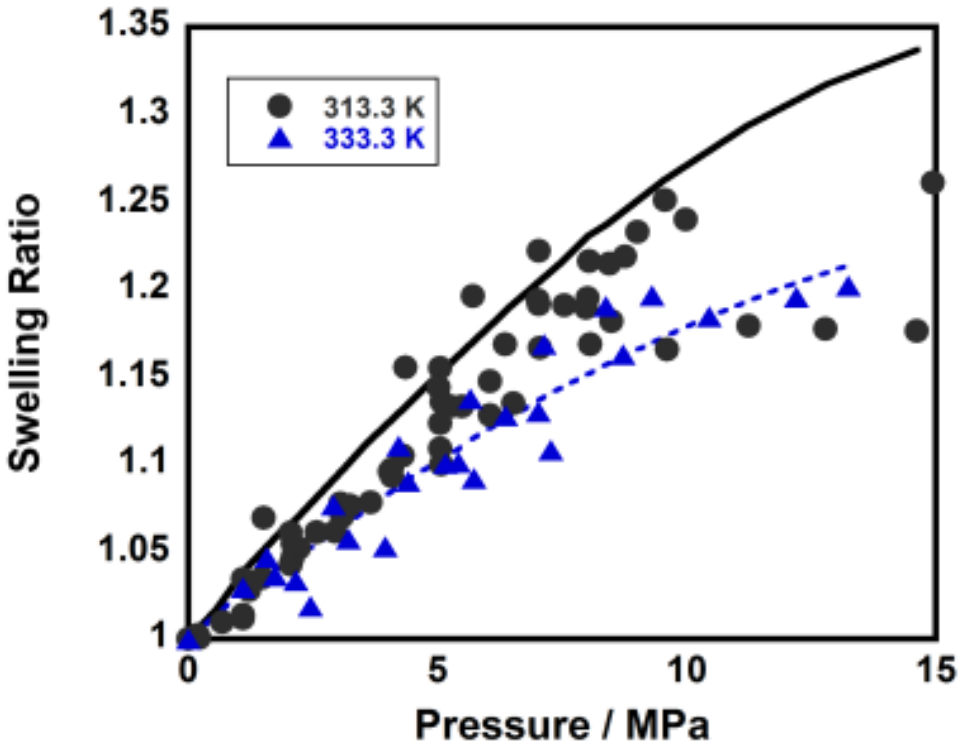


**Figure 5.4** Swelling of $[C_4mim][PF_6]$ due to $CO_2$ ; lines are calculated from the model and points are experimental results [16, 20, 21].

**Table 5.1** Characteristic Constants of the ALF and SL Equations for Pure Components

| ILs | $T^*$ / K | $P^*$ / MPa | $\rho^*$ / kg·m$^{-3}$ | $v^*r$ / cm$^3$·mol$^{-1}$ | Ref. | Data Ref |
|---|---|---|---|---|---|---|
| [$C_1$mim][$Tf_2$N] | 638.3 | 845.8 | 1669.87 | 225.94 | This | [242] |
| [$C_2$mim][$Tf_2$N] | 651.6 | 723.2 | 1610.56 | 242.97 | This | [243] |
| [$C_3$mim][$Tf_2$N] | 589.8 | 497.2 | 1599.09 | 253.48 | This | [244] |
| [$C_4$mim][$Tf_2$N] | 654.1 | 498.8 | 1526.16 | 274.79 | This | [242] |
| | 592.2 | 473.1 | 1555.00 | 269.69 | [239] | |
| [$C_5$mim][$Tf_2$N] | 591.8 | 455.5 | 1519.75 | 285.17 | This | [244] |
| [$C_6$mim][$Tf_2$N] | 648.2 | 408.7 | 1457.50 | 306.98 | This | [245] |
| [$C_7$mim][$Tf_2$N] | 644.3 | 451.8 | 1433.37 | 321.93 | This | [246] |
| [$C_8$mim][$Tf_2$N] | 584.4 | 495.8 | 1433.49 | 331.69 | This | [246] |
| [$C_{10}$mim][$Tf_2$N] | 607.8 | 410.9 | 1375.54 | 366.05 | This | [238] |
| | 598.4 | 544.7 | 1382.40 | 364.30 | [238] | - |
| [$C_2$mim][$BF_4$] | 656.4 | 605.2 | 1381.79 | 143.27 | This | [246] |
| [$C_4$mim][$BF_4$] | 691.2 | 669.7 | 1263.38 | 178.91 | This | [247] |
| | 708.3 | 569.9 | 1260.00 | 179.39 | [247] | |
| [$C_6$mim][$BF_4$] | 665.0 | 491.2 | 1213.00 | 209.46 | This | [248] |
| | 684.5 | 491.0 | 1208.00 | 210.33 | [239] | |
| [$C_8$mim][$BF_4$] | 678.3 | 524.0 | 1162.89 | 242.61 | This | [249] |
| | 685.9 | 445.0 | 1162.00 | 242.80 | [239] | |
| [$C_4$mim][$PF_6$] | 677.5 | 799.7 | 1441.33 | 197.17 | This | [243] |
| | 680.5 | 542.0 | 1448.00 | 196.26 | [247] | - |
| [$C_6$mim][$PF_6$] | 637.1 | 471.5 | 1379.61 | 226.32 | This | [248] |
| | 675.9 | 487.5 | 1369.00 | 228.07 | [239] | - |
| [$C_8$mim][$PF_6$] | 645.5 | 457.3 | 1315.18 | 258.74 | This | [248] |
| | 668.2 | 485.4 | 1311.00 | 259.57 | [239] | |
| [$C_9$mim][$PF_6$] | 603.8 | 568.9 | 1285.26 | 275.68 | This | [250] |
| [$C_2$mim][TFA] | 756.4 | 776.6 | 1347.36 | 166.38 | This | [18] |
| [$C_4$mim] [TFA] | 697.5 | 761.6 | 1282.63 | 196.65 | This | [18] |
| $CO_2$ | 308.6 | 574 | 1505.00 | - | [206] | - |

**Table 5.2** Correlation of $CO_2$ Sorption in ILs

| General Formula | Systems with $CO_2$ | $\Delta H_a$ / KJ·mol$^{-1}$ | $\Delta H_a$ Ref | $K_0$ | AAD % | Solubility Data Ref |
|---|---|---|---|---|---|---|
| 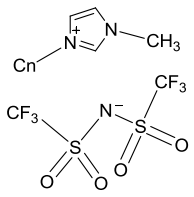 | [$C_2$mim][$Tf_2N$] | -14.20 | [14] | 0.138 | 0.60 | [17, 251] |
| | [$C_4$mim][$Tf_2N$] | -13.19 | [16] | 0.112 | 2.71 | [16, 17] |
| | [$C_5$mim][$Tf_2N$] | -12.63 | xx | 0.051 | 0.33 | [16] |
| | [$C_6$mim][$Tf_2N$] | -11.80 | [15] | 0.050 | 0.19 | [17] |
| | [$C_8$mim][$Tf_2N$] | -11.00 | xx | 0.020 | 0.32 | [17, 252] |
| | [$C_{10}$mim][$Tf_2N$] | -9.90 | xx | 0.016 | 0.24 | [252] |
| 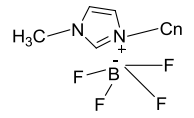 | [$C_2$mim][$BF_4$] | -17.40 | xx | 0.031 | 0.52 | [253] |
| | [$C_4$mim][$BF_4$] | -15.90 | [14] | 0.109 | 0.76 | [19] |
| | [$C_4$mim][$BF_4$] | -15.90 | [14] | 0.075 | 0.84 | [16] |
| | [$C_6$mim][$BF_4$] | -14.60 | [15] | 0.077 | 3.24 | [254] |
| | [$C_8$mim][$BF_4$] | -13.00 | [15] | 0.116 | 1.24 | [255] |
| 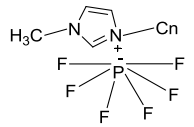 | [$C_4$mim][$PF_6$] | -16.10 | [14] | 0.140 | 3.82 | [16] |
| | [$C_6$mim][$PF_6$] | -14.65 | xx | 0.051 | 0.47 | [254] |
| | [$C_8$mim][$PF_6$] | -13.20 | xx | 0.059 | 3.84 | [21] |
| | [$C_9$mim][$PF_6$] | -12.50 | xx | 0.033 | 1.30 | [250] |
| 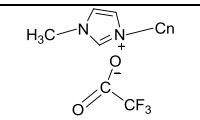 | [$C_2$mim][TFA] | -12.00 | [15] | 0.208 | 5.40 | [18] |
| | [$C_4$mim][TFA] | -10.89 | xx | 0.172 | 6.94 | [18] |

[a] Notation: xx, extrapolated value (see Figure 1).

**Table 5.3** Solubility Parameters of $[C_n mim][Tf_2N]$ ILs at 298.15 K

| ILs | $\delta$ / $MPa^{-1/2}$ |
|---|---|
| $[C_2mim][Tf_2N]$ | 27.6 [256] |
| $[C_4mim][Tf_2N]$ | 26.7 [256] |
| $[C_6mim][Tf_2N]$ | 25.6 [256] |
| $[C_8mim][Tf_2N]$ | 25.0 [256] |
| $CO_2$ | 12.3 [257] |

# CHAPTER 6: CONCLUSIONS AND RECOMMENDATIONS

## 6.1 Conclusions

A new Associated Lattice-Fluid Equation of State has been derived for $CO_2$ + polymer systems. The new EOS incorporates two mixture parameters -- the enthalpy of association $\Delta H_a$ and the equilibrium constant at a reference temperature $K_0$. These parameters were found to be independent of temperature, pressure or molecular weight. Values of $\Delta H_a$ were obtained from independent FTIR measurements in this work, whereas values of $K_0$ were obtained by fitting solubility data. The new EOS was able to correlate solubility data within experimental error (maximum AAD of about 4%). Furthermore, swelling and cloud point pressures in $CO_2$ + polymer systems were predicted without any additional parameters. Finally, it should be added that both LCST and UCST type cloud point behavior could be predicted using this approach.

A general method for estimating the strength of specific interactions between $CO_2$ and $CO_2$ – philic polymers using *in situ* ATR-FTIR experiments was outlined in this work. The application of the method was demonstrated by obtaining the enthalpies of association of $CO_2$ – polymer/copolymer systems using the bending mode of $CO_2$. $\Delta H_a$ values obtained follow regular trends with the type of the structure and functional group and its position in the polymer chain. The trend can be used for qualitative estimation of specific interactions when no experimental data are available. Enthalpies of association in $CO_2$ + $CO_2$ – philic polymer systems were observed to be between -7.3 kJ/mol and -11.5 kJ/mol in the order of $CO_2$ + PS-co-PMMA < $CO_2$ + PMMA <$CO_2$ + PBMA < $CO_2$ + PSF < $CO_2$ + PVAc < $CO_2$ + EVA40 < $CO_2$ + PEG.

The ALF EOS was also extended to the calculation of phase equilibria and swelling behavior of $CO_2$ + imidazolium-based IL systems. In these systems, $\Delta H_a$ values were obtained from enthalpy of absorption measurements. $K_0$ was treated as an adjustable parameter and obtained by fitting solubility data at one isotherm. Calculated $K_0$ values followed regular trends with the size of the cation in an IL series with a common anion. Moreover, $K_0$ values can be used to determine the influence of association, dispersion, or free volume on $CO_2$ solubility in ILs. Lastly, the extents of swelling of $CO_2$ + IL systems were predicted without any additional parameters.

## 6.2 Future work

Solubility data were used to obtain $K_0$ values. The experimental swelling data is generally less reliable due to higher experimental uncertainty and it could lead to unreliable predictions. However, it would be desirable to obtain $K_0$ values using cloud point data.

In Chapter 3, a general method to quantify specific interactions in $CO_2$ + polymer systems was established. This method can also be used to investigate specific interactions between $CO_2$ and $CO_2$ – philic ILs, poly (ILs), and Metal Organic Framework (MOF). MD simulations have suggested that an anion in ionic liquids affects the bending mode of $CO_2$ [258] so that it should be possible to use ATR – FTIR to measure enthalpies of interaction. This needs to be confirmed so that novel ILs for $CO_2$ capture may be designed.

The new ALF EOS needs to be extended to phase equilibria in $CO_2$ + small molecules. This will require both FTIR and phase equilibrium measurements. Several studies have used quantum calculations to study specific interactions between $CO_2$ and $CO_2$ – philic organic materials using the bending mode of $CO_2$ to quantify specific interactions [1, 39]. Meredith et al. [69] used FTIR experiments quantify specific interactions between $CO_2$ and a few $CO_2$ – philic organic materials using the bending mode of $CO_2$. More systems need to be investigated.

Recently, Neau et al. [259] suggested that fugacity rather than chemical potentials should be employed when the SL EOS is used for phase equilibrium calculations in $CO_2$ + organic solids. The fugacity coefficient can be derived from the residual Helmholtz free energy ( $A^{res}$ ) as follows:

$$\ln \varphi_i = \frac{1}{RT}\left(\frac{\partial A^{res}(T,V,N)}{\partial N_i}\right)_{(T,V,N_j)} - \ln Z \tag{6.1}$$

where $Z$ is the compressibility factor. From classical thermodynamics:

$$A^{res}(T,V,N) = -\int_{\infty}^{V}\left(P - N\frac{RT}{V}\right)dV = -NRT\int_{\infty}^{V}(Z-1)\frac{dV}{V} \tag{6.2}$$

The compressibility and the fugacity coefficient can be expressed as follows:

$$Z = \frac{Pv}{RT} = \frac{\tilde{P}P^*\tilde{v}V^*}{R\tilde{T}T^*} = \frac{\tilde{P}P^*\tilde{v}rv^*}{R\tilde{T}T^*} = \frac{\tilde{P}\tilde{v}r}{\tilde{T}} \times \frac{P^*v^*}{RT^*} = \frac{r\tilde{P}}{\tilde{T}\tilde{\rho}} \tag{6.3}$$

$$\ln \varphi_i = r_i\left(-\frac{2\tilde{\rho}}{\tilde{T}} - \ln(1-\tilde{\rho})\right) + \left(\frac{Z-1}{r}\right)\left(\frac{\hat{N}\hat{r}}{v^*}\left(\frac{\partial v^*}{\partial N_i}\right)\right) - \frac{\tilde{\rho}}{\tilde{T}} \times \frac{\hat{N}\hat{r}}{\varepsilon^*}\left(\frac{\partial \varepsilon^*}{\partial N_i}\right) - \ln Z \tag{6.4}$$

The above equation needs to be tested for extending the model in describing the phase equilibria of $CO_2$ + organic solid systems.

The new ALF model could be combined with the Gibbs-DiMarzio criterion (which states that the mixture entropy is zero at the glass transition) [129] to predict glass transition temperatures in $CO_2$ + polymer mixtures. The equation for the entropy using ALF model can be expressed as follows:

$$-\frac{S_c}{NR}=\left(\frac{f_0}{1-f_0}\right)\ln f_0+\frac{1}{\hat{r}}\ln(1-f_0)-\left(\phi_2-\frac{\phi_2}{r_2}\right)\ln(z-1)+\frac{\phi_2}{r_2}\ln\frac{\phi_2}{r_2}-\frac{\phi_2}{r_2}+\phi_2+\alpha\phi_2\ln\alpha$$
$$+(\frac{\phi_1-\alpha\phi_2}{1+\alpha})\ln(\phi_1-\alpha\phi_2)-\phi_1\ln\left(\frac{\phi_1}{\phi_1-\alpha\phi_2}\right)+\alpha\phi_2\ln\left(\frac{\alpha\phi_2}{\phi_1-\alpha\phi_2}\right)+\phi_2(1-\alpha)\ln(1-\alpha) \quad (6.5)$$

Finally, the ALF equation can be further reformulated by introducing the crystallinity and polydispersity in the lattice to derive a model for $CO_2$ + polymer systems. This model will be able to describe equally well for amorphous as well as crystalline polymers with any MW distribution of polymers.

# APPENDIX A: A NEW MODEL FOR THE THERMAL CONDUCTIVITY OF MOLTEN SALTS

In this chapter, a new model is proposed based on rough hard sphere theory for describing the thermal conductivity of molten salts. The model incorporates characteristic parameters based on the melting point of the molten salt, as well as a smooth hard sphere contribution using the properties of argon. It is shown that this approach is able to correlate the thermal conductivity of monovalent and multivalent molten salts within experimental error. Moreover, in salts with a common anion, the single adjustable parameter in the model exhibits regular trends with the molecular weight per ion of the salt. In addition, it is shown that no mixture parameter is needed to predict the thermal conductivity of molten salt mixtures. The contents of this chapter have been published in International Journal of Thermophysics, 35, 246–255, 2014.

## A.1 Introduction

Liquid salts (which are generally called molten salts at high temperatures and ionic liquids at low temperatures) play an important role in the production and processing of various materials. For instance, molten chlorides are used in the heat treatment of steel [260], and molten fluorides and oxides are crucial in the processing of aluminum and nuclear fuel [261]. In addition, molten nitrates and chlorides are gaining popularity as energy storage media in concentrated solar power (CSP) plants. The advantages of using the molten salts in high temperature applications are that the molten salts are nonflammable, non-toxic, inexpensive, and have the capability to transport heat at temperatures that are compatible with modern-day turbines [262-264]. Subsequently, 125,000 metric tons of molten salt used to store and deliver heat in the 280 MW Solana

plant in Arizona (the world's largest solar thermal plant). The fundamental knowledge on thermophysical properties such as the thermal conductivity of the molten salts is essential in these applications [265]. Unfortunately, such data are hardly available and, even when available, are often not reliable due to the large experimental uncertainties [266]. Therefore, there is need for a realistic model that can be used to predict and/or describe thermal conductivity data, particularly at high temperatures.

Most of the models for the thermal conductivity of molten salts (MS) treat the salt as a quasi-crystalline solid or a quasi-crystalline liquid, although a number of corresponding states models based on the properties of actual (reference) liquids are also available. Models that consider the molten salt as a quasi-crystalline solid make use of the fact that heat travels at the speed of sound in solids [267] and usually provide the expressions such as that of Kincaid and Eyring [268]:

$$\lambda = \left(\frac{0.931}{\gamma^{1/2}}\right)\left(\frac{N_A}{V}\right)^{2/3} 3kU \qquad \text{(A.1)}$$

where $\lambda$ is the thermal conductivity of the molten salt, $k$ is Boltzmann's constant, $U$ is the speed of sound in the salt, $V$ is the molar volume of the salt, $N_A$ is Avogadro's number, and $\gamma$ is the ratio of heat capacities $\left(C_p / C_v\right)$. A major drawback of this type of model is the necessity for speed of sound and heat capacity data, which are not often available. Furthermore, such models are unable to provide good agreement between calculated and experimental values (of the order of 20 - 40 %) as demonstrated by several authors [24, 266].

In Quasi-crystalline liquid models, molten salts assume a lattice structure for the molten salt and are able to consider for both vibrational (due to higher energy molecules colliding with each other) and diffusive (due to higher energy molecules diffusing to

regions of lower energy) contributions to the thermal conductivity. However, the diffusive contribution is often ignored since it has been estimated to contribute less than 4 % to the thermal conductivity of molten salts [25]. By incorporating this assumption with the vibrational frequency of a harmonic oscillator, Rao [269] derived the expression for the thermal conductivity as:

$$\lambda = A\left(\frac{R^{3/2}}{N_{\mathrm{A}}^{1/3}}\right)\left(\frac{T_{\mathrm{m}}}{M_{\mathrm{w}}V_{\mathrm{m}}^{4/3}}\right)^{1/2} \tag{A.2}$$

where $A$ is a constant that is equal to 23.44 when the thermal conductivity $\lambda$ is expressed in $\mathrm{W\cdot m^{-1}\cdot K^{-1}}$, the molecular weight $M_{\mathrm{w}}$ in $\mathrm{kg\cdot mol^{-1}}$, the gas constant $R$ in $\mathrm{J\cdot mol^{-1}\cdot K^{-1}}$, Avogadro's number $N_{\mathrm{A}}$ in $\mathrm{mol^{-1}}$, the melting temperature $T_{\mathrm{m}}$ in K, and the melt molar volume $V_{\mathrm{m}}$ in $\mathrm{m^3\cdot mol^{-1}}$. Turnbull [25] substitute $M_{\mathrm{w}}$ by $M_{\mathrm{w}}$ per ion ($M_{\mathrm{w}} / n$) and $V_{\mathrm{m}}$ by $V_{\mathrm{m}}$ per ion ($V_{\mathrm{m}} / n$) in Equation A.2 to consider the dissociation of molten salts and derived the thermal conductivity expression as:

$$\lambda = B\left(\frac{R^{3/2}}{N_{\mathrm{A}}^{1/3}}\right)\left(\frac{T_{\mathrm{m}}}{(M_{\mathrm{w}}/n)(V_{\mathrm{m}}/n)^{4/3}}\right)^{1/2} \tag{A.3}$$

where $n$ is the number of ions in each molecule of molten salt. Several molten salts thermal conductivity was fitted to obtain the value of constant $B$ as equal to 13.28. If the melt volume is expressed in $\mathrm{m^3\cdot kg^{-1}}$, then Equation A.3 becomes:

$$\lambda = B\left(\frac{R^{3/2}}{N_{\mathrm{A}}^{1/3}}\right)\left(\frac{T_{\mathrm{m}}}{(M_{\mathrm{w}}/n)^{7/3}\hat{V}_{\mathrm{m}}^{4/3}}\right)^{1/2} \tag{A.4}$$

where $\hat{V}_{\mathrm{m}}$ represents the specific volume of the melt in $\mathrm{m^3\cdot kg^{-1}}$. Note that the Equation A.2 and A.4 are limited to conditions near the melting point of the molten salt as the quasi-crystalline treatment of the molten salt used in their derivation. Agreement with

experiment is reported to be of the order of 20 % when using the Rao model (Equation A.2) for common liquids, and 15.4 % when using the Turnbull model (Equation A.4) for a number of molten salts, even though errors have also been reported as large as 39 % [25].

In corresponding states models for the thermal conductivity of molten salts, the reduced thermal conductivity $\lambda / \lambda_c$ express as a function of the reduced volume $V/V_c$ or reduced temperature $T / T_c$ using the properties of a reference fluid [270, 271]. The characteristic parameters ($\lambda_c$ and $V_c$ or $T_c$) as well as the reference fluid are sometimes chose arbitrarily, and a number of choices have been proposed for molten salts. Consequently, White and Davis [270] used the liquid density and thermal conductivity at the melting point to describe the reducing parameters in their corresponding states correlation of the thermal conductivity of alkali nitrates, with one of the nitrates acting as a reference fluid. On the other hand, Young and O'Connell [271] selected an arbitrary point on the saturation curve to estimate their characteristic parameters and correlated the thermal conductivity of nitrates and halides using one of the nitrates/halides as a reference fluid. In the hard sphere theory, the reference fluid is consisting of hard spheres and the characteristic parameters are estimated from the properties of (spherical) hard sphere molecules. The characteristic properties can be obtained from the properties of fluids with spherical molecules such as argon. This rough hard spheres (or fluids with non-spherical molecules) approach extended by Chandler [272] by incorporating a translational-rotational coupling parameter in the theory. Li et al. [273] used the rough hard sphere theory to calculate the thermal conductivity as well as the viscosity of the alkanes (with one of the alkanes effectively acting as a reference fluid), but found that

they required different characteristic volumes to correlate thermal conductivity and viscosity simultaneously. This drawback was overcome by Assael et al. [274, 275] who were able to use one characteristic volume for each fluid to correlate the thermal conductivity as well as viscosity of aromatic hydrocarbons [276], alcohols [277], and refrigerants [278]. DiGuilio and Teja [266] further extended to monovalent molten salts and their mixtures by using one molten salt as the reference fluid and the characteristic parameters are defined by the melting point of the molten salt. However, multivalent molten salts are not considered in their approach.

In this chapter, we have described a new model for the thermal conductivity of molten salts based on argon as the smooth hard sphere fluid in Chandler's theory. However, the characteristic parameters in the new model were defined according to Turnbull [11] and DiGuilio and Teja [7] and obtained from the properties of the molten salt at its melting point. We have demonstrated below that this approach can be used for both monovalent and multivalent molten salts and that the translational-rotational coupling parameter estimated in this new approach exhibits regular trends in series of salts with a common anion. Finally, we show that the thermal conductivity of simple mixtures of molten salts can be predicted using a linear mixing rule without any additional parameters.

## A.2 Development of the Model

As proposed by Chandler [272], the reduced viscosity of rough hard spheres can be correlated to that of smooth hard spheres according to:

$$\eta^*_{\mathrm{RHS}} = C_\eta \eta^*_{\mathrm{SHS}} \tag{A.5}$$

where $C_\eta$ is a coupling constant that accounts for energy transfer resulting from the coupling between translational and rotational motions. In fact, the translational-rotational constant accounts for the non – spherical shape of molecules, as well as the molecular internal energy [279]. Similarly, reduced thermal conductivity of rough hard spheres can be express by the following relation:

$$\lambda^*_{\mathrm{RHS}} = C_\lambda \lambda^*_{\mathrm{SHS}} \tag{A.6}$$

where $C_\lambda$ is again the translational – rotational coupling constant that is unique to each salt and it is independent of temperature and density. The reduced thermal conductivity of rough hard spheres can be expressed according to Li et al. [273] as:

$$\lambda^*_{\mathrm{RHS}} = \frac{\lambda}{\{0.5165\times10^{-7}\left(RT/M_{\mathrm{W}}\right)^{1/2} V^{-2/3}\}} \tag{A.7}$$

where $T$ is the temperature in $\mathrm{K}$, $R$ is the gas constant in $\mathrm{J\cdot mol^{-1}\cdot K^{-1}}$, $M_{\mathrm{w}}$ is the molecular weight in $\mathrm{kg\cdot mol^{-1}}$, and $V$ is the molar volume in $\mathrm{m^3\cdot mol^{-1}}$. Also, as shown by Assael et al. [274, 276] and Li et al. [273], the reduced thermal conductivity of smooth hard spheres in Equation A.6 is only a function of the reduced volume as follows:

$$\lambda^*_{\mathrm{SHS}} = F\left[V/V_0\right] \tag{A.8}$$

where $V_0$ represents the molar volume at closest packing. For hard spheres, $V_0 = N_{\mathrm{A}}\sigma^3/\sqrt{2}$ with $\sigma$ being the molecular diameter. This approach is extended by DiGuilio and Teja [266] to molten salts by replacing the molar volume at closest packing by the solid molar volume $V_{\mathrm{s}}$ and using the properties of one salt in a series of salts with a common anion to obtain the function *F* for that series. In addition, the origin of function $F$ in Equation A.8 was shifted to the melting point. Therefore

$$\lambda^{*}_{\mathrm{MS}} = C_{\lambda} F\left[\left(V - V_{\mathrm{m}}\right)/V_{\mathrm{s}}\right] \tag{A.9}$$

where $\lambda^{*}_{\mathrm{MS}}$ denotes the reduced thermal conductivity of the molten salt. The advantage of using $(V - V_{\mathrm{m}})/V_{\mathrm{s}}$ instead of $V/V_{\mathrm{s}}$ or $V/V_0$ to describe the functional dependence of $F$ is that the melting point thermal conductivity is obtained at $F$ [0]. DiGuilio and Teja showed that the thermal conductivity of a series of molten salts with a common anion can be correlated using Equation A.9 with a single value of coupling parameter $(C_{\lambda})$ provided that the function $F$ is estimated from the thermal conductivity of one member of the series. However, their model was restricted only to monovalent molten salts.

In this work, we follow the original rough hard sphere theory of Chandler [272] to obtain the properties of smooth hard spheres from the properties of argon. However, we follow Turnbull [25] approach in defining the reduced thermal conductivity in terms of the properties at the melting point, and DiGuilio and Teja [266] approach in shifting the origin of the function $F$ to the melting point. The resulting expression for the reduced thermal conductivity of a molten salt can be expressed as [280]:

$$\lambda^{*} = \frac{\lambda}{B\left(R^{3/2} N_A^{-1/3}\right)\left[T_{\mathrm{m}}\left(M_{\mathrm{w}}/n\right)^{-7/3} \hat{V}_{\mathrm{m}}^{-4/3}\right]^{1/2}} = C_{\lambda}\ \ F\left[\left(V - V_{\mathrm{m}}\right)/V_{\mathrm{s}}\right] \tag{A.10}$$

The function $F$ is then obtained by correlating the properties of argon to yield:

$$\lambda^{*}_{\mathrm{Ar}} = F\left(\xi\right) = 0.68285 - 0.84286\,\xi + 0.66370\,\xi^{2} - 0.21015\,\xi^{3} \tag{A.11}$$

where $\xi = (V - V_{\mathrm{m}})/V_{\mathrm{S}}$. The Equation A.11 is obtain from the thermal conductivity data for saturated liquid argon reported by Touloukian et al. [281], Younglove and Hanley [282], and Roder et al. [283]. The properties of argon, such as $V_{\mathrm{m}}$, $T_{\mathrm{m}}$ and $V_{\mathrm{s}}$ (calculated

from closed pack volume $N_A\sigma^3/\sqrt{2}$) were obtained from Rabinovich et al. [284]. The argon data in Equation A.11 cover a range of $\xi$ values between 0 and 1.11 between its melting and near critical points. This range of $\xi$ values is sufficiently large to cover molten salt data to very high temperatures (For example $\xi$ = 0.115 for NaBr at 1264 K). This allows us to extrapolate or interpolate molten salt thermal conductivity over the entire liquid range using this function, since the thermal conductivity data of argon is established up to its critical point [281].

## A.3 Results and Discussion

The new hard sphere model was first applied to the thermal conductivity behavior of monovalent chlorides (NaCl, KCl, RbCl, CsCl, and LiCl), a divalent chloride ($ZnCl_2$), and the monovalent nitrates ($LiNO_3$, $NaNO_3$, and $KNO_3$) for which reliable thermal conductivity data are available in the literature [22, 24, 25]. As discussed by DiGuilio and Teja [266] and others [22, 26, 285, 286], only the thermal conductivity data of molten salt that exhibit negative temperature coefficients ($d\lambda/dT < 0$) are considered reliable and were used in evaluating the model. On the other hand, data that exhibited positive temperature coefficients ($d\lambda/dT > 0$) were not considered for this the study. Molar volumes and melting temperatures of the molten salts were collected from Janz [287]. Figure A.1 and Table A.1 demonstrate the results of our calculations. Figure A.1 clearly illustrates that the reduced thermal conductivity *vs.* reduced volume data for a family of salts having a common anion collapse onto a single curve, regardless of the number of ions in the salt. Note that $d\lambda/dT < 0$ for argon and all molten salt data shown in Figure A.1. Table A.1 shows the $C_\lambda$ values for each salt, estimated by fitting experimental $\lambda^*$ vs.

$\xi$ data, and the average absolute percentage deviations between experimental and calculated values of the thermal conductivity. In general, we were able to correlate all thermal conductivity data within experimental error (which are quite large for some molten salts, as included in the table).

Figure A.2 illustrates the value of $C_\lambda$ that was plotted as a function of molecular weight per ion for each series of salts with a common anion. It is apparent that $C_\lambda$ exhibits a linear trend for each molten salt series. What is surprising is that all chlorides, bromides, and iodides fall on the same (chloride) line, even though there is considerable scatter due to large uncertainties in the experimental thermal conductivity data (claimed experimental uncertainties range from ± 3 % to ± 20 %) [22, 25, 26, 286]. Noted that $C_\lambda$ for $ZnCl_2$, which is the only divalent salt for which reliable data are available, apparently also lies on the (monovalent) chloride line as shown in Figure A.2.

Figure A.3 illustrates the predictive capability of the approach. In this Figure, the thermal conductivity of iodide salts was predicted using $C_\lambda$ values obtained from the chloride correlation of Figure A.2. The predictions are reasonable, keeping in mind the large uncertainties in experimental data (claimed uncertainties range from ± 9 % to ± 20 %) [26].

### A.4 Extension to Molten Salt Mixtures

DiGuilio and Teja demonstrated that a linear mixing rule can be used to obtain the thermal conductivity of chloride and nitrate molten salts [266]. As a result, we have used a similar mixing rule to extend the new model to mixtures using the following relation:

$$\lambda_{\text{mix}} = \sum_{i=1}^{m} x_i \lambda_{\text{i}} \tag{A.12}$$

where $m$ represents the number of components and $x_i$ represents the mole fraction of the $i^{th}$ component. The pure component thermal conductivity $\lambda_i$ can be obtained as described in the previous section. Table A.2 listed experimental and calculated thermal conductivities for mixtures of nitrate salts, along with the average percentage error. Table A.2 also include the mixture compositions that are reported in mole percent. The values of the calculated thermal conductivity are generally within experimental error. Table A.3 shows the predicted results of calculations when pure component values are not available, as is the case for fluoride molten salts. We have obtained the thermal conductivity of pure fluoride salts using $C_\lambda$ values from Figure A.2 (i.e. the line for chloride molten salts). Equation A.12 was then used to predict the mixture thermal conductivity for fluoride mixtures. Experimental and predicted thermal conductivities of these mixtures are of the same magnitude, even though it should be noted that the experimental data exhibit the wrong trend for the slope $d\lambda/dT$.

## A.5 Conclusions

A new model based on the rough hard sphere theory has been derived in this work for describing the thermal conductivity of molten salts. This model is able to correlate and predict thermal conductivity of molten salts and their mixtures with minimal experimental data. This new model successfully accounts for the temperature, density, and ion dependency of the thermal conductivity. The single parameter in the model ($C_\lambda$) displays a linear trend with molecular weight per ion for a series of salts with a common anion (and also, apparently, for related ions such as the halogens). In addition, thermal

conductivities of salt mixtures can be predicted without any additional parameters (in the cases studied).

Mohammad Z. Hossain, Mohamad H. Kassaee, Sheldon Jeter, Amyn S. Teja, A New Model for the Thermal Conductivity of Molten Salts, International Journal of Thermophysics, 35, 246–255, 2014

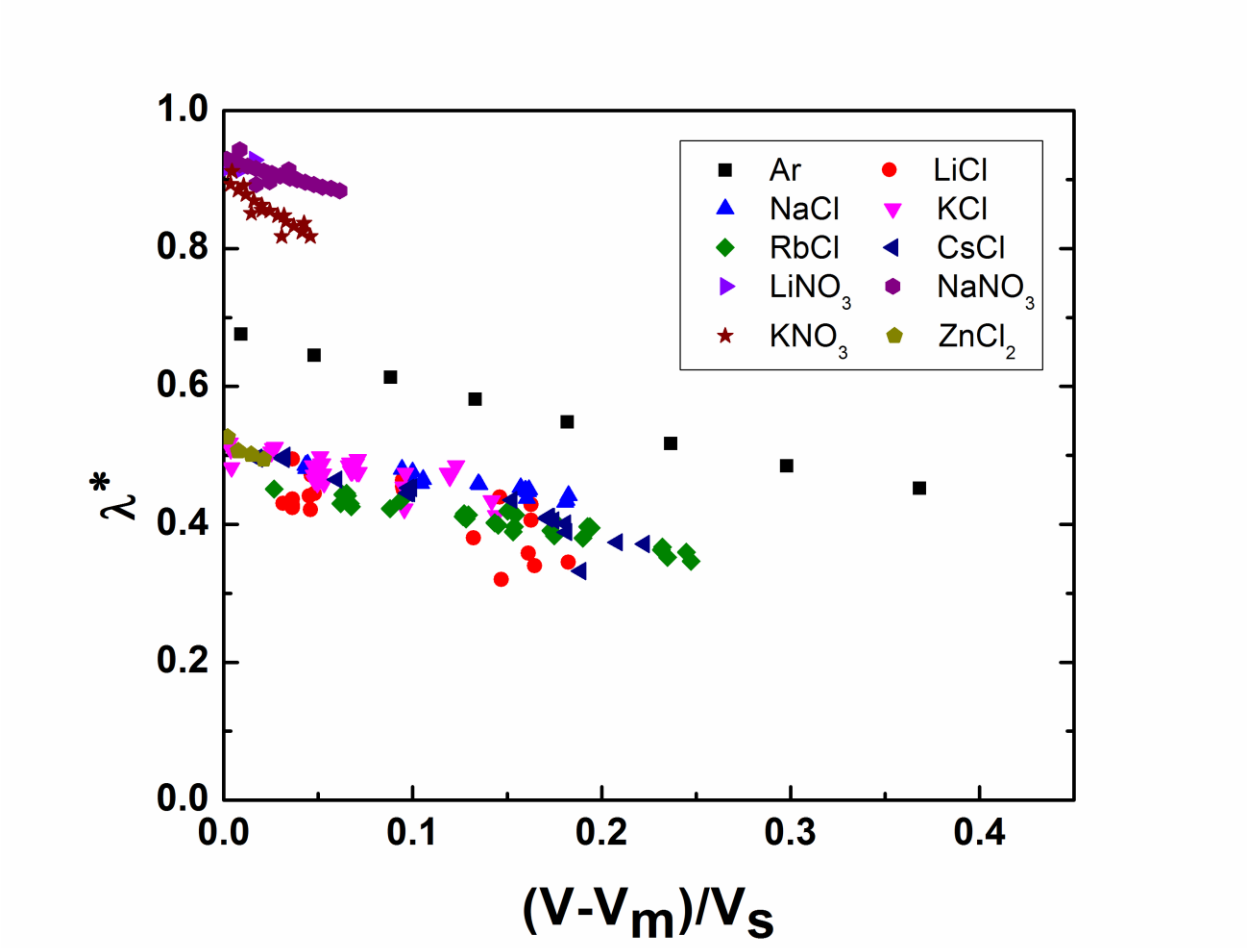


**Figure A.1** Reduced thermal conductivity $\lambda^*$ as a function of $(V-V_m)/V_s$ for argon and molten salts [22-25].

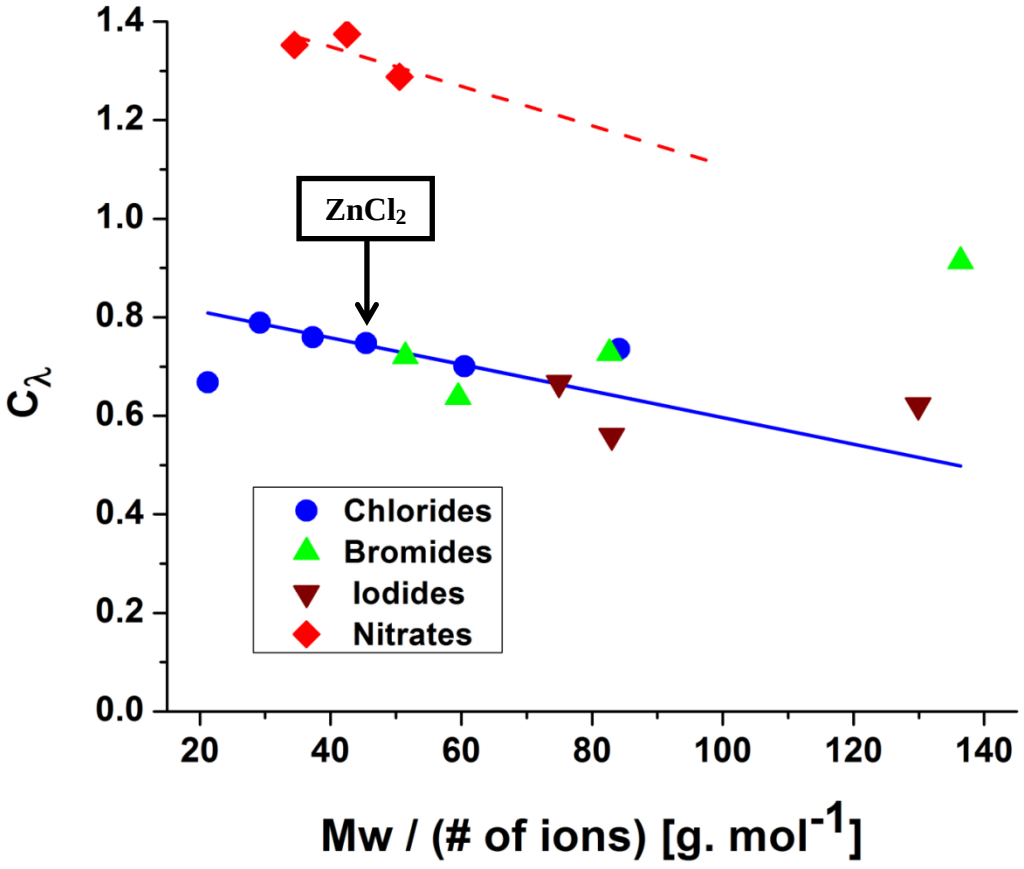


**Figure A.2** Coupling parameter $C_\lambda$ as a function of molecular weight per ion for nitrate and halide molten salts.

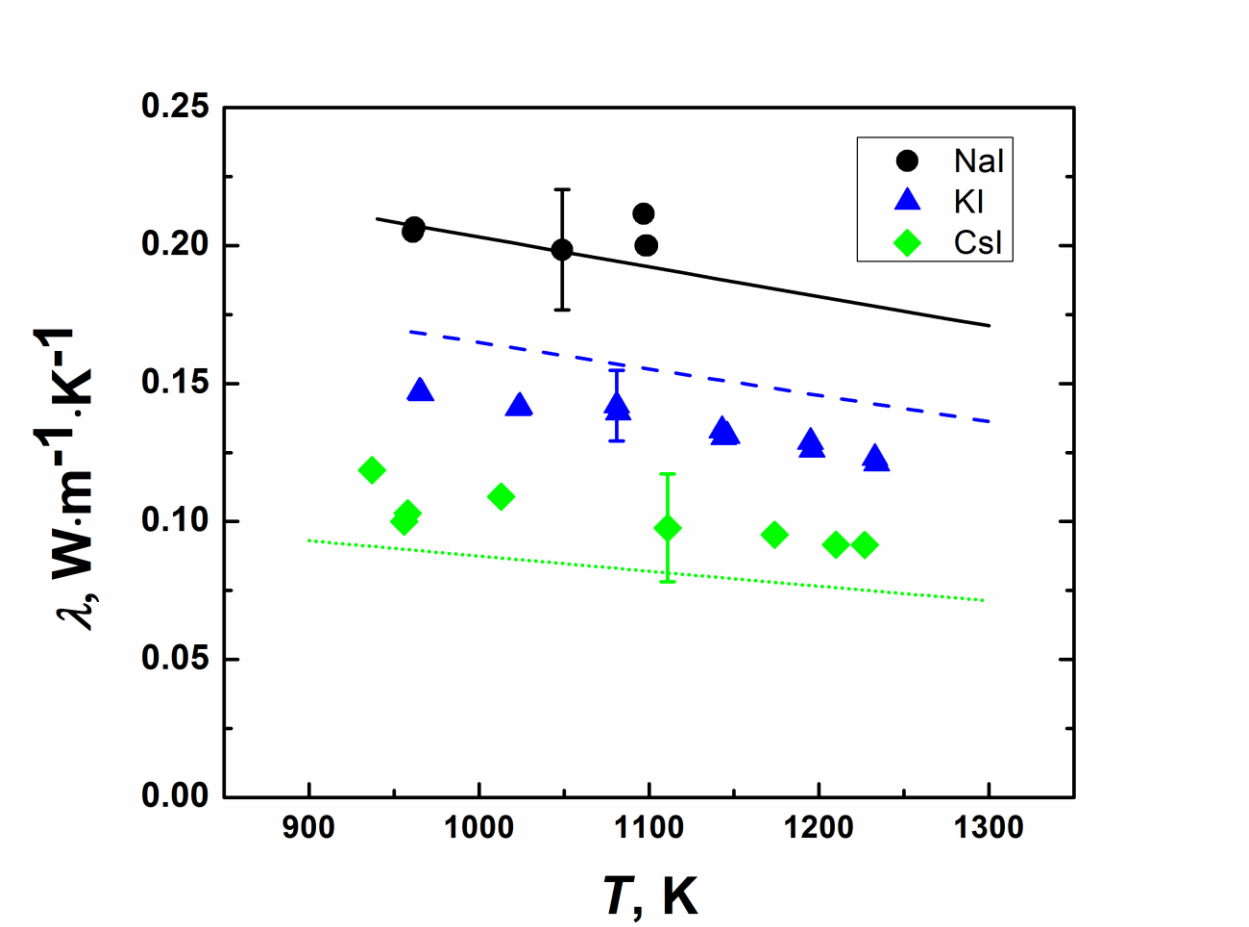


**Figure A.3** Experimental and calculated thermal conductivity for iodide salts [26]; lines are calculated using the model (solid line is for NaI, dashed line is for KI, and dotted line is for CsI)

**Table A.1** Results of thermal conductivity calculations using the new model

| Molten Salt | Number of points | Temperature range / K | Claimed uncertainties of data (%) | $C_\lambda$ | AAD % [a] |
|---|---|---|---|---|---|
| $LiNO_3$ | 3 | 531.1 – 567.8 | ± 3 | 1.35 | 0.96 |
| $NaNO_3$ | 23 | 590 – 720 | ± 4 | 1.37 | 0.89 |
| $KNO_3$ | 19 | 620 – 720 | ± 4 | 1.29 | 1.30 |
| LiCl | 21 | 967 – 1321 | ± 20 | 0.67 | 7.34 |
| NaCl | 19 | 1170 – 1439 | ± 8 | 0.79 | 1.86 |
| KCl | 33 | 1056 – 1335 | ± 8 | 0.76 | 2.75 |
| Rbcl | 32 | 1046 – 1441 | ± 15 | 0.70 | 1.79 |
| CsCl | 20 | 960 – 1360 | ± 18 | 0.74 | 2.71 |
| $ZnCl_2$ | 4 | 564 – 640 | ± 3 | 0.75 | 0.99 |
| NaBr | 21 | 1050 – 1267 | ± 15 | 0.72 | 2.22 |
| KBr | 14 | 1035 – 1245 | ± 7 | 0.64 | 2.36 |
| RbBr | 25 | 1031 – 1326 | ± 15 | 0.73 | 2.41 |
| CsBr | 17 | 948 – 1314 | ± 19 | 0.91 | 7.06 |
| NaI | 6 | 961 – 1094 | ± 11 | 0.67 | 2.95 |
| KI | 13 | 965 – 1234 | ± 9 | 0.56 | 1.09 |
| CsI | 8 | 937 – 1227 | ± 20 | 0.62 | 3.48 |

[a] $\mathrm{AAD\%} = 100 \cdot \sum \left| \frac{\lambda_{\mathrm{calc}} - \lambda_{\mathrm{exp}}}{\lambda_{\mathrm{exp}}} \right|$; Data references [22, 24-26, 286, 288]

**Table A.2** Prediction of thermal conductivity of nitrate mixtures

| Molten Salt Mixture | $T$ (K) | $\lambda_{exp}$ / W·m$^{-1}$·K$^{-1}$ | $\lambda_{calc}$ / W·m$^{-1}$·K$^{-1}$ | AAD% | Data Ref. |
|---|---|---|---|---|---|
| 0.3 $NaNO_3$ + 0.7 $KNO_3$ | 543.3 | 0.433 | 0.453 | | |
| | 566.7 | 0.425 | 0.448 | 4.36[a] | [289] |
| | 589.5 | 0.429 | 0.443 | | |
| 0.46 $NaNO_3$ + 0.54 $KNO_3$ | 526.2 | 0.4675 | 0.472 | | |
| | 541.5 | 0.4650 | 0.468 | | |
| | 557.5 | 0.4579 | 0.465 | 1.31[b] | [266] |
| | 572.4 | 0.4543 | 0.461 | | |
| | 588.0 | 0.4484 | 0.457 | | |
| 0.50 $NaNO_3$ + 0.50 $KNO_3$ | 497.5 | 0.620 | 0.482 | | |
| | 509.4 | 0.460 | 0.480 | | |
| | 545.3 | 0.457 | 0.471 | 3.65[c] | [289] |
| | 573.7 | 0.446 | 0.464 | | |
| | 592.2 | 0.446 | 0.460 | | |
| 0.75 $NaNO_3$ + 0.25 $KNO_3$ | 546.4 | 0.479 | 0.494 | | |
| | 569.6 | 0.471 | 0.488 | 3.39[d] | [289] |
| | 587.3 | 0.465 | 0.484 | | |
| | 592.8 | 0.470 | 0.482 | | |

Experimental uncertainty; a – (±3), b – (±1), c – (±3-4), and d – (±3)

**Table A.3** Prediction of the thermal conductivity of fluoride salt mixtures

| Molten Salt Mixture | $T$ (K) | $\lambda_{exp}$ / W·m$^{-1}$·K$^{-1}$ | $\lambda_{calc}$ / W·m$^{-1}$·K$^{-1}$ | AAD% |
|---|---|---|---|---|
| 20 % KF + 80 % NaF | 1185 | 0.97 | 0.999 | 5.91 |
| | 1206 | 0.99 | 0.989 | |
| | 1233 | 0.99 | 0.977 | |
| | 1254 | 1.01 | 0.968 | |
| | 1270 | 1.10 | 0.960 | |
| | 1288 | 1.11 | 0.952 | |
| 40 % KF + 60 % NaF | 1134 | 0.80 | 0.929 | 7.83 |
| | 1160 | 0.82 | 0.918 | |
| | 1189 | 0.86 | 0.906 | |
| | 1213 | 0.90 | 0.896 | |
| | 1247 | 0.93 | 0.882 | |
| 60 % KF + 40 % NaF | 1063 | 0.70 | 0.864 | 10.63 |
| | 1094 | 0.73 | 0.852 | |
| | 1171 | 0.80 | 0.822 | |
| | 1210 | 0.81 | 0.807 | |
| | 1244 | 0.88 | 0.794 | |
| 80 % KF + 20 % NaF | 1133 | 0.71 | 0.744 | 9.48 |
| | 1174 | 0.76 | 0.730 | |
| | 1200 | 0.78 | 0.720 | |
| | 1226 | 0.80 | 0.711 | |
| | 1248 | 0.81 | 0.703 | |
| | 1267 | 0.83 | 0.696 | |

Data reference [290]; Experimental uncertainty is ± 4 % for these mixtures

# APPENDIX B: DERIVATION OF ASSOCIATION RATIO

This chapter discusses the relationship between the association ratio and the equilibrium constant for association.

## B.1 Associated solutions

For the purposes of this work, it is assumed that there are three different types of molecules in a polymer solution: polymer-solvent complexes, unassociated solvent molecules, and unassociated polymer molecules. The following equilibrium reaction may be postulated between a polymer molecule and $\mu$ solvent molecules

$$P + \mu S \Leftrightarrow PS_{\mu} \tag{B.1}$$

where $P$ is the solute (polymer), $S$ is the solvent, $\mu$ is the solute/solvent binding ratio, and $PS_{\mu}$ is the associated solute-solvent complex. The equilibrium constant $K$ for the association can be expressed as:

$$K = \frac{[PS\mu]}{[P][S]^{\mu}} \tag{B.2}$$

where $[P]$, $[S]$, and $[PS_{\mu}]$ are the concentration of solute, solvent, and associated solute-solvent complex, respectively. For a solution with $r_1 N_1$ solvent molecules and $r_2 N_2$ molecules of solute (or $N_2$ polymer molecules, each of which consists of $r_2$ segments), the following table can be constructed for $\alpha$ which is the fraction of polymer segments associated with the solvent

| Component | Initial | Change | Final |
|---|---|---|---|
| $S$ | $r_1N_1$ | $\mu\alpha r_2N_2$ | $r_1N_1-\mu\alpha r_2N_2$ |
| $P$ | $r_2N_2$ | $\alpha r_2N_2$ | $(1-\alpha)r_2N_2$ |

where, sum of the stoichiometric coefficient $\sum_i \upsilon_i = 1-1-\mu = -\mu$, $N_{initial} = r_1N_1 + r_2N_2 = N$, and the extent of reactions is $\alpha r_2N_2$. The total number of molecule can be expressed as $N_T = N_{initial} + \alpha r_2N_2\sum_i \upsilon_i = N - \mu\alpha r_2N_2$.

$$[P] = \frac{(1-\alpha)r_2N_2}{N-\mu\alpha r_2N_2}; [S] = \frac{r_1N_1-\mu\alpha r_2N_2}{N-\mu\alpha r_2N_2} = \frac{\phi_1-\mu\alpha\phi_2}{1-\mu\alpha\phi_2}; \left[PS_\mu\right] = \frac{\alpha r_2N_2}{N-\mu\alpha r_2N_2} \tag{B.3}$$

$$K = \frac{\dfrac{\alpha r_2N_2}{N-\mu\alpha r_2N_2}}{\left(\dfrac{(1-\alpha)r_2N_2}{N-\mu\alpha r_2N_2}\right)\left(\dfrac{\phi_1-\mu\alpha\phi_2}{1-\mu\alpha\phi_2}\right)^\mu} = \frac{\alpha}{(1-\alpha)}\left(\frac{1-\mu\alpha\phi_2}{\phi_1-\mu\alpha\phi_2}\right)^\mu \tag{B.4}$$

If we assume the solute/solvent binding ratio $\mu$ is equal to one, then

$$K = \frac{\alpha}{(1-\alpha)}\left(\frac{1-\mu\alpha\phi_2}{\phi_1-\mu\alpha\phi_2}\right)$$
$$\Rightarrow K(1-\alpha)(\phi_1-\alpha\phi_2) = \alpha(1-\alpha\phi_2)$$
$$\Rightarrow \alpha^2\phi_2(K+1) - (1+K)\alpha + K\phi_1 = 0$$

$$\alpha = \frac{(1+K) \pm \sqrt{(1+K)^2 - 4\phi_1\phi_2K(1+K)}}{2\phi_2(1+K)} \tag{B.5}$$

Ignoring the positive values, we can have

$$\alpha = \frac{(1+K) - \sqrt{(1+K)^2 - 4\phi_1\phi_2K(1+K)}}{2\phi_2(1+K)} \tag{B.6}$$

$$\Rightarrow \alpha = \frac{1}{2\phi_2} - \sqrt{\frac{(1+K)^2 - 4\phi_1\phi_2 K(1+K)}{4\phi_2^2(1+K)^2}};\ \frac{\partial \phi_2}{\partial N_1} = -\frac{\phi_2}{N} \text{ and } \frac{\partial \phi_1}{\partial N_1} = \frac{\phi_2}{N}$$

$$\Rightarrow \frac{\partial \alpha}{\partial N_1} = -\frac{1}{2\phi_2^2}\frac{\partial \phi_2}{\partial N_1} - \frac{1}{2}\sqrt{\frac{4\phi_2^2(1+K)^2}{(1+K)^2 - 4\phi_1\phi_2 K(1+K)}}\left[\left(-\frac{2}{4\phi_2^3}\frac{\partial \phi_2}{\partial N_1}\right) - \frac{K}{1+K}\frac{\phi_2\frac{\phi_2}{N} + \phi_1\frac{\phi_1}{N}}{\phi_2^2}\right]$$

then,

$$\beta = -\frac{1}{2\phi_2^2}\left(-\frac{\phi_2}{N}\right) - \frac{1}{2}\frac{2\phi_2}{1-2\alpha\phi_2}\left[\left(\frac{1}{2\phi_2^3}\frac{\phi_2}{N}\right) - \frac{K}{1+K}\frac{1}{\phi_2 N}\right];\ \frac{\partial \alpha}{\partial N_1} = \beta \tag{B.7}$$

$$\Rightarrow N\beta = \frac{1}{2\phi_2} - \frac{1}{1-2\alpha\phi_2}\left[\frac{1}{2\phi_2} - \frac{K}{1+K}\right];\ \left[\sqrt{\frac{(1+K)^2 - 4\phi_1\phi_2 K(1+K)}{4\phi_2^2(1+K)^2}} = \frac{1-2\alpha\phi_2}{2\phi_2}\right]$$

$$\Rightarrow \beta_1 = \frac{1}{2\phi_2} + \frac{1}{1-2\alpha\phi_2}\left[\frac{1+K-2\phi_2 K}{2\phi_2(1+K)}\right];\ N\beta = \beta_1$$

$$\Rightarrow \beta_1 = \frac{\alpha(1+K) - K}{(1+K)(2\alpha\phi_2 - 1)} \tag{B.8}$$

The equilibrium constant $K$ in Equation (B.8) can be expressed via van't Hoff relation as follows:

$$\ln\frac{K}{K_0} = -\frac{\Delta H_a}{R}\left(\frac{1}{T} - \frac{1}{T_0}\right) \tag{B.9}$$

Where, $K_0$ is the association constant at reference temperature $T_0$ (298.15 K).

# REFERENCES


[1] M.R. Nelson, R.F. Borkman, Ab initio calculations on $CO_2$ binding to carbonyl groups, The Journal of Physical Chemistry A, 102 (1998) 7860-7863.

[2] M.A. McHugh, V.J. Krukonis, Supercritical Fluid Extraction: Principles and Practice, 2nd edition ed., Butterworths-Heinemann, Boston, 1994

[3] F. Rindfleisch, T.P. DiNoia, M.A. McHugh, Solubility of polymers and copolymers in supercritical $CO_2$, The Journal of Physical Chemistry, 100 (1996) 15581-15587.

[4] Z. Shen, M.A. McHugh, J. Xu, J. Belardi, S. Kilic, A. Mesiano, S. Bane, C. Karnikas, E. Beckman, R. Enick, $CO_2$-solubility of oligomers and polymers that contain the carbonyl group, Polymer, 44 (2003) 1491-1498.

[5] S. Kilic, S. Michalik, Y. Wang, J.K. Johnson, R.M. Enick, E.J. Beckman, Phase Behavior of Oxygen-Containing Polymers in $CO_2$, Macromolecules, 40 (2007) 1332-1341.

[6] M.Z. Hossain, Y. Yuan, A.S. Teja, A lattice fluid equation of state for associating $CO_2$ + polymer systems, Industrial & Engineering Chemistry Research, 52 (2013) 12654–12660.

[7] Y. Sato, T. Takikawa, S. Takishima, H. Masuoka, Solubilities and diffusion coefficients of carbon dioxide in poly(vinyl acetate) and polystyrene, The Journal of Supercritical Fluids, 19 (2001) 187-198.

[8] M. Pantoula, C. Panayiotou, Sorption and swelling in glassy polymer/carbon dioxide systems: Part I. Sorption, The Journal of Supercritical Fluids, 37 (2006) 254-262.

[9] N.-H.T. Wang, S.; Masuoka, H., Measurement and correlation of solubility of a high pressure gas in a polymer by Piezoelectric quartz soprtion -$CO_2$+PVAc and $CO_2$+PBMA systems, International Chemical Engineering, 34 (1994) 255-262.

[10] D. Liu, D.L. Tomasko, Carbon dioxide sorption and dilation of poly(lactide-co-glycolide), The Journal of Supercritical Fluids, 39 (2007) 416-425.

[11] A. Kasturirangan, C. Grant, A.S. Teja, Compressible lattice model for phase equilibria in $CO_2$ + polymer systems, Industrial & Engineering Chemistry Research, 47 (2008) 645-649.

[12] Y. Sato, T. Takikawa, A. Sorakubo, S. Takishima, H. Masuoka, M. Imaizumi, Solubility and diffusion coefficient of carbon dioxide in biodegradable polymers, Industrial & Engineering Chemistry Research, 39 (2000) 4813-4819.

[13] S.E. Conway, H.S. Byun, M.A. McHugh, J.D. Wang, F.S. Mandel, Poly(lactide-co-glycolide) solution behavior in supercritical $CO_2$, $CHF_3$, and $CHClF_2$, Journal of Applied Polymer Science, 80 (2001) 1155-1161.

[14] C. Cadena, J.L. Anthony, J.K. Shah, T.I. Morrow, J.F. Brennecke, E.J. Maginn, Why Is $CO_2$ So Soluble in Imidazolium-Based Ionic Liquids?, Journal of the American Chemical Society, 126 (2004) 5300-5308.

[15] S.S. Moganty, R.E. Baltus, Regular Solution Theory for Low Pressure Carbon Dioxide Solubility in Room Temperature Ionic Liquids: Ionic Liquid Solubility Parameter from Activation Energy of Viscosity, Industrial & Engineering Chemistry Research, 49 (2010) 5846-5853.

[16] S.N.V.K. Aki, B.R. Mellein, E.M. Saurer, J.F. Brennecke, High-Pressure Phase Behavior of Carbon Dioxide with Imidazolium-Based Ionic Liquids, The Journal of Physical Chemistry B, 108 (2004) 20355-20365.

[17] E.-K. Shin, B.-C. Lee, J.S. Lim, High-pressure solubilities of carbon dioxide in ionic liquids: 1-Alkyl-3-methylimidazolium bis (trifluoromethylsulfonyl)imide, Journal of Supercritical Fluids, 45 (2008) 282-292.

[18] A. Yokozeki, M.B. Shiflett, C.P. Junk, L.M. Grieco, T. Foo, Physical and Chemical Absorptions of Carbon Dioxide in Room-Temperature Ionic Liquids, The Journal of Physical Chemistry B, 112 (2008) 16654-16663.

[19] M.C. Kroon, A. Shariati, M. Costantini, J. van Spronsen, G.J. Witkamp, R.A. Sheldon, C.J. Peters, High-pressure phase Behavior of systems with ionic liquids: Part V. The binary system carbon dioxide+1-butyl-3-methylimidazolium tetrafluoroborate, Journal of Chemical and Engineering Data, 50 (2005) 173-176.

[20] J.-M. Andanson, F. Jutz, A. Baiker, Supercritical $CO_2$/Ionic Liquid Systems: What Can We Extract from Infrared and Raman Spectra?, The Journal of Physical Chemistry B, 113 (2009) 10249-10254.

[21] L.A. Blanchard, Z. Gu, J.F. Brennecke, High-Pressure Phase Behavior of Ionic Liquid/$CO_2$ Systems, The Journal of Physical Chemistry B, 105 (2001) 2437-2444.

[22] Y. Nagasaka, N. Nakazawa, A. Nagashima, Experimental determination of the thermal diffusivity of molten alkali halides by the forced Rayleigh scattering method. I. Molten LiCl, NaCl, KCl, RbCl, and CsCl, Int. J. Thermophys., 13 (1992) 555-574.

[23] T. Omotani, A. Nagashima, Thermal conductivity of molten salts, HTS and the lithium nitrate-sodium nitrate system, using a modified transient hot-wire method, J. Chem. Eng. Data, 29 (1984) 1-3.

[24] Y. Nagasaka, A. Nagashima, The thermal conductivity of molten NaNO3 and KNO3, Int. J. Thermophys., 12 (1991) 769-781.

[25] A.G. Turnbull, The Thermal Conductivities of Molten Salts II. Theory and Results for Pure Salts, Aust. J. of Appl. Sci., 9 (1961) 324.

[26] N. Nakazawa, Y. Nagasaka, A. Nagashima, Experimental determination of the thermal diffusivity of molten alkali halides by the forced Rayleigh scattering method. III. molten NaI, KI, RbI, and CsI, Int. J. Thermophys., 13 (1992) 763-772.

[27] A.I. Cooper, Polymer synthesis and processing using supercritical carbon dioxide, Journal of Materials Chemistry, 10 (2000) 207-234.

[28] J.L. Kendall, D.A. Canelas, J.L. Young, J.M. DeSimone, Polymerizations in supercritical carbon dioxide, Chemical Reviews, 99 (1999) 543-564.

[29] S.D. Yeo, E. Kiran, Formation of polymer particles with supercritical fluids: A review, The Journal of Supercritical Fluids, 34 (2005) 287-308.

[30] A.R.C. Duarte, J.F. Mano, R.L. Reis, Supercritical fluids in biomedical and tissue engineering applications: a review, International Materials Reviews, 54 (2009) 214-222.

[31] S. Kazarian, Polymer processing with supercritical fluids, Polymer Science Series Cc/C of Vysokomolekuliarnye Soedineniia, 42 (2000) 78-101.

[32] D.L. Tomasko, H. Li, D. Liu, X. Han, M.J. Wingert, L.J. Lee, K.W. Koelling, A review of $CO_2$ applications in the processing of polymers, Industrial & Engineering Chemistry Research, 42 (2003) 6431-6456.

[33] H.Y. Shin, J. Wu, Equation of state for the phase behavior of carbon dioxide−polymer systems, Industrial & Engineering Chemistry Research, 49 (2010) 7678-7684.

[34] R. Dohrn, S. Peper, J.M.S. Fonseca, High-pressure fluid-phase equilibria: experimental methods and systems investigated (2000–2004), Fluid Phase Equilibria, 288 (2010) 1-54.

[35] S.G. Kazarian, M.F. Vincent, F.V. Bright, C.L. Liotta, C.A. Eckert, Specific intermolecular interaction of carbon dioxide with polymers, Journal of the American Chemical Society, 118 (1996) 1729-1736.

[36] S.P. Nalawade, F. Picchioni, J.H. Marsman, L.P.B.M. Janssen, The FT-IR studies of the interactions of $CO_2$ and polymers having different chain groups, The Journal of Supercritical Fluids, 36 (2006) 236-244.

[37] Y.T. Shieh, K.H. Liu, The effect of carbonyl group on sorption of $CO_2$ in glassy polymers, The Journal of Supercritical Fluids, 25 (2003) 261-268.

[38] Y. Yuan, A.S. Teja, Quantification of specific interactions between $CO_2$ and the carbonyl group in polymers via ATR-FTIR measurements, The Journal of Supercritical Fluids, 56 (2011) 208-212.

[39] Jamroz, M. H., Dobrowolski, J. CZ., Bajdor, K., Borowiak, M. A., AB initio study of the *v* ($CO_2$) mode in EDA complexes, Elsevier, Amsterdam, PAYS-BAS, 1995.

[40] I.A. Ozkan, A.S. Teja, Phase equilibria in systems with specific $CO_2$–polymer interactions, Fluid Phase Equilibria, 228–229 (2005) 487-491.

[41] Y. Yuan, Specific Interactions in polymer + $CO_2$ + sosolvent systems: experiment and modeling, in: School of Chemical and Biomolecular Engineering Georgia Institute of Technology, Atlanta, Georgia, 2010.

[42] A. Kasturirangan, A.S. Teja, Phase behavior of $CO_2$ + biopolymer and $CO_2$ + fluoropolymer systems, Fluid Phase Equilibria, 261 (2007) 64-68.

[43] A. Kasturirangan, Specific interactions in $CO_2$ + polymer systems, in: Chemical and Biomolecular Engineering, Goergia Institute of Technology, Goergia Institute of Technology, 2007.

[44] Y. Yuan, A.S. Teja, Extension of a compressible lattice model to $CO_2$ + cosolvent + polymer systems, The Journal of Supercritical Fluids, 55 (2010) 358-362.

[45] I.C. Sanchez, R.H. Lacombe, An elementary molecular theory of classical fluids. pure fluids, The Journal of Physical Chemistry, 80 (1976) 2352-2362.

[46] T. Sukhadia, Prediction of phase equilibria in solutions: an associative reformulation of thermodynamic theories of solutions, in, Georgia Institute of Technology, Atlanta, Georgia, 1998.

[47] N. Variankaval, Structure and thermodynamics of associationg solutions: prediction of phase equilibria, in, Georgia Institute of Technology, Atlanta, Georgia, 2001.

[48] S.P. Nalawade, F. Picchioni, L.P.B.M. Janssen, Supercritical carbon dioxide as a green solvent for processing polymer melts: Processing aspects and applications, Progress in Polymer Science, 31 (2006) 19-43.

[49] P.F. Arce, M. Aznar, Thermodynamic modeling of liquid–fluid phase equilibrium in supercritical ethylene + copolymer + co-solvent systems using the PC-SAFT equation of state, The Journal of Supercritical Fluids, 52 (2010) 18-29.

[50] I. Stoychev, J. Galy, B. Fournel, P. Lacroix-Desmazes, M. Kleiner, G. Sadowski, Modeling the phase behavior of PEO−PPO−PEO surfactants in carbon dioxide using the PC-SAFT equation of state: application to dry decontamination of solid substrates, Journal of Chemical & Engineering Data, 54 (2009) 1551-1559.

[51] H.S. Byun, M.A. McHugh, High pressure phase behavior of poly[isopropyl acrylate] and poly[isopropyl methacrylate] in supercritical fluid (SCF) solvent and SCF solvent + cosolvent mixtures, The Journal of Supercritical Fluids, 41 (2007) 482-491.

[52] C.F. Kirby, M.A. McHugh, Phase Behavior of Polymers in Supercritical Fluid Solvents, Chemical Reviews, 99 (1999) 565-602.

[53] J.H. Hildebrand, Prausnitz, J. M. & Scott, R. L., Regular and Related Solutions Van Nostrand-Reinhold Co, New York, 1970.

[54] C.M. Hansen, The three-dimensional solubility parameter - key to paint component affinities: solvents, plasticizers, polymers, and resins. II. Dyes, emulsifiers, mutual solubility and compatibility, and pigments. III. Independent cal-culation of the parameter components, Journal of paint technology, 39 (1967 ) 505-510.

[55] J.C. Giddings, M.N. Myers, L. McLaren, R.A. Keller, High Pressure Gas Chromatography of Nonvolatile Species, Science, 162 (1968) 67-73.

[56] L.L. Williams, J.B. Rubin, H.W. Edwards, Calculation of Hansen Solubility Parameter Values for a Range of Pressure and Temperature Conditions, Including the Supercritical Fluid Region, Industrial & Engineering Chemistry Research, 43 (2004) 4967-4972.

[57] J. Emsley, Very strong hydrogen bonding, Chemical Society Reviews, 9 (1980) 91-124.

[58] J.W. Larson, T.B. McMahon, Gas-phase bihalide and pseudobihalide ions. An ion cyclotron resonance determination of hydrogen bond energies in XHY- species (X, Y = F, Cl, Br, CN), Inorganic Chemistry, 23 (1984) 2029-2033.

[59] M.O. Steinhauser, Computational Multiscale Modeling of Fluids and Solids: Theory and Applications, Springer, 2008.

[60] S. Kilic, S. Michalik, Y. Wang, J.K. Johnson, R.M. Enick, E.J. Beckman, Effect of grafted lewis base groups on the phase behavior of model poly(dimethyl siloxanes) in $CO_2$, Industrial & Engineering Chemistry Research, 42 (2003) 6415-6424.

[61] K.H. Kim, Y. Kim, Theoretical Studies for Lewis Acid−Base Interactions and C−H···O Weak Hydrogen Bonding in Various $CO_2$ Complexes, The Journal of Physical Chemistry A, 112 (2008) 1596-1603.

[62] B.L. Bhargava, A.C. Krishna, S. Balasubramanian, Molecular dynamics simulation studies of $CO_2$ – [bmim][PF6] solutions: Effect of $CO_2$ concentration, Aiche Journal, 54 (2008) 2971-2978.

[63] M. Saharay, S. Balasubramanian, Ab initio molecular-dynamics study of supercritical carbon dioxide, The Journal of chemical physics, 120 (2004) 9694-9702.

[64] M. Saharay, S. Balasubramanian, Electron Donor−Acceptor Interactions in Ethanol−$CO_2$ Mixtures: An Ab Initio Molecular Dynamics Study of Supercritical Carbon Dioxide, The Journal of Physical Chemistry B, 110 (2005) 3782-3790.

[65] M. Saharay, S. Balasubramanian, Evolution of Intermolecular Structure and Dynamics in Supercritical Carbon Dioxide with Pressure: An ab Initio Molecular Dynamics Study, The Journal of Physical Chemistry B, 111 (2006) 387-392.

[66] B.C. Smith, Fundamentals of Fourier Transform Infrared Spectroscopy CRC Press, Boca Raton, 1996.

[67] S.G. Kazarian, Polymers and supercritical fluids: opportunities for vibrational spectroscopy, Macromolecular Symposia, 184 (2002) 215-228.

[68] M.M. Coleman, X. Yang, P.C. Painter, J.F. Graf, Equilibrium constants and the prediction of phase behavior for phenoxy blends with aliphatic polyesters, Macromolecules, 25 (1992) 4414-4424.

[69] J.C. Meredith, K.P. Johnston, J.M. Seminario, S.G. Kazarian, C.A. Eckert, Quantitative Equilibrium Constants between $CO_2$ and Lewis Bases from FTIR Spectroscopy, The Journal of Physical Chemistry, 100 (1996) 10837-10848.

[70] K. Dharmalingam, K. Ramachandran, P. Sivagurunathan, G.M. Kalamse, Molecular interactions in alcohol–ethyl methacrylate mixtures, Spectrochimica Acta Part A: Molecular and Biomolecular Spectroscopy, 69 (2008) 467-470.

[71] C.P. Nash, THE CALCULATION OF EQUILIBRIUM CONSTANTS FROM SPECTRO-PHOTOMETRIC DATA, The Journal of Physical Chemistry, 64 (1960) 950-953.

[72] R.S. Drago, N. O'Bryan, G.C. Vogel, A frequency shift-enthalpy correlation for a given donor with various hydrogen-bonding acids, Journal of the American Chemical Society, 92 (1970) 3924-3929.

[73] K.F. Purcell, J.A. Stikeleather, S.D. Brunk, Spectroscopic studies of hydrogen bonding: Hexafluoroisopropanol, Journal of Molecular Spectroscopy, 32 (1969) 202-213.

[74] F.M. Fowkes, D.O. Tischler, J.A. Wolfe, L.A. Lannigan, C.M. Ademu-John, M.J. Halliwell, Acid–base complexes of polymers, Journal of Polymer Science: Polymer Chemistry Edition, 22 (1984) 547-566.

[75] F. Cangelosi, M.T. Shaw, Hydrogen bonding in polymer systems, Polymer Engineering & Science, 23 (1983) 669-675.

[76] W. Ji, Modeling VLE and GLE of systems involving polymers by using SRK equation of state, Chinese Journal of Chemical Engineering, 15 (2007) 221-227.

[77] T. Sako, A.H. Wu, J.M. Prausnitz, A cubic equation of state for high-pressure phase equilibria of mixtures containing polymers and volatile fluids, Journal of Applied Polymer Science, 38 (1989) 1839-1858.

[78] F. Gharagheizi, M. Mehrpooya, A. Vatani, Modification of Sako-Wu-Prausnitz equation of state for fluid phase equilibria in polyethylene-ethylene systems at high pressures, Brazilian Journal of Chemical Engineering, 23 (2006) 383-394.

[79] Z.h. Chen, K. Cao, Z. Yao, Z.-m. Huang, Modeling solubilities of subcritical and supercritical fluids in polymers with cubic and non-cubic equations of state, The Journal of Supercritical Fluids, 49 (2009) 143-153.

[80] P. Arce, M. Aznar, S. Mattedi, Fluid phase behavior modeling of $CO_2$ + molten polymer systems using cubic and theoretically based equations of state, Polymer Engineering & Science, 48 (2008) 1157-1167.

[81] P.F. Arce, M. Aznar, Phase behavior of polypropylene + n-pentane and polypropylene + n-pentane + carbon dioxide: modeling with cubic and non-cubic equations of state, The Journal of Supercritical Fluids, 34 (2005) 177-182.

[82] P. Arce, M. Aznar, Modeling of phase equilibrium of binary mixtures composed by polystyrene and chlorofluorocarbons, hydrochlorofluorocarbons, hydrofluorocarbons and supercritical fluids using cubic and non-cubic equations of state, The Journal of Supercritical Fluids, 45 (2008) 134-145.

[83] J. Gwon, D.W. Cho, S.H. Kim, H.Y. Shin, H. Kim, Phase behaviour of the ternary mixture system of poly(l-lactic acid), dichloromethane and carbon dioxide, The Journal of Chemical Thermodynamics, 55 (2012) 37-41.

[84] P. Arce, M. Aznar, Modeling the thermodynamic behavior of poly(lactide-co-glycolide) + supercritical fluid mixtures with equations of state, Fluid Phase Equilibria, 244 (2006) 16-25.

[85] G.M. Kontogeorgis, I.V. Yakoumis, P.M. Vlamos, Application of the sCPA equation of state for polymer solutions, Computational and Theoretical Polymer Science, 10 (2000) 501-506.

[86] Y. Song, S.M. Lambert, J.M. Prausnitz, A perturbed hard-sphere-chain equation of state for normal fluids and polymers, Industrial & Engineering Chemistry Research, 33 (1994) 1047-1057.

[87] W.G. Chapman, K.E. Gubbins, G. Jackson, M. Radosz, SAFT: Equation-of-state solution model for associating fluids, Fluid Phase Equilibria, 52 (1989) 31-38.

[88] M.L. Michelsen, E.M. Hendriks, Physical properties from association models, Fluid Phase Equilibria, 180 (2001) 165-174.

[89] G. Soave, Equilibrium constants from a modified Redlich-Kwong equation of state, Chemical Engineering Science, 27 (1972) 1197-1203.

[90] M.S. Wertheim, Fluids with highly directional attractive forces. IV. Equilibrium polymerization, Journal of Statistical Physics, 42 (1986) 477-492.

[91] M.B. Oliveira, J.A.P. Coutinho, A.J. Queimada, Mutual solubilities of hydrocarbons and water with the CPA EoS, Fluid Phase Equilibria, 258 (2007) 58-66.

[92] Y.C. Chiew, Percus-Yevick integral-equation theory for athermal hard-sphere chains, Molecular Physics, 70 (1990) 129-143.

[93] J.M. Prausnitz, R.N. Lichtenthaler, E.G.d. Azevedo, Moleular thermodynamics of fluid - phase equilibria, Third Edition ed., Prentice - Hall, Inc., New Jersey, 1999.

[94] S.H. Huang, M. Radosz, Equation of state for small, large, polydisperse, and associating molecules, Industrial & Engineering Chemistry Research, 29 (1990) 2284-2294.

[95] N. von Solms, M.L. Michelsen, G.M. Kontogeorgis, Prediction and correlation of high-pressure gas solubility in polymers with simplified PC-SAFT, Industrial & Engineering Chemistry Research, 44 (2005) 3330-3335.

[96] J. Gross, G. Sadowski, Perturbed-chain SAFT: An equation of state based on a perturbation theory for chain molecules, Industrial & Engineering Chemistry Research, 40 (2001) 1244-1260.

[97] S.H. Huang, M. Radosz, Equation of state for small, large, polydisperse, and associating molecules: extension to fluid mixtures, Industrial & Engineering Chemistry Research, 30 (1991) 1994-2005.

[98] X.S. Li, P. Englezos, Vapor–liquid equilibrium of systems containing alcohols, water, carbon dioxide and hydrocarbons using SAFT, Fluid Phase Equilibria, 224 (2004) 111-118.

[99] X. Chen, Y. Sato, S. Takishima, H. Masuoka, Liquid–liquid equilibria of solvent + polymer solutions with a chain-referenced perturbed hard-sphere-chain equation of state, Fluid Phase Equilibria, 237 (2005) 162-169.

[100] X. Chen, Y. Hou, W. Wu, S. Ren, J. Zhang, J. Fan, High pressure phase behavior and density of the carbon dioxide+1-methylimidazole binary system, Journal of Supercritical Fluids, 49 (2009) 310-314.

[101] I.A. Kouskoumvekaki, N. von Solms, T. Lindvig, M.L. Michelsen, G.M. Kontogeorgis, Novel method for estimating pure-component parameters for polymers: application to the PC-SAFT equation of state, Industrial & Engineering Chemistry Research, 43 (2004) 2830-2838.

[102] P. Paricaud, A. Galindo, G. Jackson, Modeling the cloud curves and the solubility of gases in amorphous and semicrystalline polyethylene with the SAFT-VR approach and flory theory of crystallization, Industrial & Engineering Chemistry Research, 43 (2004) 6871-6889.

[103] J. Chmelar, T. Gregor, H. Hajova, A. Nistor, J. Kosek, Experimental study and PC-SAFT simulations of sorption equilibria in polystyrene, Polymer, 52 (2011) 3082-3091.

[104] G. Li, H. Li, J. Wang, C.B. Park, Investigating the solubility of $CO_2$ in polypropylene using various EOS models, Cellular Polymers, 25 (2006) 237-248.

[105] T. Lindvig, M.L. Michelsen, G.M. Kontogeorgis, Liquid−liquid equilibria for binary and ternary polymer solutions with PC-SAFT, Industrial & Engineering Chemistry Research, 43 (2004) 1125-1132.

[106] J. Gross, G. Sadowski, Modeling Polymer Systems Using the Perturbed-Chain Statistical Associating Fluid Theory Equation of State, Industrial & Engineering Chemistry Research, 41 (2001) 1084-1093.

[107] P.J. Flory, Statistical thermodynamics of liquid mixtures, Journal of the American Chemical Society, 87 (1965) 1833-1838.

[108] P.C. Painter, Y. Park, M.M. Coleman, Thermodynamics of hydrogen bonding in polymer blends. 1. The application of association models, Macromolecules, 22 (1989) 570-579.

[109] M.M. Coleman, G.J. Pehlert, P.C. Painter, Functional group accessibility in hydrogen bonded polymer blends, Macromolecules, 29 (1996) 6820-6831.

[110] M.M. Coleman, P.C. Painter, Hydrogen bonded polymer blends, Progress in Polymer Science, 20 (1995) 1-59.

[111] M. Coleman, J. Graf, and P. Painter, Specific Interactions and the Miscibility of Polymer Blends, Technomic Publishing AG, Pennsylvania, 1991.

[112] I.C. Sanchez, R.H. Lacombe, Statistical thermodynamics of polymer solutions, Macromolecules, 11 (1978) 1145-1156.

[113] K. Matsuyama, K. Mishima, Phase behavior of $CO_2$ + polyethylene glycol + ethanol at pressures up to 20 MPa, Fluid Phase Equilibria, 249 (2006) 173-178.

[114] C. Panayiotou, M. Pantoula, E. Stefanis, I. Tsivintzelis, I.G. Economou, Nonrandom hydrogen-bonding model of fluids and their mixtures. 1. pure fluids, Industrial & Engineering Chemistry Research, 43 (2004) 6592-6606.

[115] C. Panayiotou, I. Tsivintzelis, I.G. Economou, Nonrandom hydrogen-bonding model of fluids and their mixtures. 2. multicomponent mixtures, Industrial & Engineering Chemistry Research, 46 (2007) 2628-2636.

[116] A.J. Staverman, The entropy of high polymer solutions. Generalization of formulae, Recueil des Travaux Chimiques des Pays-Bas, 69 (1950) 163-174.

[117] E.A. Guggenheim, Mixtures, Oxford University Press, London, 1952.

[118] C. Panayiotou, I.C. Sanchez, Hydrogen bonding in fluids: an equation-of-state approach, The Journal of Physical Chemistry, 95 (1991) 10090-10097.

[119] B.A. Veytsman, Are lattice models valid for fluids with hydrogen bonds?, The Journal of Physical Chemistry, 94 (1990) 8499-8500.

[120] M. Pantoula, J. von Schnitzler, R. Eggers, C. Panayiotou, Sorption and swelling in glassy polymer/carbon dioxide systems: Part II—Swelling, The Journal of Supercritical Fluids, 39 (2007) 426-434.

[121] P.F. Arce, M. Aznar, Modeling of thermodynamic behavior of PVT properties and cloud point temperatures of polymer blends and polymer blend + carbon dioxide systems using non-cubic equations of state, Fluid Phase Equilibria, 286 (2009) 17-27.

[122] B. Bonavoglia, G. Storti, M. Morbidelli, Modeling of the sorption and swelling behavior of semicrystalline polymers in supercritical $CO_2$, Industrial & Engineering Chemistry Research, 45 (2005) 1183-1200.

[123] M.A. Jacobs, M.F. Kemmere, J.T.F. Keurentjes, Foam processing of poly(ethylene-co-vinyl acetate) rubber using supercritical carbon dioxide, Polymer, 45 (2004) 7539-7547.

[124] Y. Sato, T. Takikawa, M. Yamane, S. Takishima, H. Masuoka, Solubility of carbon dioxide in PPO and PPO/PS blends, Fluid Phase Equilibria, 194–197 (2002) 847-858.

[125] C. Gutiérrez, J.F. Rodríguez, I. Gracia, A. de Lucas, M.T. García, High-pressure phase equilibria of Polystyrene dissolutions in Limonene in presence of $CO_2$, The Journal of Supercritical Fluids, 84 (2013) 211-220.

[126] E. Aionicesei, M. Škerget, Ž. Knez, Measurement and Modeling of the $CO_2$ Solubility in Poly(ethylene glycol) of Different Molecular Weights, Journal of Chemical & Engineering Data, 53 (2007) 185-188.

[127] A. Galia, A. Cipollina, O. Scialdone, G. Filardo, Investigation of multicomponent sorption in polymers from fluid mixtures at supercritical conditions: The case of the carbon dioxide/vinylidenefluoride/poly(vinylidenefluoride) system, Macromolecules, 41 (2008) 1521-1530.

[128] F. Favari, A. Bertucco, N. Elvassore, M. Fermeglia, Multiphase multicomponent equilibria for mixtures containing polymers by the perturbation theory, Chemical Engineering Science, 55 (2000) 2379-2392.

[129] M.N. Lotfollahi, R.D. Salehi, H. Modarress, Ternary phase diagram for polymer/solvent/supercritical - $CO_2$ by Sanchez - Lacombe model, Iranian Association of Chemical Engineers (IAChE), 3 (2006) 64 - 72.

[130] H.S. Byun, Phase behavior on the binary and ternary mixtures of poly(cyclohexyl acrylate) and poly(cyclohexyl methacrylate) in supercritical $CO_2$, Journal of Applied Polymer Science, 94 (2004) 1117-1125.

[131] H.S. Byun, C.H. Bang, J.S. Lim, Effect of cosolvent concentration on phase behavior for the poly(isodecyl acrylate) in supercritical carbon dioxide, propane, propylene, butane, 1-butene and dimethyl ether, Journal of Macromolecular Science Part B, 47 (2008) 150-165.

[132] S. Liu, H.Y. Lee, S.D. Yoon, K.P. Yoo, H.S. Byun, High-pressure phase behavior for poly[dodecyl methacrylate] + supercritical solvents + cosolvents and carbon dioxide + dodecyl methacrylate mixture, Industrial & Engineering Chemistry Research, 48 (2009) 7821-7827.

[133] T.A. Walker, C.M. Colina, K.E. Gubbins, R.J. Spontak, Thermodynamics of poly(dimethylsiloxane)/poly(ethylmethylsiloxane) (PDMS/PEMS) blends in the presence of high-pressure $CO_2$, Macromolecules, 37 (2004) 2588-2595.

[134] F. Becker, M. Buback, H. Latz, G. Sadowski, F. Tumakaka, Cloud-point curves of ethylene−(meth)acrylate copolymers in fluid ethene up to high pressures and temperatures—experimental study and PC–SAFT modeling, Fluid Phase Equilibria, 215 (2004) 263-282.

[135] M. Haruki, Y. Takakura, H. Sugiura, S.I. Kihara, S. Takishima, Phase behavior for the supercritical ethylene + hexane + polyethylene systems, The Journal of Supercritical Fluids, 44 (2008) 284-293.

[136] M. Haruki, K. Sato, S.I. Kihara, S. Takishima, High pressure phase behavior for the supercritical ethylene + cyclohexane + hexane + polyethylene systems, The Journal of Supercritical Fluids, 49 (2009) 125-134.

[137] L.A. Blanchard, D. Hancu, E.J. Beckman, J.F. Brennecke, Green processing using ionic liquids and $CO_2$, Nature, 399 (1999) 28-29.

[138] L.A. Blanchard, J.F. Brennecke, Recovery of organic products from ionic liquids using supercritical carbon dioxide, Industrial & Engineering Chemistry Research, 40 (2001) 287-292.

[139] A.M. Scurto, S.N.V.K. Aki, J.F. Brennecke, $CO_2$ as a Separation Switch for Ionic Liquid/Organic Mixtures, Journal of the American Chemical Society, 124 (2002) 10276-10277.

[140] P.J. Carvalho, V.H. Alvarez, J.J.B. Machado, J. Pauly, J.-L. Daridon, I.M. Marrucho, M. Aznar, J.A.P. Coutinho, High pressure phase behavior of carbon dioxide in 1-alkyl-3-methylimidazolium bis(trifluoromethylsulfonyl)imide ionic liquids, Journal of Supercritical Fluids, 48 (2009) 99-107.

[141] J.L. Anderson, J.K. Dixon, J.F. Brennecke, Solubility of $CO_2$, CH4, C2H6, C2H4, O2, and N2 in 1-Hexyl-3-methylpyridinium Bis(trifluoromethylsulfonyl)imide: Comparison to Other Ionic Liquids, Accounts of Chemical Research, 40 (2007) 1208-1216.

[142] S.G. Kazarian, B.J. Briscoe, T. Welton, Combining ionic liquids and supercritical fluids: ATR-IR study of $CO_2$ dissolved in two ionic liquids at high pressures, Chemical Communications, (2000) 2047-2048.

[143] A. Shariati, C.J. Peters, High-pressure phase behavior of systems with ionic liquids: measurements and modeling of the binary system fluoroform+1-ethyl-3-methylimidazolium hexafluorophosphate, The Journal of Supercritical Fluids, 25 (2003) 109-117.

[144] P.J. Carvalho, V.H. Alvarez, I.M. Marrucho, M. Aznar, J.A.P. Coutinho, High pressure phase behavior of carbon dioxide in 1-butyl-3-methylimidazolium bis(trifluoromethylsulfonyl)imide and 1-butyl-3-methylimidazolium dicyanamide ionic liquids, Journal of Supercritical Fluids, 50 (2009) 105-111.

[145] J.O. Valderrama, V.H. Alvarez, A versatile thermodynamic consistency test for incomplete phase equilibrium data of high-pressure gas–liquid mixtures, Fluid Phase Equilibria, 226 (2004) 149-159.

[146] M.B. Shiflett, A. Yokozeki, Solubility of $CO_2$ in Room Temperature Ionic Liquid [hmim][Tf2N], The Journal of Physical Chemistry B, 111 (2007) 2070-2074.

[147] M.B. Shiflett, D.J. Kasprzak, C.P. Junk, A. Yokozeki, Phase behavior of {carbon dioxide plus bmim Ac } mixtures, Journal of Chemical Thermodynamics, 40 (2008) 25-31.

[148] L.F. Vega, O. Vilaseca, F. Llovell, J.S. Andreu, Modeling ionic liquids and the solubility of gases in them: Recent advances and perspectives, Fluid Phase Equilibria, 294 (2010) 15-30.

[149] Z. Lei, J. Zhang, Q. Li, B. Chen, UNIFAC Model for Ionic Liquids, Industrial & Engineering Chemistry Research, 48 (2009) 2697-2704.

[150] T. Banerjee, M.K. Singh, R.K. Sahoo, A. Khanna, Volume, surface and UNIQUAC interaction parameters for imidazolium based ionic liquids via Polarizable Continuum Model, Fluid Phase Equilibria, 234 (2005) 64-76.

[151] S. Nebig, R. Bölts, J. Gmehling, Measurement of vapor–liquid equilibria (VLE) and excess enthalpies (HE) of binary systems with 1-alkyl-3-methylimidazolium bis(trifluoromethylsulfonyl)imide and prediction of these properties and $\gamma\infty$ using modified UNIFAC (Dortmund), Fluid Phase Equilibria, 258 (2007) 168-178.

[152] Y.S. Kim, W.Y. Choi, J.H. Jang, K.P. Yoo, C.S. Lee, Solubility measurement and prediction of carbon dioxide in ionic liquids, Fluid Phase Equilibria, 228 (2005) 439-445.

[153] E.K. Karakatsani, I.G. Economou, M.C. Kroon, C.J. Peters, G.-J. Witkamp, tPC-PSAFT Modeling of Gas Solubility in Imidazolium-Based Ionic Liquids†, The Journal of Physical Chemistry C, 111 (2007) 15487-15492.

[154] S.A. Bhamidipati M, Detamore MS, The future of carbon dioxide for polymer processing in tissue engineering Tissue Engineering Part B: Reviews, 19 (2013) 221-232.

[155] M.B. Oliveira, J.F. Mano, Polymer-based microparticles in tissue engineering and regenerative medicine, Biotechnology Progress, 27 (2011) 897-912.

[156] E. Reverchon, S. Cardea, Supercritical fluids in 3-D tissue engineering, The Journal of Supercritical Fluids, 69 (2012) 97-107.

[157] K. Takahashi, Polymer analysis by supercritical fluid chromatography, Journal of Bioscience and Bioengineering, 116 (2013) 133-140.

[158] D. Sanli, S.E. Bozbag, C. Erkey, Synthesis of nanostructured materials using supercritical $CO_2$: Part I. Physical transformations, Journal of Materials Science, 47 (2012) 2995-3025.

[159] J.P. Rao, K.E. Geckeler, Polymer nanoparticles: Preparation techniques and size-control parameters, Progress in Polymer Science, 36 (2011) 887-913.

[160] F. Cansell, C. Aymonier, Design of functional nanostructured materials using supercritical fluids, The Journal of Supercritical Fluids, 47 (2009) 508-516.

[161] F. Mattea, Á. Martín, M.J. Cocero, Carotenoid processing with supercritical fluids, Journal of Food Engineering, 93 (2009) 255-265.

[162] C.A. Scholes, G.W. Stevens, S.E. Kentish, Membrane gas separation applications in natural gas processing, Fuel, 96 (2012) 15-28.

[163] C.A. Scholes, K.H. Smith, S.E. Kentish, G.W. Stevens, $CO_2$ capture from pre-combustion processes-strategies for membrane gas separation, International Journal of Greenhouse Gas Control, 4 (2010) 739-755.

[164] A. Brunetti, F. Scura, G. Barbieri, E. Drioli, Membrane technologies for $CO_2$ separation, Journal of Membrane Science, 359 (2010) 115-125.

[165] S.E. Bozbag, C. Erkey, Supercritical fluids in fuel cell research and development, The Journal of Supercritical Fluids, 62 (2012) 1-31.

[166] Y. Haldorai, J.J. Shim, K.T. Lim, Synthesis of polymer–inorganic filler nanocomposites in supercritical $CO_2$, The Journal of Supercritical Fluids, 71 (2012) 45-63.

[167] J. Yang, T. Hasell, D.C. Smith, S.M. Howdle, Deposition in supercritical fluids: from silver to semiconductors, Journal of Materials Chemistry, 19 (2009) 8560-8570.

[168] M.I. Burguete, E. García-Verdugo, S.V. Luis, Efficient and selective chemical transformations under flow conditions: The combination of supported catalysts and supercritical fluids, Beilstein Journal of Organic Chemistry, 7 (2011) 1347-1359.

[169] K. M., Y. R., Application of supercritical antisolvent method in drug encapsulation: a review, International Journal of Nanomedicine, 6 (2011) 1429-1442.

[170] M.J. Cocero, Á. Martín, F. Mattea, S. Varona, Encapsulation and co-precipitation processes with supercritical fluids: Fundamentals and applications, The Journal of Supercritical Fluids, 47 (2009) 546-555.

[171] O.R. Davies, A.L. Lewis, M.J. Whitaker, H. Tai, K.M. Shakesheff, S.M. Howdle, Applications of supercritical $CO_2$ in the fabrication of polymer systems for drug delivery and tissue engineering, Advanced Drug Delivery Reviews, 60 (2008) 373-387.

[172] M.E.M. Braga, M.T.V. Pato, H.S.R.C. Silva, E.I. Ferreira, M.H. Gil, C.M.M. Duarte, H.C. de Sousa, Supercritical solvent impregnation of ophthalmic drugs on chitosan derivatives, The Journal of Supercritical Fluids, 44 (2008) 245-257.

[173] J.M.S. Fonseca, R. Dohrn, S. Peper, High-pressure fluid-phase equilibria: experimental methods and systems investigated (2005–2008), Fluid Phase Equilibria, 300 (2011) 1-69.

[174] E. Kiran, Polymer miscibility, phase separation, morphological modifications and polymorphic transformations in dense fluids, The Journal of Supercritical Fluids, 47 (2009) 466-483.

[175] Ž. Knez, E. Markocic, Z. Novak, M.K. Hrncic, Processing polymeric biomaterials using supercritical $CO_2$, Chemie Ingenieur Technik, 83 (2011) 1371-1380.

[176] M. Sauceau, J. Fages, A. Common, C. Nikitine, E. Rodier, New challenges in polymer foaming: A review of extrusion processes assisted by supercritical carbon dioxide, Progress in Polymer Science, 36 (2011) 749-766.

[177] T.A. Walker, D.J. Frankowski, R.J. Spontak, Thermodynamics and kinetic processes of polymer blends and block copolymers in the presence of pressurized carbon dioxide, Advanced Materials, 20 (2008) 879-898.

[178] H. Ruckdäschel, P. Gutmann, V. Altstädt, H. Schmalz, A.E. Müller, Foaming of microstructured and nanostructured polymer blends, in: A.H.E. Müller, H.-W. Schmidt (Eds.) Complex Macromolecular Systems I, Springer Berlin Heidelberg, 2010, pp. 199-252.

[179] L. Du, J.Y. Kelly, G.W. Roberts, J.M. DeSimone, Fluoropolymer synthesis in supercritical carbon dioxide, The Journal of Supercritical Fluids, 47 (2009) 447-457.

[180] I. Kikic, Polymer–supercritical fluid interactions, The Journal of Supercritical Fluids, 47 (2009) 458-465.

[181] K.P. Johnston, S.R.P.d. Rocha, Colloids in supercritical fluids over the last 20 years and future directions, The Journal of Supercritical Fluids, 47 (2009) 523-530.

[182] N.F. Carnahan, K.E. Starling, Equation of state for nonattracting rigid spheres, The Journal of chemical physics, 51 (1969) 635-636.

[183] J.A. Barker, D. Henderson, Perturbation theory and equation of state for fluids. II. a successful theory of liquids, The Journal of chemical physics, 47 (1967) 4714-4721.

[184] Y.H. Fu, S.I. Sandler, A simplified SAFT equation of state for associating compounds and mixtures, Industrial & Engineering Chemistry Research, 34 (1995) 1897-1909.

[185] K.H. Lee, M. Lombardo, S.I. Sandler, The generalized van der Waals partition function. II. application to the square-well fluid, Fluid Phase Equilibria, 21 (1985) 177-196.

[186] A. Gil-Villegas, A. Galindo, P.J. Whitehead, S.J. Mills, G. Jackson, A.N. Burgess, Statistical associating fluid theory for chain molecules with attractive potentials of variable range, The Journal of chemical physics, 106 (1997) 4168-4186.

[187] E. Aionicesei, M. Škerget, Ž. Knez, Mathematical modelling of the solubility of supercritical $CO_2$ in poly(l-lactide) and poly(d,l-lactide-co-glycolide), The Journal of Supercritical Fluids, 50 (2009) 320-326.

[188] N. Elvassore, K. Vezzù, A. Bertucco, Measurement and modeling of $CO_2$ absorption in poly(lactic-co-glycolic acid), The Journal of Supercritical Fluids, 33 (2005) 1-5.

[189] Z. Lei, H. Ohyabu, Y. Sato, H. Inomata, R.L. Smith Jr, Solubility, swelling degree and crystallinity of carbon dioxide–polypropylene system, The Journal of Supercritical Fluids, 40 (2007) 452-461.

[190] X. Xu, D.E. Cristancho, S. Costeux, Z.-G. Wang, Density-functional theory for polymer-carbon dioxide mixtures: A perturbed-chain SAFT approach, The Journal of chemical physics, 137 (2012 ) 054902-054908.

[191] D. Liu, H. Li, M.S. Noon, D.L. Tomasko, $CO_2$-induced PMMA swelling and multiple thermodynamic property analysis using Sanchez−Lacombe EOS, Macromolecules, 38 (2005) 4416-4424.

[192] D.c. Li, T. Liu, L. Zhao, W.-k. Yuan, Solubility and diffusivity of carbon dioxide in solid-state isotactic polypropylene by the pressure−decay method, Industrial & Engineering Chemistry Research, 48 (2009) 7117-7124.

[193] R. Pini, G. Storti, M. Mazzotti, H. Tai, K.M. Shakesheff, S.M. Howdle, Sorption and swelling of poly(DL-lactic acid) and poly(lactic-co-glycolic acid) in supercritical

$CO_2$: An experimental and modeling study, Journal of Polymer Science Part B: Polymer Physics, 46 (2008) 483-496.

[194] Z.Y. Li, T.Y. Meng, X.W. Liu, Y.J. Xia, D.P. Hu, Phase equilibrium characteristics of supercritical CO2/poly(ethylene terephthalate) binary system, Journal of Applied Polymer Science, 109 (2008) 2836-2841.

[195] H.S. Byun, Y.J. Park, J.S. Lim, Phase behavior on the binary and ternary mixtures of poly(isooctyl acrylate) + supercritical fluid solvents + isooctyl acrylate and $CO_2$ + isooctyl acrylate system, Journal of Applied Polymer Science, 107 (2008) 1124-1132.

[196] E. de Paz, A. Martín, S. Rodríguez-Rojo, J. Herreras, M.J. Cocero, Determination of phase equilibrium (eolid−liquid−gas) in poly-(ε-caprolactone)−carbon dioxide systems, Journal of Chemical & Engineering Data, 55 (2010) 2781-2785.

[197] M. Görnert, G. Sadowski, Phase-equilibrium measurement and modeling of the PMMA/MMA/carbon dioxide ternary system, The Journal of Supercritical Fluids, 46 (2008) 218-225.

[198] M.A. Fanovich, P. Jaeger, Sorption and diffusion of compressed carbon dioxide in polycaprolactone for the development of porous scaffolds, Materials Science and Engineering: C, 32 (2012) 961-968.

[199] A.-Z. Chen, Z. Zhao, S.-B. Wang, Y. Li, C. Zhao, Y.-G. Liu, A continuous RESS process to prepare PLA–PEG–PLA microparticles, The Journal of Supercritical Fluids, 59 (2011) 92-97.

[200] I.-I. Jung, S. Haam, G. Lim, J.-H. Ryu, Preparation of peptide-loaded polymer microparticles using supercritical carbon dioxide, Biotechnology and Bioprocess Engineering, 17 (2012) 185-194.

[201] S. Palakodaty, P. York, Phase Behavioral Effects on Particle Formation Processes Using Supercritical Fluids, Pharmaceutical Research, 16 (1999) 976-985.

[202] S.-S. Ashrafmansouri, S. Raeissi, Modeling gas solubility in ionic liquids with the SAFT-γ group contribution method, The Journal of Supercritical Fluids, 63 (2012) 81-91.

[203] M.S. Shin, H. Kim, A quasi-chemical nonrandom lattice fluid model for phase equilibria of associating systems, Fluid Phase Equilibria, 256 (2007) 27-33.

[204] S.I. Sandler, Models for Thermodynamic and Phase Equilibria Calculations, Marcel Dekker, Inc., New York, 1994.

[205] C.P.J.H. Vera, Statistical Thermodynamics of r-Mer Fluids and Their Mixtures, Polymer Journal, 14 (1982) 681 - 694.

[206] P.D. Condo, I.C. Sanchez, C.G. Panayiotou, K.P. Johnston, Glass transition behavior including retrograde vitrification of polymers with compressed fluid diluents, Macromolecules, 25 (1992) 6119-6127.

[207] M.L. Cecopieri-Gómez, J. Palacios-Alquisira, Interaction parameter (c); expansion factor (e); steric hindrance factor (s); and shielding function F(x); for the system PEA-organic solvents by intrinsic viscosity measurements, Journal of the Brazilian Chemical Society, 16 (2005) 426-433.

[208] P. Zoller, D.J. Walsh, Standard Pressure-volume-temperature data for polymers, Technomic Publishing Company, Inc., Lancaster, Pennsylvania 1995.

[209] P. Zoller, R.K. Jain, R. Simha, Equation of state of copolymer melts: The poly(vinyl acetate)–polyethylene pair, Journal of Polymer Science Part B: Polymer Physics, 24 (1986) 687-696.

[210] P.A. Rodgers, Pressure–volume–temperature relationships for polymeric liquids: A review of equations of state and their characteristic parameters for 56 polymers, Journal of Applied Polymer Science, 48 (1993) 1061-1080.

[211] Y.I. Sato, Kenzo; Takishima, Shigeki; Masuoka, Hirokatsu, Pressure-volume-temperature behavior of polylactide, poly(butylene succinate), and poly(butylene succinate-co-adipate), Polymer Engineering and Science, 40 (2000) 2602-2609.

[212] O. Olabisi, R. Simha, Pressure-Volume-Temperature Studies of Amorphous and Crystallizable Polymers. I. Experimental, Macromolecules, 8 (1975) 206-210.

[213] A. Quach, R. Simha, Pressure-Volume-Temperature Properties and Transitions of Amorphous Polymers; Polystyrene and Poly (orthomethylstyrene), Journal of Applied Physics, 42 (1971) 4592-4606.

[214] D.-c. Li, T. Liu, L. Zhao, W.-k. Yuan, Solubility and Diffusivity of Carbon Dioxide in Solid-State Isotactic Polypropylene by the Pressure−Decay Method, Industrial & Engineering Chemistry Research, 48 (2009) 7117-7124.

[215] S. Beret, J.M. Prausnitz, Densities of Liquid Polymers at High Pressure. Pressure-Volume-Temperature Measurements for Polythylene, Polyisobutylene, Poly(vinyl acetate), and Poly(dimethylsiloxane) to 1 kbar, Macromolecules, 8 (1975) 536-538.

[216] J. Li, Y. Ye, L. Chen, Z. Qi, Solubilities of $CO_2$ in Poly(ethylene glycols) from (303.15 to 333.15) K, Journal of Chemical & Engineering Data, 57 (2011) 610-616.

[217] R.G. Wissinger, M.E. Paulaitis, Swelling and sorption in polymer–$CO_2$ mixtures at elevated pressures, Journal of Polymer Science Part B: Polymer Physics, 25 (1987) 2497-2510.

[218] Y. Sato, K. Fujiwara, T. Takikawa, Sumarno, S. Takishima, H. Masuoka, Solubilities and diffusion coefficients of carbon dioxide and nitrogen in polypropylene,

high-density polyethylene, and polystyrene under high pressures and temperatures, Fluid Phase Equilibria, 162 (1999) 261-276.

[219] P. Alessi, A. Cortesi, I. Kikic, F. Vecchione, Plasticization of polymers with supercritical carbon dioxide: Experimental determination of glass-transition temperatures, Journal of Applied Polymer Science, 88 (2003) 2189-2193.

[220] J.S. Chiou, J.W. Barlow, D.R. Paul, Plasticization of glassy polymers by $CO_2$, Journal of Applied Polymer Science, 30 (1985) 2633-2642.

[221] O.W. Kolling, FTIR study of the solvent influence on the carbonyl absorption peak of ethyl acetate, The Journal of Physical Chemistry, 96 (1992) 6217-6220.

[222] J.R. Fried, W. Li, High-pressure FTIR studies of gas–polymer interactions, Journal of Applied Polymer Science, 41 (1990) 1123-1131.

[223] A. Higuchi, T. Nakagawa, Infrared spectroscopic studies of $CO_2$ sorbed in glassy and rubbery polymeric membranes, Journal of Polymer Science Part B: Polymer Physics, 32 (1994) 149-157.

[224] Y. Danten, T. Tassaing, M. Besnard, Vibrational Spectra of $CO_2$-Electron Donor−Acceptor Complexes from ab Initio, The Journal of Physical Chemistry A, 106 (2002) 11831-11840.

[225] M.I. Cabaço, Y. Danten, T. Tassaing, S. Longelin, M. Besnard, Raman spectroscopy of $CO_2$–acetone and $CO_2$–ethanol complexes, Chemical Physics Letters, 413 (2005) 258-262.

[226] R.S. Drago, G.C. Vogel, T.E. Needham, Four-parameter equation for predicting enthalpies of adduct formation, Journal of the American Chemical Society, 93 (1971) 6014-6026.

[227] J. Wang, M. Wang, J. Hao, S.-i. Fujita, M. Arai, Z. Wu, F. Zhao, Theoretical study on interaction between $CO_2$ and carbonyl compounds: Influence of $CO_2$ on infrared spectroscopy and activity of CO, The Journal of Supercritical Fluids, 54 (2010) 9-15.

[228] N. Tekin, M. Cebe, Solvents effect on infrared spectra of trimethyl phosphate in organic solvents, Vibrational Spectroscopy, 36 (2004) 129-133.

[229] Y. Park, Specific interactions between phosphorus compounds and carbon dioxide: Ab initio approach, Journal of Supercritical Fluids, 36 (2005) 154-159.

[230] E.D. Bates, R.D. Mayton, I. Ntai, J.H. Davis, $CO_2$ Capture by a Task-Specific Ionic Liquid, Journal of the American Chemical Society, 124 (2002) 926-927.

[231] W. Leitner, Recent advances in catalyst immobilization using supercritical carbon dioxide, Pure and Applied Chemistry, 76 (2004) 635-644.

[232] R. Sheldon, Catalytic reactions in ionic liquids, Chemical Communications, (2001) 2399-2407.

[233] F. Liu, M.B. Abrams, R.T. Baker, W. Tumas, Phase-separable catalysis using room temperature ionic liquids and supercritical carbon dioxide, Chemical Communications, (2001) 433-434.

[234] M.T. Reetz, W. Wiesenhofer, G. Francio, W. Leitner, Biocatalysis in ionic liquids: batchwise and continuous flow processes using supercritical carbon dioxide as the mobile phase, Chemical Communications, 0 (2002) 992-993.

[235] M.C. Kroon, E.K. Karakatsani, I.G. Economou, G.-J. Witkamp, C.J. Peters, Modeling of the Carbon Dioxide Solubility in Imidazolium-Based Ionic Liquids with the tPC-PSAFT Equation of State, The Journal of Physical Chemistry B, 110 (2006) 9262-9269.

[236] J.S. Andreu, L.F. Vega, Capturing the Solubility Behavior of $CO_2$ in Ionic Liquids by a Simple Model, The Journal of Physical Chemistry C, 111 (2007) 16028-16034.

[237] J.S. Andreu, L.F. Vega, Modeling the Solubility Behavior of $CO_2$, $H_2$, and Xe in [Cn-mim][Tf2N] Ionic Liquids, The Journal of Physical Chemistry B, 112 (2008) 15398-15406.

[238] L.I.N. Tomé, P.J. Carvalho, M.G. Freire, I.M. Marrucho, I.M.A. Fonseca, A.G.M. Ferreira, J.o.A.P. Coutinho, R.L. Gardas, Measurements and Correlation of High-Pressure Densities of Imidazolium-Based Ionic Liquids, Journal of Chemical & Engineering Data, 53 (2008) 1914-1921.

[239] H. Machida, T. Kawasumi, W. Endo, Y. Sato, R.L. Smith, Jr., Ionic liquid structural effects on solute partitioning in biphasic ionic liquid and supercritical carbon dioxide systems, Fluid Phase Equilibria, 294 (2010) 114-120.

[240] M.Z. Hossain, A.S. Teja, Extension of an Associated Lattice–Fluid Equation of State to $CO_2$ + Ionic Liquid Systems, Journal of Chemical & Engineering Data, 59 (2013) 1038-1044.

[241] A. Finotello, J.E. Bara, D. Camper, R.D. Noble, Room-temperature ionic liquids: Temperature dependence of gas solubility selectivity, Industrial & Engineering Chemistry Research, 47 (2008) 3453-3459.

[242] P.W. Michael Krummen, and Jurgen Gmehling, Measurement of Activity Coefficients at Infinite Dilution in Ionic Liquids Using the Dilutor Technique, J. Chem. Eng. Data, 47 (2002) 1411-1417.

[243] J. Jacquemin, P. Husson, V. Mayer, I. Cibulka, High-pressure volumetric properties of imidazolium-based ionic liquids: Effect of the anion, Journal of Chemical and Engineering Data, 52 (2007) 2204-2211.

[244] J.M.S.S. Esperança, Z.P. Visak, N.V. Plechkova, K.R. Seddon, H.J.R. Guedes, L.P.N. Rebelo, Density, Speed of Sound, and Derived Thermodynamic Properties of Ionic Liquids over an Extended Pressure Range. 4. [C3mim][NTf2] and [C5mim][NTf2], Journal of Chemical & Engineering Data, 51 (2006) 2009-2015.

[245] M.E. Kandil, K.N. Marsh, A.R.H. Goodwin, Measurement of the Viscosity, Density, and Electrical Conductivity of 1-Hexyl-3-methylimidazolium Bis(trifluorosulfonyl)imide at Temperatures between (288 and 433) K and Pressures below 50 MPa, Journal of Chemical & Engineering Data, 52 (2007) 2382-2387.

[246] R.L. Gardas, M.G. Freire, P.J. Carvalho, I.M. Marrucho, I.M.A. Fonseca, A.G.M. Ferreira, J.A.P. Coutinho, P rho T measurements of imidazolium-based ionic liquids, Journal of Chemical and Engineering Data, 52 (2007) 1881-1888.

[247] H. Machida, Y. Sato, R.L. Smith, Jr., Pressure-volume-temperature (PVT) measurements of ionic liquids ( bmim(+) PF6- , bmim(+) BF4- , bmim(+) OcSO(4)(-) ) and analysis with the Sanchez-Lacombe equation of state, Fluid Phase Equilibria, 264 (2008) 147-155.

[248] R. Taguchi, H. Machida, Y. Sato, R.L. Smith, High-Pressure Densities of 1-Alkyl-3-methylimidazolium Hexafluorophosphates and 1-Alkyl-3-methylimidazolium Tetrafluoroborates at Temperatures from (313 to 473) K and at Pressures up to 200 MPa, Journal of Chemical & Engineering Data, 54 (2009) 22-27.

[249] R.L. Gardas, M.G. Freire, P.J. Carvalho, I.M. Marrucho, I.M.A. Fonseca, A.G.M. Ferreira, J.A.P. Coutinho, High-Pressure Densities and Derived Thermodynamic Properties of Imidazolium-Based Ionic Liquids, Journal of Chemical & Engineering Data, 52 (2007) 80-88.

[250] J.E. Kim, J.S. Lim, J.W. Kang, Measurement and correlation of solubility of carbon dioxide in 1-alkyl-3-methylimidazolium hexafluorophosphate ionic liquids, Fluid Phase Equilibria, 306 (2011) 251-255.

[251] A.M. Schilderman, S. Raeissi, C.J. Peters, Solubility of carbon dioxide in the ionic liquid 1-ethyl-3-methylimidazolium bis(trifluoromethylsulfonyl)imide, Fluid Phase Equilibria, 260 (2007) 19-22.

[252] W. Ren, B. Sensenich, A.M. Scurto, High-pressure phase equilibria of {carbon dioxide (CO(2)) + n-alkyl-imidazolium bis(trifluoromethylsulfonyl)amide} ionic liquids, Journal of Chemical Thermodynamics, 42 (2010) 305-311.

[253] S. Hwang, Y. Park, K. Park, Measurement and prediction of phase behaviour for 1-alkyl-3-methylimidazolium tetrafluoroborate and carbon dioxide: Effect of alkyl chain length in imidazolium cation, Journal of Chemical Thermodynamics, 43 (2011) 339-343.

[254] M. Costantini, V.A. Toussaint, A. Shariati, C.J. Peters, I. Kikic, High-pressure phase Behavior of systems with ionic liquids: Part IV. Binary system carbon dioxide+1-

hexyl-3-methylimidazolium tetrafluoroborate, Journal of Chemical and Engineering Data, 50 (2005) 52-55.

[255] K.I. Gutkowski, A. Shariati, C.J. Peters, High-pressure phase behavior of the binary ionic liquid system 1-octyl-3-methylimidazolium tetrafluoroborate plus carbon dioxide, Journal of Supercritical Fluids, 39 (2006) 187-191.

[256] A. Marciniak, The Solubility Parameters of Ionic Liquids, International Journal of Molecular Sciences, 11 (2010) 1973-1990.

[257] M.A. LaPack, J.C. Tou, V.L. McGuffin, C.G. Enke, The correlation of membrane permselectivity with Hildebrand solubility parameters, Journal of Membrane Science, 86 (1994) 263-280.

[258] S.Y. Sudha, A. Khanna, Evaluating the Interactions of $CO_2$-Ionic Liquid Systems through Molecular Modeling, World Academy of Science, Engineering and Technology, 57 (2009) 539-542.

[259] C. Nicolas, E. Neau, S. Meradji, I. Raspo, The Sanchez–Lacombe lattice fluid model for the modeling of solids in supercritical fluids, Fluid Phase Equilibria, 232 (2005) 219-229.

[260] E.A. Smol'nikov, Sarmanova, L. M., Lukhvich, A. A., and Sharando, V. I., Means of Checking the Decarburizing Activity of Hot Salt Baths for the Heat Treatment of Tools, Met. Sci. Heat Treat., 29 (1987) 131-134.

[261] B.J.S. R. E. Thoma, and E. X, Guinn, Molten - Salt Solvents for Fluoride Volatility Processing of Aluminium - Matrix Nuclear Fuel Elements, in, Oak Ridge National Laboratory, Oak Ridge, Tennessee, 1964, pp. 1.

[262] Q. Peng, X. Yang, J. Ding, X. Wei, J. Yang, Design of new molten salt thermal energy storage material for solar thermal power plant, Appl. Energ., 112 (2013) 682-689.

[263] T. Bauer, N. Pfleger, N. Breidenbach, M. Eck, D. Laing, S. Kaesche, Material aspects of Solar Salt for sensible heat storage, Appl. Energ., 111 (2013) 1114-1119.

[264] J.W. Raade, D. Padowitz, Development of Molten Salt Heat Transfer Fluid With Low Melting Point and High Thermal Stability, J. Sol. Energ., 133 (2011) 031013-031013.

[265] T.O. Norikazu Ohtori, and Keiichi Takase Thermal conductivity of molten alkali halides: Temperature and density dependence, J. Chem. Phys., 130 (2009) 044505

[266] R.M. DiGuilio, A.S. Teja, A rough hard-sphere model for the thermal conductivity of molten salts, Int. J. Thermophys., 13 (1992) 855-871.

[267] P.W. Bridegman, The Physics of High Pressures, G. Bell and Sons Ltd., London, 1949.

[268] J.F. Kincaid, H. Eyring, Free Volumes and Free Angle Ratios of Molecules in Liquids, J. Chem. Phys., 6 (1938) 620-629.

[269] M.R. Rao, Thermal Conductivity of Liquids., J. Chem. Phys., 9 (1941) 120.

[270] L.R. White, H.T. Davis, Thermal Conductivity of Molten Alkali Nitrates, J. Chem. Phys., 47 (1967) 5433-5439.

[271] R.E. Young, J.P. O'Connell, An Empirical Corresponding States Correlation of Densities and Transport Properties of 1-1 Alkali Metal Molten Salts, Ind. Eng. Chem. Fund., 10 (1971) 418-423.

[272] D. Chandler, Rough hard sphere theory of the self diffusion constant for molecular liquids, J. Chem. Phys., 62 (1975) 1358.

[273] S.F.Y. Li, R.D. Trengove, W.A. Wakeham, M. Zalaf, The transport coefficients of polyatomic liquids, Int. J. Thermophys., 7 (1986) 273-284.

[274] M.J. Assael, J.H. Dymond, M. Papadaki, P.M. Patterson, Correlation and prediction of dense fluid transport coefficients. I. n-alkanes, Int. J. Thermophys., 13 (1992) 269-281.

[275] M.J. Assael, J.H. Dymond, M. Papadaki, P.M. Patterson, Correlation and prediction of dense fluid transport coefficients: II. Simple molecular fluids, Fluid Phase Equilibr., 75 (1992) 245-255.

[276] M.J. Assael, J.H. Dymond, P.M. Patterson, Correlation and prediction of dense fluid transport coefficients. V. Aromatic hydrocarbons, Int. J. Thermophys., 13 (1992) 895-905.

[277] M.J. Assael, J.H. Dymond, S.K. Polimatidou, Correlation and prediction of dense fluid transport coefficients. VI.n-alcohols, Int. J. Thermophys., 15 (1994) 189-201.

[278] M.J. Assael, J.H. Dymond, S.K. Polimatidou, Correlation and prediction of dense fluid transport coefficients. VII. Refrigerants, Int. J. Thermophys., 16 (1995) 761-772.

[279] T. Sun, A.S. Teja, Correlation and Prediction of the Viscosity and Thermal Conductivity of Dense Fluids†, J. Chem. Eng. Data, 54 (2009) 2527-2531.

[280] M. Hossain, M. Kassaee, S. Jeter, A. Teja, A New Model for the Thermal Conductivity of Molten Salts, International Journal of Thermophysics, 35 (2014) 246-255.

[281] Y.S.L. Touloukian, P. E.; Saxena, S. C., Thermal Conductivity of Argon. Thermal Conductivity: Non-metallic Liquids and Gases, Plenum Press, New York, 1970.

[282] B.A. Younglove, H.J.M. Hanley, The Viscosity and Thermal Conductivity Coefficients of Gaseous and Liquid Argon, J. Phys. Chem. Ref. Data, 15 (1986) 1323.

[283] H.M. Roder, C.A. Nieto de Castro, U.V. Mardolcar, The thermal conductivity of liquid argon for temperatures between 110 and 140 K with pressures to 70 MPa, Int. J. Thermophys., 8 (1987) 521-540.

[284] A.A.V. V. A. Rabinovich, V. I. Nedostup, and L. S. Veksler, Properties of Neon, Argon, Krypton and Xenon. Thermophysical Properties of Neon, Argon, Krypton and Xenon, Hemisphere Publishing Co., New York, 1988.

[285] S. Kitade, Kobayashi, Y. and Nagashima, A., Measurement of the Thermal Conductivity of Molten KNO3 and NaNO3 by the Transient Hot-Wire Method with Ceramic Coated Probes, High Temp. High Press., 21 (1989) 219-224.

[286] N. Nakazawa, Y. Nagasaka, A. Nagashima, Experimental determination of the thermal diffusivity of molten alkali halides by the forced Rayleigh scattering method. II. Molten NaBr, KBr, RbBr, and CsBr, Int. J. Thermophys., 13 (1992) 753-762.

[287] G.J. Janz., Density. Molten Salts Handbook, Academic Press, New York, 1967.

[288] R. Tufeu, J.P. Petitet, L. Denielou, B. Neindre, Experimental determination of the thermal conductivity of molten pure salts and salt mixtures, Int. J. Thermophys., 6 (1985) 315-330.

[289] T. Omotani, Y. Nagasaka, A. Nagashima, Measurement of the thermal conductivity of $KNO_3$-$NaNO_3$ mixtures using a transient hot-wire method with a liquid metal in a capillary probe, Int. J. Thermophys., 3 (1982) 17-26.

[290] M.V. Smirnov, V.A. Khokhlov, E.S. Filatov, Thermal conductivity of molten alkali halides and their mixtures, Electrochim. Acta, 32 (1987) 1019-1026.

# VITA

MOHAMMAD ZAHID HOSSAIN

Hossain was born in Brahmanbaria, Bangladesh. He attended school in Dhaka, Bangladesh, and received a B. S. in chemical engineering from Bangladesh University of Engineering and Technology in 2004. He worked in a fertilizer industry named KAFCO (Karnaphuli Fertilizer Company Limited, Bangladesh) from 2005 to 2008 as a Process Engineer. He received his master's degree in chemical engineering from North Carolina A & T State University in 2010 before coming to Georgia Tech to pursue a doctorate degree in chemical engineering. He develops a new thermodynamic EOS for associating systems in his PhD work. He is looking for a long time career in research and development to contribute 21$^{st}$ century scientific advancement in green technology. Mr. Hossain enjoys playing soccer at CRC at weekend.